Oljato-Monument Valley, Utah, United States

ΕΛΛΗΝΙΚΗ
ΕΠΙΣΤΗΜΟΝΙΚΗ
ΕΤΑΙΡΕΙΑ
ΕΔΑΦΟΜΗΧΑΝΙΚΗΣ
& ΓΕΩΤΕΧΝΙΚΗΣ
ΜΗΧΑΝΙΚΗΣ

Τα Νέα της Ε Ε Ε Ε Γ Μ

93

Αρ. 93 – ΑΥΓΟΥΣΤΟΣ 2016

Potential Pitfalls for an Expert Witness

Many of us in the technical services industry aspire to be experts in our field. To receive a request to provide expert witness services can be flattering and could be seen as validation of that status. However, ultimately provision of this service can result in the requirement to provide expert evidence at an inquiry or in court where rules and behaviour can be very different to our day to day experience.

Therefore, before accepting instructions to provide expert witness services on a particular matter, practitioners from member companies would be well advised to;

- refer to the recently published LPA 62 [Advice to Expert Witnesses] and
- reflect upon the following Magnificent Seven potential pitfalls drawn from recent experience, that potential expert witnesses can face and must fully understand:

1. Responsibility of an expert.

First and foremost experts must be aware that their responsibility is to provide independent evidence to the court unaffected by any desire to support their client's case (see also LPA 62). An expert should be formally instructed by the solicitor acting for the client and this should clearly define the terms of reference and responsibilities.

(συνέχεια στην σελίδα 3)

SIMSG ISSMGE

ISRM

Π Ε Ρ Ι Ε Χ Ο Μ Ε Ν Α

(συνέχεια από την πρώτη σελίδα)

2. **Ensure you are Fully independent.**

Before accepting an instruction, an expert must carefully consider if there are any conflicts in the appointment. This could be a question of being previously involved in the case, a connection with other parties dealing with or affecting the case or a less obvious connection with a matter that could influence the case. As a minimum the expert should advise the instructing solicitor and be entirely transparent in the proof of evidence of the potential conflict and how it could have affected the opinions given.

3. **Ensure you really are an expert.**

Although you might be expert in the general aspects of the case consider whether you truly are an expert in all the specific details you are required to give evidence on. For example you might be an expert remediation engineer but have never dealt with a petrol filling station. If the case is about a PFS, you should seriously consider whether you should accept or decline the instruction.

4. **Make sure you are fully conversant with all the documents**

It is easy to be tripped up if you are unaware of documents. On cross examination of a politician who admitted she had not had time to read all the documents, the barrister stated "Madam, you do not have an opinion!"

5. **Make absolutely sure your proof of evidence is correct**

There is nothing a barrister likes more than to find errors in a proof of evidence. So when writing your expert report or proof of evidence make doubly sure that everything is factually correct, that any calculations you have made are not flawed and your opinions cannot be disputed or undermined by virtue of simple factual or typographic errors. There is nothing worse than having to amend errors in a proof identified during cross examination and the barrister will use this to question the reliability of all your evidence. Although it is your evidence it always makes sense to get another expert to undertake a sense check before it is submitted to the court

6. **Do not be drawn under cross examination to stray beyond your area of expertise.**

It is very easy to be drawn under cross examination to make statements that are be beyond your area of expertise. A common pitfall is to bluff your way through but this could destroy the credibility of your entire evidence. It is far better to admit the limitations of your knowledge and not offer an opinion that is outside your area of expertise.

7. **And finally**

It is important to recognise the seriousness of being an expert. This is not just an exercise in mental gymnastics; beware that barristers do this day in day out and excel in getting under your skin to undermine your credibility – this is what they are paid to do! If anyone needs a confirmation of how merciless the process can be, it is worth reading the judgement of Justice Aikenhead on the Corby case and how he dealt with some of the witnesses. But more important than personal credibility, many of these cases can affect the lives of real people (as in the Corby case) and we must remember we have a responsibility to them as well.

Peter Witherington and Hugh Mallett

AGS - Association of Geotechnical & Geoenvironmental Specialists

8th Aug 2016

http://ags.org.uk/2016/08/potential-pitfalls-for-an-expert-witness/

ΑΡΘΡΑ

Παρουσίαση άρθρων, στην συγγραφή των οποίων μετείχαν Έλληνες, στο XVI European Conference on Soil Mechanics and Geotechnical Engineering, Edinburgh, 13-17 September 2015 (κατ’ αλφαβητική σειρά, στα ελληνικά, του ονόματος του πρώτου συγγραφέα).

Factors affecting the degree of improvement of NC clays reinforced with stone columns

Facteurs qui influencent le degré du progrès de NC argiles reinforcées par les colonnes en pierre

V. Papadopoulos & P. Andreou

ABSTRACT The main objective of this paper is to examine through 2D and 3D numerical analyses the effect of several important factors on the behaviour of NC clayey soils, reinforced with stone columns. In order to estimate the improvement degree as the settlement reduction factor, β, extensive analyses were performed for a wide range of the parameters involved. Apart from some well known factors, as the replacement ratio and the gravel pile deformability and strength, the effect of other parameters as the loading conditions, the intensity and the undrained shear strength of the clay as well, are investigated. The F.E. programs ABAQUS and PLAXIS (2D and 3D) are used for the examination of typical gravel pile groups, under varying loading level. From the comparison of the results from three dimensional analyses with those of the widely used simple unit cell model, under axisymmetric conditions, useful practical conclusions may be drawn.

1 INTRODUCTION

Stone columns installation in soft soils, usually achieved by vibro-replacement methods, is a widely used and effective ground improvement method. This technique provides better behaviour of the foundations, by increasing bearing capacity, reducing the settlements, accelerating the consolidation process and mitigating the liquefaction risk, as well.

In an attempt to understand and predict the behaviour of vibrated stone columns, many studies based on physical modeling, mathematical analysis, and full-scale testing have been carried out. These studies have highlighted various parameters that influence the overall performance of this technique. Laboratory research as f.e., by Hughes & Withers (1974), Charles & Watts (1984), Andreou et al (2006), Black et al (2007) has contribute considerably in understanding the behaviour of stone columns. These experimental studies have identified most of the particular parameters that control the behaviour of a vertically loaded stone column.

Many analytical and numerical approaches for estimating bearing capacity and settlement of soft soils improved by stone columns have been proposed. The analytical method after Priebe (1976, 1995) is commonly used to predict the settlements, using the unit cell approach, where a single column with the influenced soil zone is modeled in axisymmetric conditions. Methods based on the assumption of linear elastic behaviour of the gravel pile-soil system, seem to overestimate the settlement reduction. Dheerendra Babu et al (2013) reported and commended analytical methods based either on elastic or elastoplastic gravel pile and soil models.

Several factors, which influence the improvement, as the gravel pile and soil stress-strain relationship, boundary conditions, rigidity of the foundation surface, etc, can be modeled during the application of the finite element method. However, most of the cases are analysed by the simple axisymmetric simulation or the plain-strain one, mainly due to practical reasons. Comparative analyses under 2-D and 3-D conditions after Elshazly et al (2008), verified that the unit cell analyses, lead to inaccurate estimation of settlements, in some cases, therefore settlement correction factors must be applied, when 2-D F.E. simulations are performed. Extensive three-dimensional F.E. analyses were presented by Andreou (2009) for representative stone column groups and comparative results as well, from 2-D axisymmetric ones.

In the present paper the case of soft clayey soils improved by stone columns is examined. From the results of 3-D and 2-D finite element analyses, useful conclusions may be drawn, regarding the effect of several parameters on the settlement reduction ratio.

2 F.E. SIMULATION AND SOIL PARAMETERS

The detailed parametric 3-D analyses are carried out on group configuration of gravel piles on square grids, using the F.E. codes ABAQUS and PLAXIS 3D. Two basic cases are investigated in the present paper, as shown in Figure 1: Case A: The uniformly distributed pressure q, is immediately applied through a rigid plate on the improved soil surface, while the gravel piles are based on a rigid layer underlying the soft clay’s one. Case B: The pressure q is applied on a gravel blanket and the loading area is assumed either rigid or perfectly flexible. The stone columns are based on hard clay.

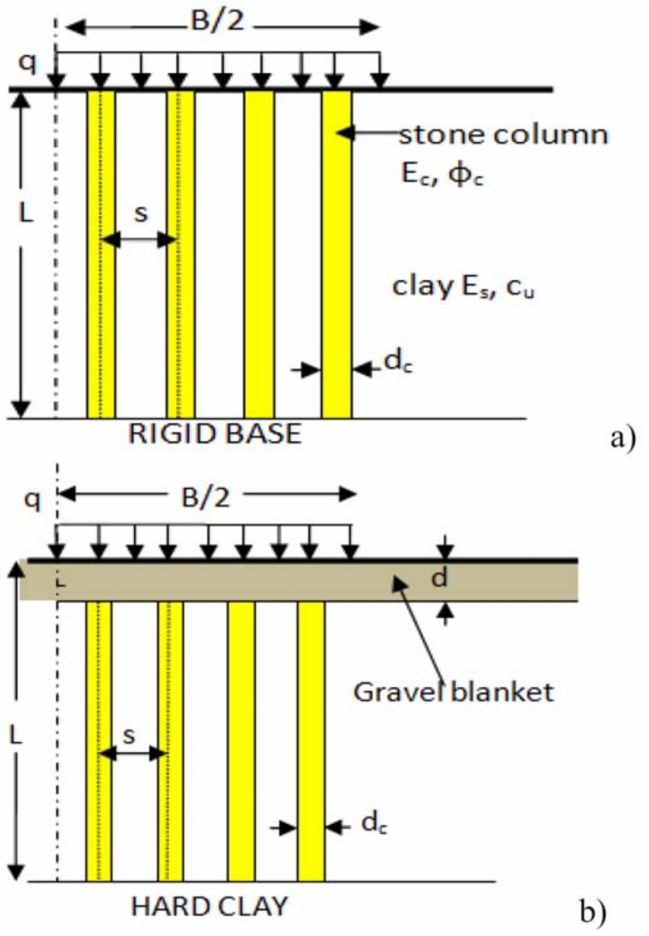

Figure 1. Geometrical model of the presented vases: Stone column grid 6*6 or 8*8.

In both cases A and B, the examined stone columns square grids are 6*6 or 8*8 (36 or 64 stone columns totally). The diameter of the stone columns in any case is assumed constant (dc=0.80 m), in Case B d=d_c is considered, while the center to center spacing s is varied 1.6 m-3.2 m. Therefore, the normalized spacing is s/d_c=2-4 and the replacement ratio of the improved soil, a_s=0.05-0.196.

The thickness of the compressible clay layer (equal to the gravel pile length) varied in the range of: L=6 m-20 m. In any case, the ratio B/L (where B is the width of the loading area) depends on the ratio s/d_s and the length L, as well. For the larger ratio s/d_s =4 and the lower L value, the loading conditions of the improved soil are almost 1-D ones. However, in most cases 3-D deformation conditions are clearly developed.

Several cases of the soft clay parameters were examined, mainly regarding the variation of shear strength with depth. The presented analyses are carried out by the simplest assumption of constant undrained shear strength over the thickness L. The investigated range of the used geotechnical parameters is given in Table 1. The ratio of the moduli of elasticity (gravel pile and clay) ranges between E_c/E=15-100. The comparative analyses under axisymmetric conditions (according to the unit cell model) are performed by the F.E. codes ABAQUS and PLAXIS V8.6. In the latter case 15-node finite elements were selected. In both 3-D and 2-D axisymmetric analyses, firstly the settlement so of the soft clayey soil without any improvement is calculated and the final settlement s_f of the reinforced soil by the stone columns, thus the settlement reduction factor β (equal to s_o/s_f) is resulted in any case.

Table 1. Range of geotechnical parameters used in F.E. analyses.

Description	Bulk density	Strength parameters		Elastic parameters	
	γ (kN/m^3)	φ΄(°)	c΄,c_u (kPa)	ν	E_c,E_s (MPa)
Soft clay	18	0-2	20-50	0.3-0.4	4-10
Stone columns	20	37-43	1	0.25	60-400
Hard clay	20	0	200	0.30	60

3. THREE DIMENSIONAL NUMERICAL RESULTS

It is well known that the replacement ratio as (or the normalized distance s/d_c in case of rectangular grid) and the angle of internal friction of the stone column φ΄$_c$ results in a remarkable improvement of the composite system. It is also shown that an increase of the normalized distance results to the significant decrease of the settlement reduction factor β, especially in the range of s/d_c=2-3.

It seems from the analyses, that for a given value φ'$_c$, the factor β increases when the undrained shear strength of the soft clay decreases. It is also clear from Figure 2 that the reduction factor β depends on the applied pressure q. The non-linear behaviour of both the stone columns, as well as the soft clay and especially the development of plastic zones and deformations by the increase of the loading, affect the relationship β-q/c_u.

Furthermore, the relationship between the applied pressure q (through a rigid plate) and the unique settlement of the surface, s, is a cumulatively presented in the specific case of Figure 3 for the soil without improvement and two cases of the ratio E_c/E_s, as well.

Three parts of the diagrams can be distinguished, as follows:

Part I: For very low pressures q, both the stone columns and the soil's behaviour is almost linear elastic, so the settlement reduction factor has relatively high values, similar to those provided by the elastic theory. For the higher value E_c/E_s is also higher, although these differences are not clear in Figure 3 due to the scale of the settlements.

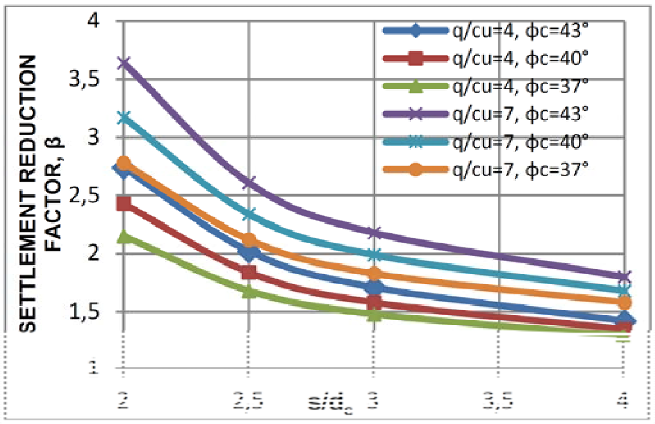

Figure 2. Influence of the normalized stone column spacings on the settlement reduction factor: Case A, L=12 m, grid 6*6, E_c/E_s=15.

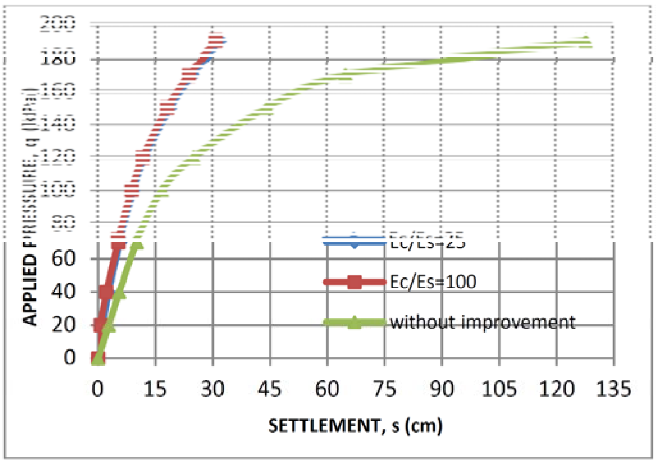

Figure 3. Comparative pressure-settlement diagrams: c_u=30 kPa, grid 8*8, H=12m, s/d_c=2,0.

Part II: The increase of the loading q results in the development of plastic zones, near the heads of the stone columns, due to stress overconcentration. In Figure 4a, these zones are shown for normalized pressure q/c_u=1.33. The soil for such loading, even in case of not any improvement, remains in the almost linear range, thus the factor β is slightly decreasing. For higher loading values, due to nonlinear response of the soil, the factor β remains almost constant or slightly increases.

Part III: For high loading values, the not improved soil approaches the limit equilibrium. Additionally, the rate of increase of the settlements is higher than this of the stone columns. As a result, the settlement reduction factor increases, reaching high values. The distribution of plastic zones for q/c_u=6.33 is shown in Figure 4b.

The effect of the normalized pressure and the ratio of moduli of elasticity E_c/E_s on the factor β are presented in Figure 5. The abovementioned three parts of the diagrams are clearly presented, as well as the very important effect of the normalized loading q/c_u on the settlement reduction factor, β. The effect of the ratio E_c/E_s is significant, only at low pressures, q and it seems that for higher values q/c_u, the vertical displacement of the stone columns is governed mainly from the plastic deformations and not from the modulus of elasticity E_c at the linear elastic area.

In case of flexible loading area, the settlement reduction factor, β depends on the point of reference and could be defined as the ratio of max s_o/max s_f, where the maximum settlements, without and after the improvement, correspond to the center of the grid. From Figure 6, important differences between a rigid and a perfectly flexible loading area resulted, only for high values, q/c_u.

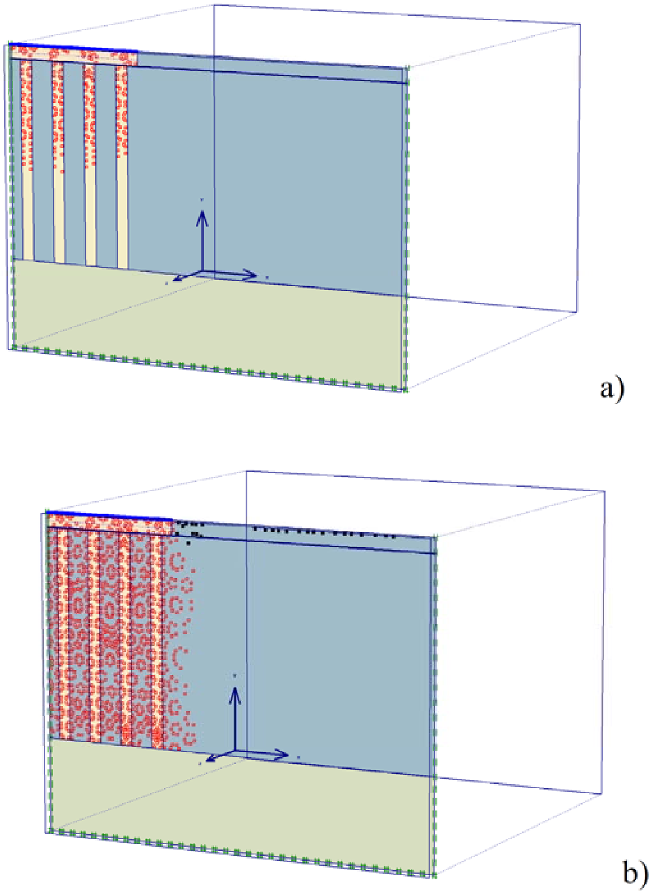

Figure 4. Development of plastic zones, case B, s/d_c=2: a) q/c_u=1.33, b) q/c_u=6.33.

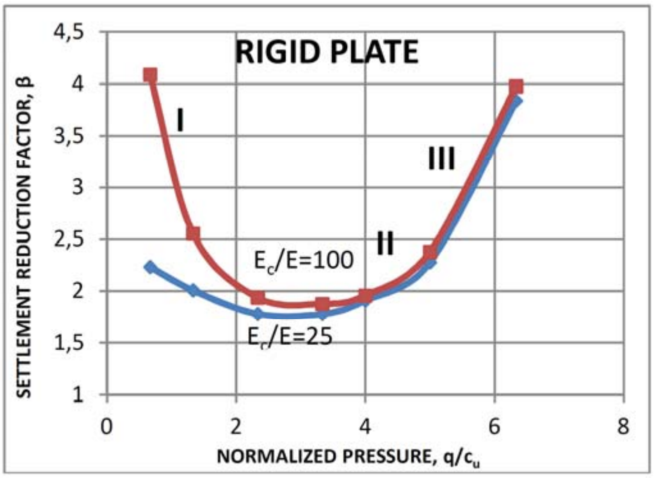

Figure 5. Effect of the normalized pressure on factor β: Case B, grid 8*8, H=12m, s/d_c=2,0.

The effect of the ratio B/L (B is the width of the square loading area) is examined for various lengths of the stone columns (L=6 m, 12 m and 18 m), keeping the constant value B=16 m. From Figure 7, it can be concluded that for the lower length (higher B /L ratio) the factor β is calculated with the lower values. In contrary, higher values β, correspond to geometrical conditions, clearly triaxial.

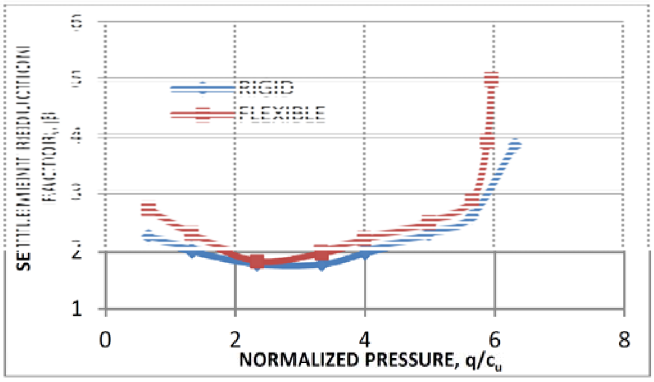

Figure 6. Effect of the flexibility of the loading area on the factor β (E_c/E_s=25).

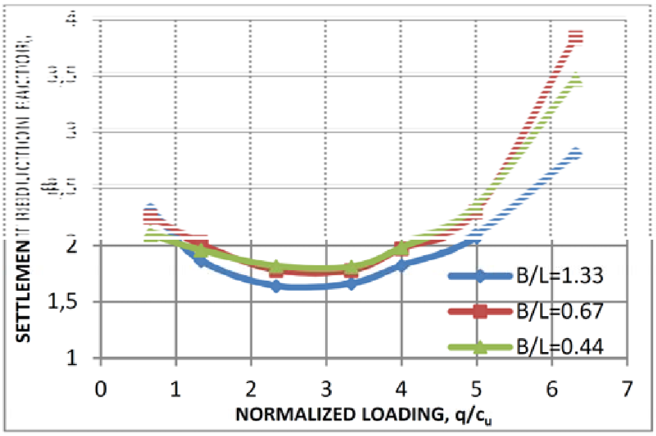

Figure 7. Effect of the length of stone columns on the factor β: φ'_c=43° , E_c/E_s=25.

4. COMPARISON OF THE RESLUTS FROM 3-D AND UNIT CELL

Due to the complexity of 3-D F.E. analysis, most cases of soil improvement, using stone columns are presently studied by axisymmetric finite element computations. Otherwise, it is the analytical method of Priebe (1995) that is commonly used to predict the settlements of the composite system, consisting from a single gravel pile and the surrounding soil. Both methods are based on the simulation of unit cell, where the main parameter affecting the settlement reduction factor, β, is the replacement factor, as. The response of the improved soil under 3-D conditions is quite complicated. Several parameters have minor or major effect on the settlements of the composite system and on the reduction factor, as follows:

i) The non-linear relationship s-q in both the clayey soil without any improvement and the reinforced one.

ii) The development of relatively high horizontal displacements under the perimeter of the loading area, both in case of improved soil (Figure 8) and the untreated one.

iii) The non-uniform distribution of the vertical stresses on the pile's heads, depending on the location of each of them (either near the center or at the perimeter of the grid).

On the other hand, in case of unit cell, several hypotheses seem unrealistic in some cases, as:

i) The conditions are similar to 1-dimensional compression, where the bearing capacity of the system is out of interest and the settlements are almost proportional to the applied loading q.

ii) The outer boundary of the model is assumed as rigid. In this way, no horizontal displacements take place under the perimeter.

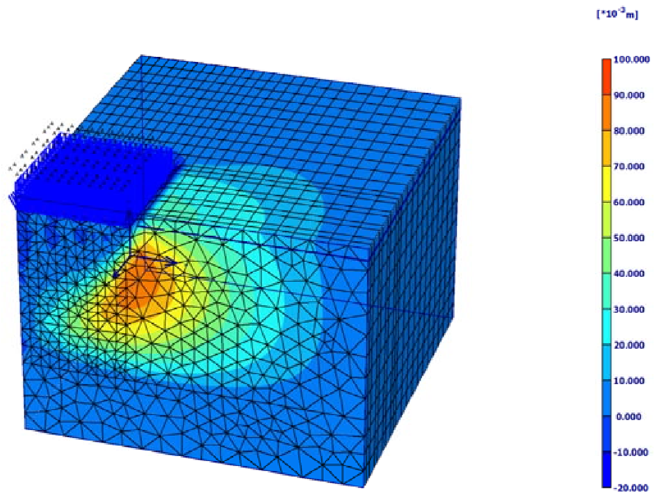

Figure 8. Horizontal displacements in case of B/L=0.67 (simulation of a quarter of the loading area).

The effect of the normalized spacing (center to center), s/d_s on the settlement reduction factor, β, either from 3-D analyses or 2-d ones (unit cell), is presented in Figure 9. The 3-D analyses are carried out for a grid 6*6 stone columns and L=12 m, therefore the ratio B/L varies in this case, between 0.8-1.6. The axisymmetric analyses are performed using the program PLAXIS V8.6 (comparative analyses by the code ABAQUS resulted in almost identical β values).

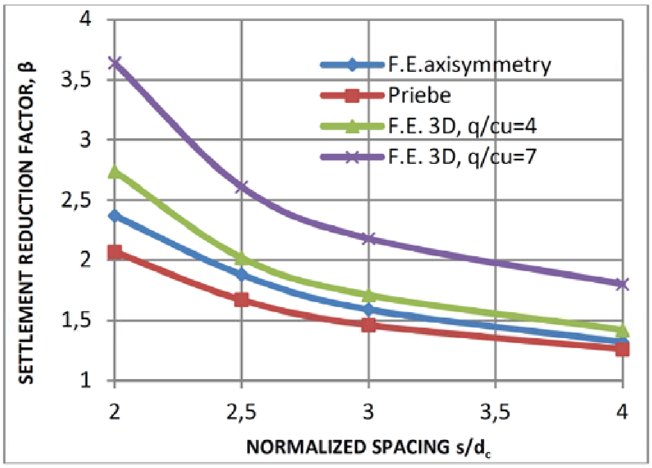

Figure 9. Comparison of 3D and unit cell analyses: Case A, L=12 m, grid 6*6, E_c/E_s=15.

The following inferences can be drawn from Fig. 9:

a) 2-D analyses underestimate the reduction factor, β. The differences from the 3-D ones are higher for lower s/d_c values.

b) Factor β is highly depended on the loading level (q/c_u). In contrast, neither the unit cell assumptions nor the axisymmetric analyses correlate the degree of improvement with the q values.

c) Although the 2-D analyses resulted in higher values of the factor β than the Priebe's method, generally the differences aren't remarkable.

Similar results were reported by Andreou and Papadopoulos (2014), by comparison of measured and back calculated settlement reduction factors.

5. CONCLUSIONS

From 3-D parametric analyses, it can be concluded that apart from several factors affecting the settlement reduction of the improved clayey soil by stone columns, other parameters as the loading level and the ratio B/L have also a quite significant effect. Three distinct parts of the diagrams relating the reduction factor β with the normalized pressure q/c_u can be distinguished, the higher β values corresponding to the first and third of them.

The ratio of modulus of elasticity E_c/E_s has a significant impact on the β ratio, only at relatively low loading levels, where the response of the composite system is almost linear elastic.

The results from well known methods based on the unit cell model seem that they underestimate the improvement degree, while they ignore the effect of the loading level. However, the deviations from the 3-D F.E. results become insignificant, as the conditions approach the 1-D ones (high B/L values) and the ratio q/c_u obtains lower values.

REFERENCES

ABAQUS Inc. (2004), ABAQUS V.6.4. User's manual. Providence, Rhode Island, USA.

Andreou, P., Frikha, W., Frank, R., Canou, J., Papadopoulos V.& Dupla J.C. (2008). Experimental study on sand and gravel columns in clay. *Proceedings of the Institution of Civil Engineers. Ground Improv.* 161 (GI4): 189-198.

Andreou, P. (2009). Modeling the behavior of soil improved by stone columns, *PhD Thesis*, National Technical University of Athens, School of Civil Engineering, Geotechnical Division (in Greek).

Andreou, P.& Papadopoulos, V. (2014). Factors affecting the settlements estimation of the stone column reinforced soils. *Geotech.Geol.Eng*.32: 1175-1185.

Bachus, R.C. & Barksdale, R.D. (1984). Vertical and lateral behavior of model stone columns. *Proceedings of Actes du Colloque International*: Renforcement en place des sols et de roches, Paris, 1: 99-104.

Black, J.A., Sivakumar, V. & McKinley J.D. (2007). Performance of clay samples reinforced with vertical granular columns. *Can. Geotech. J.* 44:89-95.

Charles, J.A.& Watts, K.S. (1983). Compressibility of soft clay reinforced with granular columns. *Proceedings of the 8th European Conference on Soil Mechanics and Foundation Engineering*, Helsinki, 1:347-352 (Eds: Rathmayer H.G. & Saari, K.H.O.).

Dherrendra Babu, M.R., Sitaran Nayak & Shivashankar, R. (2013). A critical review of construction, analysis and behaniour of stone columns, *Geotech. Geol.Eng*. 31: 1-22 (State-of-the-art-review).

Elshazly, H.A., Hafez, D.H.& Mossaad, M.E. (2008). Reliability of conventional settlement evaluation for circular foundations on stone columns. *Goetech. Geol. Eng*. 26: 323-334.

Hughes, J.M.O. & Withers, N.J. (1974). Reinforcing of soft cohesive soils with stone columns. *Ground Eng.* 7 (3): 42-49.

Plaxis b.v. (2007). Plaxis 3D.V2 user's manual. The Netherlands Plaxis b.v. (2012). Plaxis V.8 user's manual. The Netherlands.

Priebe H.J. (1976). Abschätzung des Setzungsverhaltes eines durch Stopverdinhtung verbesserten Baugrundes. *Die Bautechnik*, Vol.53, No 5: 160-162.

Priebe H.J. (1995). The design of vibro-replacement, Ground Engineering*, Keller Grundbau GmbH*, Technical paper, 12-61E.

Slope instabilities in clayey marls: two case studies

Glissement de Talus en Marnes Argileuses: Deux cas examinés

K.Papadopoulou and G.Gazetas

ABSTRACT Two cases of slope failures are analysed in conjunction with some factors affecting the instability of clayey marls, such as the pore pressures due to the rain infiltration, the weathering and the residual strength mobilization along pre-sheared surfaces. The first case concerns a failure of a major cutting 20-25 m deep, excavated during the earthworks for a new highway. The pleistocene deposits mainly consist of very stiff to hard clayey marls of high plasticity containing sandy thin layers and intercalations. Joints, which have unfavourable dip directions, were reported in some cases, while the failure was triggered by excessive water pressures after a period of heavy rainfalls. The second case refers to a major 30 m high slope failure, during construction. The plio-pleistocene deposits of the area consist from an upper very stiff marly clay layer, with sandy horizons weakly cemented and the underlying neogene hard marl. The failure, which was developed along a pre-sheared surface and was mainly triggered by the high water pressures, before any dissipation through toe drainage could ameliorate the situation.

1 INTRODUCTION

In overconsolidated clays or even clay shales and very weak rocks, factors as time-depended softening, weathering and strain-depended weakening influence the long term stability of slopes and contribute to delayed failures.

On the other hand, in such soil formations slope failures are usual during the construction or shortly after this, if high water pore pressures develop after intense rainfalls. Several factors affecting the slope stability of slopes in very stiff or hard soils have been investigated by many researchers. Picarelli (2013) concluded that the combination of peculiar features as weak bonds, fissuring and easy deterioration result in high landslide susceptibility. The effect of the presence of thin sand layers within a hard till formation was investigated by Orr (2013). The significance of the residual strength of clays in landslides was underlined by Skempton (1985), while Tika (2013) reviewed the main factors influencing the residual strength of cohesive soils, especially in overconsolidated ones with pre-existing shear zones. The importance of the anisotropy in the case of instability in hard soils or weak rocks has been reported by Simic (2013). Sotiropoulos and Cavournidis (1981) reported a case of progressive failures of slopes in clayey marls, attributed to an irregular stress-strain relationship, where the shear stresses passing to the softening side without ever reaching the anticipate peak strength. Alexandris et al (2011) presented a case of failures (end of construction) of slopes in clayey marls.

Nowadays, several advances lab or in situ methods are available to investigate the stability of slopes in such formations and analytical tools, as well. However, as it is now widely recognized, case studies are more likely to contribute in solving these problems than theoretical or laboratory work only (Popescu, 1997).

In this paper two slope failure cases in clayey marls are revisited and analyzed.

2 CASE 1: INSTABILITY OF SLOPES IN TECTONIZED AND WEATHERED CLAYEY MARLS

2.1 Brief history and geology

The project refers to a motorway in Greece, which was constructed 20 years ago. The axis of the road crosses a region covered by lacustrine plio-pleiostocene deposits up to great depth, consisting mainly of clayey marls or marls with thin layers of sandstones and/or marly limestones. In some locations of the region the marls are covered by fluvial Pleistocene deposits, consisting by mixtures of clayey silt and sand. The deposits are tectonized, so many minor or major faults were recorded in several positions, while the upper soil layers are intensely weathered in many cases.

Although the relevant geotechnical-geological investigations concluded that caution and special measures should be applied in specific locations, generally the slopes were constructed by a unique inclination 2:3 (height over length), benches 8 m high with no support.

In the revisited case under consideration, a major failure of a slope 24 m high is presented and backanalyzed, which took place in a location with unfavourable dip direction, but triggered by the water pore pressures after continuous and intense rainfalls, just at the end of excavation. The slip surface passing at the toe of the lower bench, had an almost cylindrical shape and was rather shallow.

2.2 Geotechnical conditions

From the relevant boreholes executed in the location of the failure, prior to any excavation, from the natural surface, mainly clayey marl was met with layers of sandy clay or clayey sand and intercalations of slightly cemented silty sand or sand. No water table was met during the drilling (up to 30 m depth), nor was it reported later on the installed piezometric pipes. At the upper 6-8 m the cohesive layers are dominated, while deeper, down to 30 m the presence of cohesionless thin layers in-between the marl is frequent.

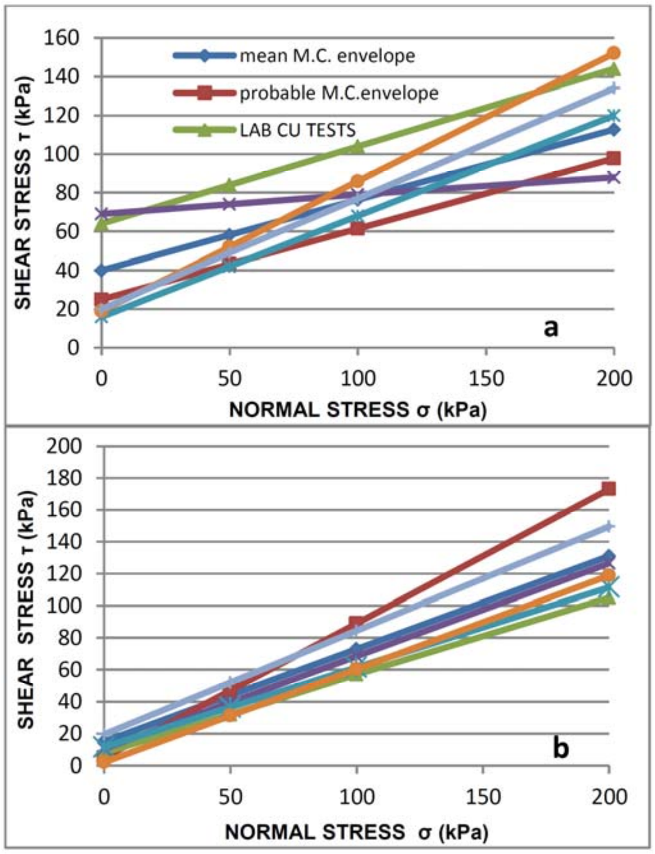

Figure 1. Shear strength envelopes from direct shear CU tests a) Samples CH, b) Samples SC-CH.

In almost all cases the examined samples from the clayey marls were classified as clay of high plasticity (CH) with high values of the liquid limit reaching LL= 100 approximately. The SPT blow counts were found to be 25<N<40 in most cases, while in the sandy intercalations reached much higher values. Moreover, a significant scatter was observed from the shear strength tests. The Mohr-Coulomb failure envelopes from CU direct shear tests are presented separately in cases of clayey marl CH and sandy samples SC-CH in Fig.1a and 1b, respectively.

2.3 New back analyses and comments

Just after the slope failure, back analyses were performed in order to design remedial measures and to improve the stability conditions at nearby positions. Those analyses were performed by the simplified Bishop's method. Using the F.E. program Plaxis V.8, the analyses were based on the original geometry before excavation, the available geotechnical data and the observations or information after the slope failure.

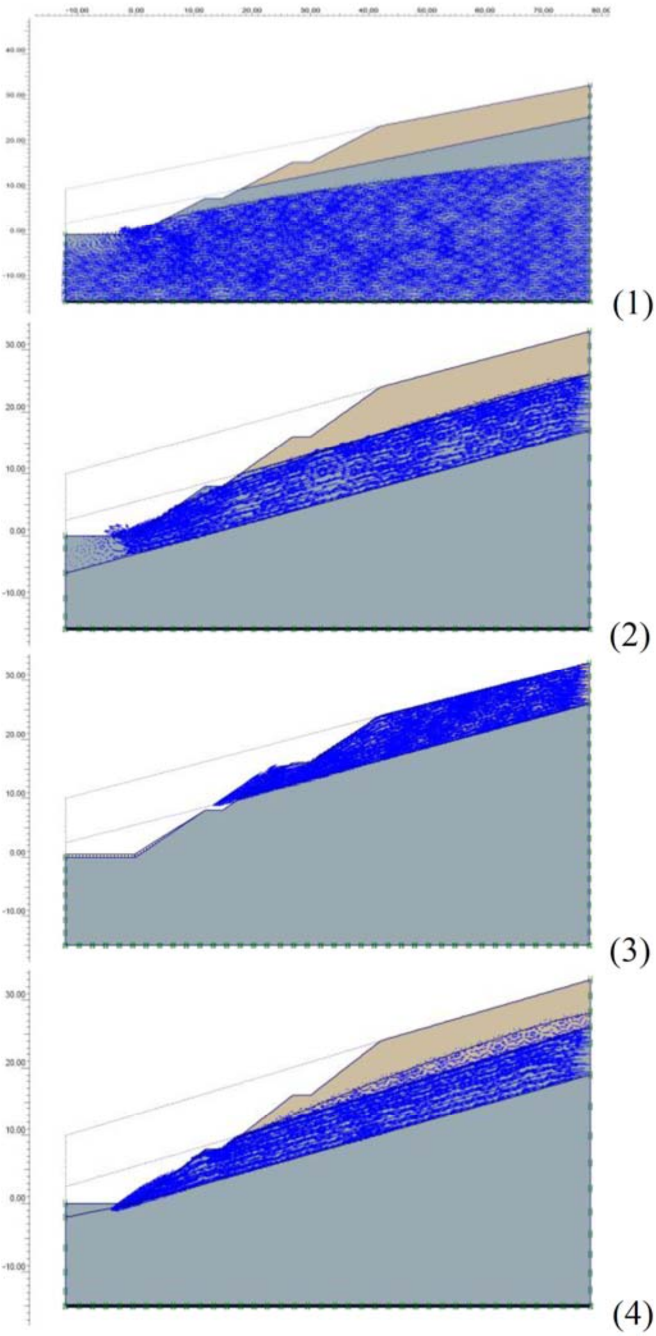

Figure 2. Four cases of temporary flow regime.

One of the main advantages of such a F.E. analysis is the capability to examine the effects of various probable flows, on the global safety factor, since the failure was attributed to the pore water pressures development. Temporary water flows, as in Figure 2, through the upper marly layers were analysed, taking into account that no water table existed, but the infiltration of the rain water from the intensively weathered surface soil zones seems certain. In any case, the ratio of coefficients of permeability at the horizontal and vertical direction was assumed $k_h/k_v=2$.

In the upper layer, I, 6-8 m thick, constant geotechnical parameters were considered, while in layer II, several combinations of the shear strength parameters were used, in the range shown in Table 1.

Table 1. Geotechnical parameters used in F.E. analyses

	Bulk density	Strength parameters		Coefficient of permeability	
Layers	γ (kN/m^3)	φ' (°)	c' (kPa)	k_v (m/s)	k_h (m/s)
I	19	20	25	$1.2\cdot10^{-6}$	$2.4\cdot10^{-6}$
IIa	16	29-33	5-15	$0.6\cdot10^{-6}$	$1.2\cdot10^{-6}$
IIb	16	29-33	5-15	$0.6\cdot10^{-8}$	$1.2\cdot10^{-8}$

The global safety factor SF for any case was estimated by the strength reduction method, which in case of Mohr-Coulomb criterion results in the so-called: "φ-c reduction". The effect of cohesion of the main second layer II on SF, depending also on the flow regime of any case, is presented in Figure 3. For comparison reasons, the case of fully drained slope (no water pressures development) was added.

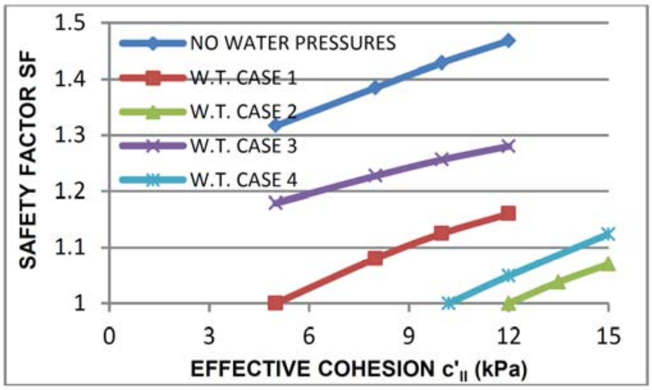

Figure 3. Effect of c'_{II} on the global safety factor for various cases of flow net (φ'_{II}=31°).

Taking into account that flow-net cases 2, 3, 4 are most probable than case 1, it may be concluded that a mean cohesion value c'_{II} = 5-10 kPa wasn't enough to prevent the slope failure under the abovementioned conditions. Furthermore, it is also concluded from Figure 1b that the probable range of the cohesion from the lab tests is c'_{II} = 8-10 kPa.

The failure mechanism from the F.E. analyses is illustrated for the three first cases of flow nets in Figure 4. Consequently, it generally matches quite well the actual one.

3 CASE 2: LANDSLIDE ALONG A PRESHEARED SURFACE

3.1 Brief history and geology

The case refers to a major slope failure during the construction of a motorway in the island of Crete, Greece, crossing a marly formation. The bedrock consists of miocene marly limestone or hard marls covered by pleistocene lacustrine clayey marls and fluvial marly clays, and/or mixtures of clay, sand and gravels. In the past, instabilities of the natural slopes had been reported, which were attributed to movements of the upper weathered mantle (4m thick), due to the temporary recharge of the water level from the springs of the area. The excavations were constructed in a dry period, mostly with two or three benches, each 8 m high. Before the completion of the excavation of the lowest bench (about 4 m above the final level), the first tension crack appeared at the crest of the higher one.

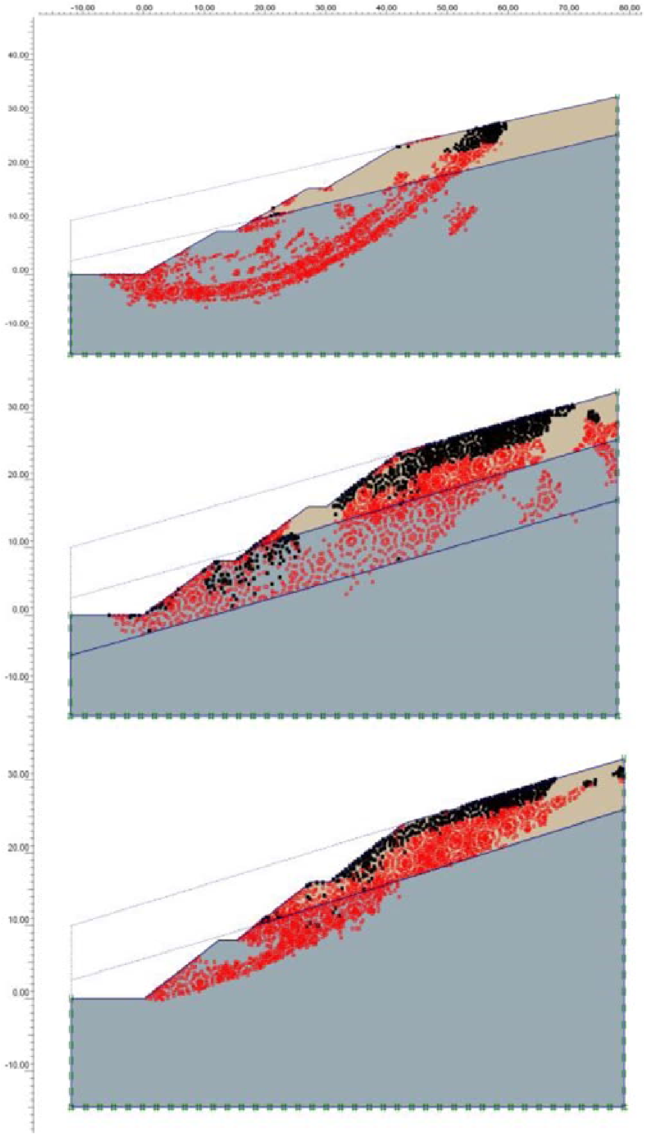

Figure 4. Three cases of slope failure mechanism from F.E. analyses (plastic zones in S.F. =1).

The slump type failure extended upwards far enough from the excavations, where the main scarp was developed. Furthermore, the failure was triggered by the infiltration of water uphill of the excavated slopes, but it was attributed to the unfavourable coincidence of some other factors.

3.2 Geotechnical conditions and back analyses

The upper soil layer (I), 2-5 m thick is weathered consisting of marly or clayey sand and disturbed soil materials. The main layer II has 6-8 m thickness and consists from overconsolidated marly clay CL-CH stiff or very stiff. The underlying Pleistocene marl (layer III) appears as hard O.C. clay CL-CH. The geotechnical investigation, which was carried out just after the landslide, focused on the shear strength of the second layer, since the failure surface, according to the observations, was developed at the contact with the marl (III).

The range of the shear strength resulted either from direct shear CU or triaxial CD tests on samples of the main layer II, is given in Figure 6. The results from residual strength tests and direct shear test on presplit samples, indicate a low residual "cohesion" in the order of c'_r= 9 kPa and φ'_r= 20°-28° for the effective overburden stress level at the contact surface (Figure 7).

Figure 5. Case 2: Tension cracks and secondary scarps on the benches.

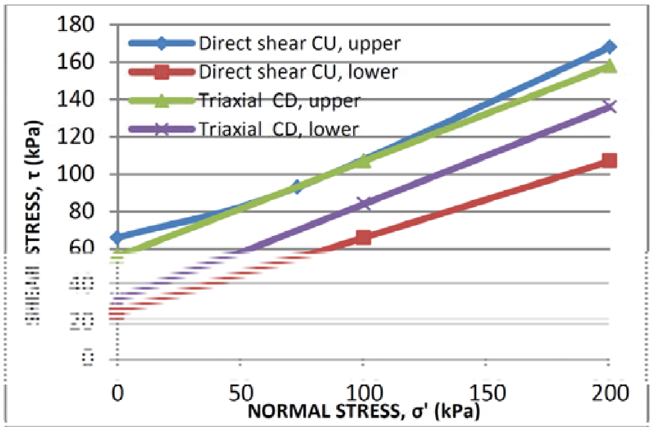

Figure 6. Shear strength envelopes from lab tests on marly clay (II) samples.

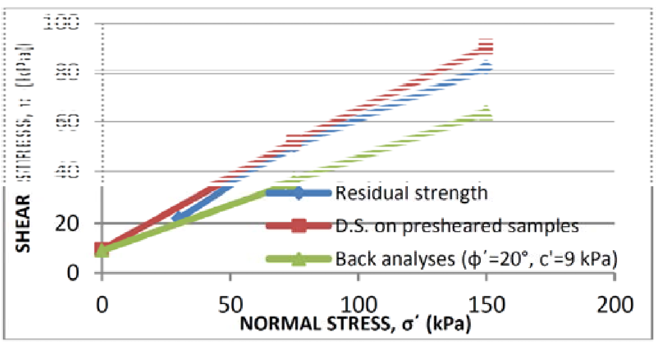

Figure 7. Residual strength of the marly clay (II) samples.

By the new back analyses, using the F.E. program Plaxis V.8 firstly, the effect of the ground water regime in conjunction with several combinations of the shear strength parameters on the failure mechanism is investigated.

Even taking into account the lowest of the φ', c' parameters of the layer II, which is considered as homogeneous one, according to Figure 6, it was not possible to explain the slope failure.

In contrast, simulating the contact surface between layers II and III, as an interface with reduced shear strength, in the order of the residual parameters or even lower (c'_r= 9 kPa and φ'_r=20°-28°), for various possible flow nets, the resulted global safety factor approached the value SF=1, during the excavation of the lower bench.

An indicative case of the analyses, which simulates a representative cross-section is shown in Figure 8. The mode of failure from these analyses approaches well the observed surface, at the crest of the excavation, which extended uphill at a relative high distance.

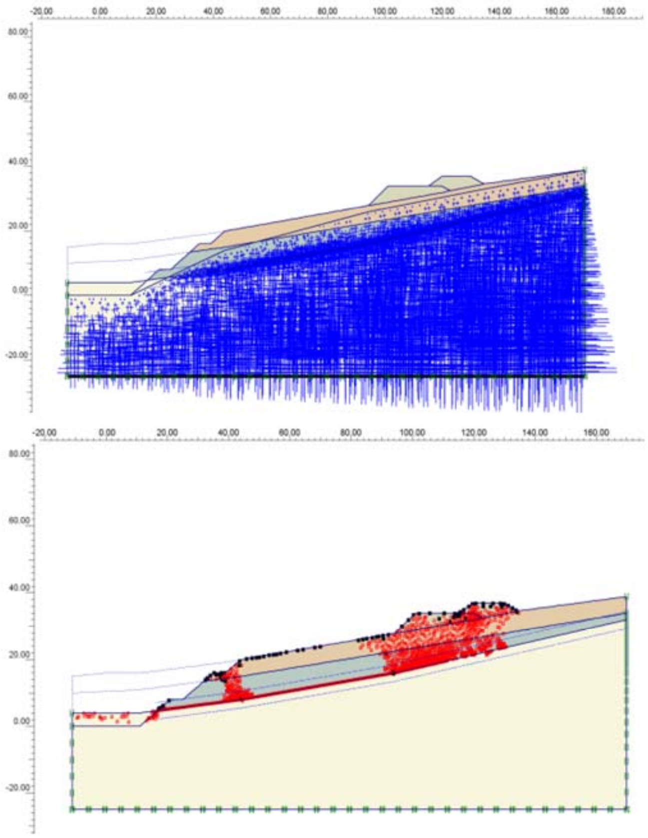

Figure 8. Flow regime and failure mechanism of the slope.

4. CONCLUSIONS

The trigger of slope failures in cases 1 and 2 was the excessive water pressures after a period of intense rainfalls and the unexpected infiltration and rise of the water table, correspondingly. However, the main reason of the first case failure was the presence of tectonized and intensely weathered clayey marls in a part of the excavations, while in the second the pre-sheared contact surface between the hard marl and the overlying stiff marly clay.

In both cases the back analyses using F.E. method, appropriate strength parameters and in situ observations can justify the mechanisms of failures quite well. Nevertheless, it is quite difficult to predict the behaviour of slopes, to be excavated in the design phase, taking into account the significant scatter of the shear strength parameters, the weathering effect, the strain-dependence on the residual strength, etc. As it is well known, in such cases, the engineering judgment, the appropriate evaluation of any information and the attention to "detail" are of peculiar interest.

ACKNOWLEDGEMENT

The authors would like to thank TOPPOS Consulting Engineers SA and Dr. V. Papadopoulos, Associate Professor for the provided geotechnical data of the back analysed cases.

REFERENCES

Alexandris, A., Paschalidou, A., Griva, E. & Kavvadas, M. (2011). End of Construction failures of cuttings in stiff clayey marls- A case from Central Greece. *Proceedings of the 15th C.S.M.G.E.* (Eds: Anagnostopoulos, A. et al), Vol.3: 1219-1224.

Alonso, E.E. Pinyol, N.M. & Puzrin, A.M. (2010). Geomechanics of failures– Advanced Topics. *Springer* Dordecht, Heildeberg, London, New York.

Orr, T.L.L. (2013). The stability of lodgement till slopes in Ireland. *Proceedings of the 15th ECSMGE* (Eds: Anagnostopoulos, A. et al), Vol.4: 413-416.

Picarelli, L (2013). Remarks on the behaviour of cuttings and natural slopes in tectonized clay shales. *Proceedings of the 15th ECSMGE* (Eds: Anagnostopoulos, A. et al), Vol.4: 401-407.

Popescu, M.E. (1997). Slope Stability and Protection, General Co-Report, session 4*, Proc. of an Int. Symposium: Geotechnical Enginering of Hard Soils –Soft Rocks*, Athens (Eds: Anagnostopoulos, A., F.Schlosser, N.Kalteziotis & R.Frank), Vol.3: 1985-2006.

Simic D. (2013). Instability phenomena in hard soils-weak rocks: Importance of the anisotropy. *Proceedings of the 15th ECSMGE* (Eds: Anagnostopoulos, A. et al), Vol.4: 409-412.

Skempton, A.W. (1985). Residual strength of clays in landslides, Folded Strata and the Laboratory. *Geotechnique*, Vol.35: 3-18.

Sotiropoulos, E. & Cavounidis, S. (1981). Irregular stress strain and progressive failure. *Proceedings 10th I.C.S.M.F.E.* (Eds: Publications Committee of 10th I.C.S.M.F.E.), Vol. 3: 527-531.

Tika, T. (2013). Residual strength of cohesive soils: A review of the main influencing factors. *Proceedings of the 15th ECSMGE* (Eds: Anagnostopoulos, A. et al), Vol.4: 417-424.

Dynamic properties of gravel – recycled rubber mixtures: resonant column and cyclic triaxial tests

Propriétés dynamiques de mélange de gravel-caoutchouc recyclé a l'aide des essais a la colonne résonnante et triaxiale cyclique

G.-A. Pistolas, A. Anastasiadis and K. Pitilakis

ABSTRACT: Strain-dependent shear modulus and damping ratio of poor-graded gravelly soil mixtures with granulated rubber, composed of recycled tire chips, are examined. On this framework, resonant column tests were performed on saturated specimens rubber percentage ranging between 0% and 60% by mixture weight; the ratio of the size of rubber versus gravel particles is equal to 0.7. Cyclic triaxial tests were also performed on identical specimens. A set of equations is proposed to describe the observed behaviour and the results are compared with previous studies. The effect of rubber content is discussed both in terms of small-strain shear modulus (Go) and small - strain damping ratio (Do), as well as in terms of strain - dependent dynamic properties in the form of G/Go – γ – D/Do curves.

1 INTRODUCTION

Experimental and theoretical studies during the last two decades have indicated alternative and interesting applications regarding the use of granulated rubber as a lightweight material in civil engineering structures, to improve the behaviour of geo-structures and foundations in static and dynamic loading. Granulated tire rubber materials composed of recycled tire shreds is used in clean form or in mixtures with granular soils in cases the reduction of the vertical and/or horizontal loads or earth pressures is requested. Recycled rubber materials mixtures with soils (mainly sand and gravels) have been also proposed as a mean to reduce vibration amplitudes and potentially to act as a short of seismic isolation layer.

2 MATERIALS TESTED AND TESTING PROGRAMME

The effect of rubber content in granular soils in terms of material stiffness, strength and damping has been studied through means of resonant column testing (Feng & Sutter, 2000; Senetakis et al., 2012; Anastasiadis et al,. 2012, Tsinaris et al., 2014), monotonic tests (Zornberg et al., 2004; Venkatapparao & Dutta, 2006; Pistolas et al., 2014), cyclic triaxial testing (Nakhaei et al., 2012; Pistolas et al., 2014), direct shear testing (Hazarika et al., 2012; Mohamad et al., 2013) and shaking table tests (Xiong et al., 2011), giving promising results as for the expediency of the implementation in civil engineer applications as a backfill, embankment or ground improvement material.

In this study, the effect of rubber content in gravel-rubber mixtures is examined by means of resonant column and cyclic triaxial testing. The small strain shear modulus (G_o) and damping ratio (D_o) are derived and their variation with rubber content, shear strain amplitude and confining pressure is presented. A modification of available equations from the literature describing the dynamic properties of soils in a wide range of shear strains γ and rubber content is proposed in order to capture the observed behaviour of the mixtures of the current study.

2.1 Materials tested

Table 1 summarizes the physical characteristics of the parent gravel material (C1D4), which is a typical quarry material. Only the particles restrained from sieve No4 are used to achieve a uniformity coefficient equal to 1. The rubber material (R3) comes from recycled tires and consists of grains with mean size $D_{50,r}$= 3.38mm. The mean grain size ratio of the materials tested is $D_{50,r}/D_{50,s}$=0.7.

Table 1. Properties and classification of physical and synthetic materials used.

Properties/Data	Physical Materials (Gravel)	Synthetic Materials (Rubber)
Material code	C1D4	R3
G_s, gr/cm^3	2.67	1.10
D_{max}, mm	4.76	4.75
D_{50}, mm	4.76	3.38
C_u	1.00	1.68
C_c	1.00	0.96
Classification	SP	Granulated Rubber
$\gamma_{d,max}$, kN/m^3	17.4	6.1
$\gamma_{d,min}$, kN/m^3	11.8	4.2

2.2 Specimen preparation and testing

In total 12 saturated specimens are tested by means of resonant column and cyclic triaxial tests. The dimension of the specimens is 70x140mm. First 6 specimens, as shown in Table 2, are tested in resonant column apparatus and then 6 identical specimens are tested in cyclic triaxial apparatus to reach higher strain level. The maximum shear strain imposed is about 2%. The specimens are tested over a wide range of confining pressures: 25kPa-50kPa-100kPa and 200kPa. For the compaction of the specimens dry tamping method is used and the relative density is kept constant, about D_r ≈70%. The void ratio of the specimens is shown in Figure 1. The rubber content in the mixtures ranges from 0% to 60% per mixture weight (Table 1) and as it is expected, the specific gravity of the specimens is reduced as the rubber content increases. For the given relative density, the void ratio of the materials ranges between 0.76 and 0.87. The equivalent void ratio e_{eq}, as proposed by (Feng & Sutter, 2000) increases as the rubber content increases (Figure 2), and is calculated as:

$$e_{eq} = \frac{V_{voids} + V_{rubber}}{V_{soil}} \tag{1}$$

Table 2. Tested mixtures and specimens.

Specimen Code	Rubber content, %	γ_d, kN/m^3	e	γ_L, %
C1D4 100	0	15.4	0.88	$0.9\text{-}1.4\cdot10^{-4}$
C1D4/R3-90/10	10	13.3	0.74	$1.2\text{-}6.4\cdot10^{-4}$
C1D4/R3-85/15	15	12.6	0.73	$1.2\text{-}6.2\cdot10^{-4}$
C1D4/R3-80/20	20	11.8	0.73	$1.7\text{-}3.9\cdot10^{-4}$
C1D4/R3-60/40	40	9.1	0.85	$9.1\cdot10^{-4}\text{-}16.8\cdot10^{-3}$
C1D4/R3-40/60	60	7.7	0.65	$9.0\text{-}16.8\cdot10^{-3}$

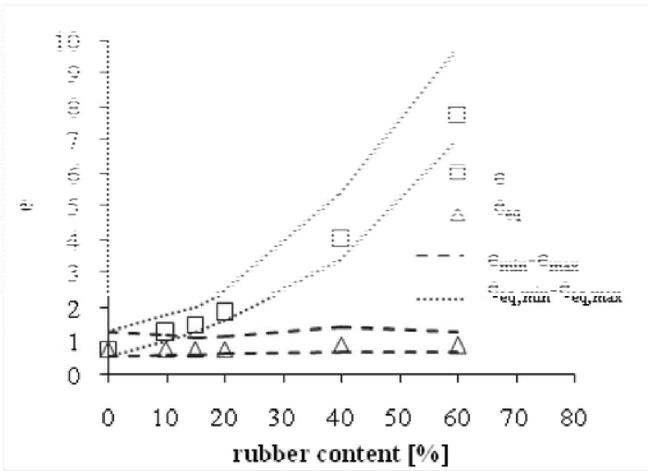

Figure 1. Void ratio to rubber content variation.

3 EXPERIMENTAL RESULTS AND ADOPTED MODEL

3.1 Experimental results

The experimental results show a constant decrease of the shear modulus G and an increase of the damping ratio D with increasing rubber content, as presented in (Figure 2).

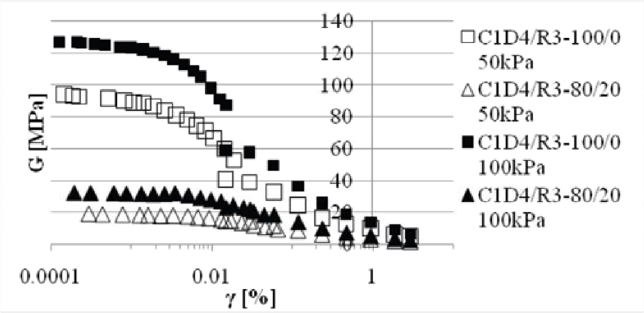

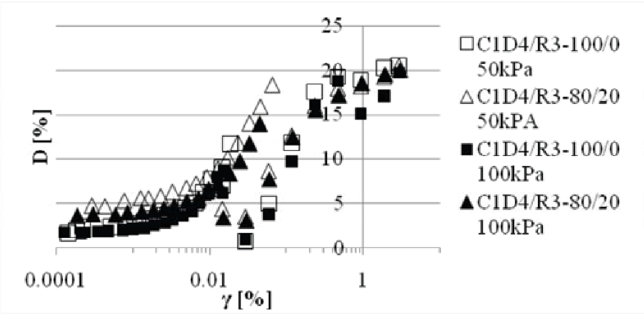

Figure 2. G-γ-D experimental results, σ'$_m$=50kPa and 100kPa.

The rate of increase of the shear modulus G with mean pressure decreases as the rubber content of the mixture increases. This can be observed from the comparison of the initial values of G at different mean pressures (50 & 100 kPa), as presented in (Figure 2). The mixture becomes more stress independent, in terms of shear modulus, as the rubber content increases, which can be attributed to the deformability of rubber grains.

The rate of decrease of the shear modulus G and the rate of increase of the damping ratio D with shear strain, reduces as the rubber content and mean confining pressure increases. The tested materials reach a rather constant maximum damping, approximately equal to 20%, for rubber content up to 20% per weight. For rubber content ≥40% the maximum damping occurs lower than 20% in the shear strain range of this study. The adapted hyperbolic model, as presented later, shows a tendency to reach higher values of damping than the parent material but at relatively high strain (γ>2%), even higher than the strain reported for sand/rubber mixtures by (Senetekis et al. (2012)) and also observed experimentally by (Pistolas et al. (2014)). The observed damping threshold is attributed to the fact that the rubber grains are smaller than the gravel grains. This leads to a soil-like behaviour of the material and the damping at high strain level is governed by dislocations of gravel grains. For rubber content ≥40% per weight, rubber like behaviour occurs, as it is also observed by (Kim & Santamarina, 2008) and the damping of the mixed material is mainly affected by the deformability of rubber grains. As a result, the D-γ curve becomes more linear at low-medium strain level. An increase of damping occurs at high strain level that dislocation of the rubber grains may occur. This tendency is captured by an abrupt increase of the proposed D-γ curves for mixtures with rubber content ≥40% per weight at high strain level.

3.2 Adopted Model

The main parameters affecting the mechanical behaviour of the mixtures are the mean grain size ratio of the mixed materials ($D_{50,r}/D_{50,s}$), the rubber content r, (rubber percentage per mixture's weight), the equivalent void ratio (e_{eq}) and the uniformity coefficient of the gravel material ($C_{u,s}$). It is noted however that the effects of the uniformity coefficient and the mean grain size of the rubber material on the mechanical properties of the mixtures, are considered of lower importance due to the high deformability of the material.

Considering this remark the proposed model is mainly governed by the rubber percentage per mixture's weight, r (%), the equivalent void ratio of the mixture e_{eq}, the properties of the initial gravel material (mean grain size $D_{50,s}$ and uniformity coefficient $C_{u,s}$) and the mean confining pressure, σ$_m$'.

To account for the rubber content of the mixtures the initial shear modulus Go and damping ratio D_o, are derived by modifying the equations proposed by (Menq, 2003) as follows. The value of $C_{u,s}$=1.0 for the tested materials leads to elimination of the influence of $C_{u,s}$. Moreover for r =0 the values for the initial gravel material are obtained.

$$G_0 = 115 \cdot C_{u,s}^{-0.2} \cdot e_{eq}^{x} \cdot \left(\frac{\sigma_m'}{p_a} \right)^{n_G} \cdot R_G \qquad (2)$$

$$D_0 = 2.8 \cdot C_{u,s}^{0.1} \cdot D_{50,s}^{-0.3} \cdot \left(\frac{\sigma_m'}{p_a} \right)^{n_D} \cdot R_D \qquad (3)$$

where p_a=101.325kPa and:

$$n_G = 0.6 \cdot C_{u,s}^{0.09} - 0.0009 \cdot r \qquad (4)$$

$$R_G = 1.025^{-r} \qquad (5)$$

$$x = -1 - \left(\frac{D_{50,s}}{20} \right)^{0.75} \qquad (6)$$

$$n_D = -0.18 \cdot 0.98^{r} \qquad (7)$$

$$R_D = -0.5 \cdot \left(1 + \frac{60 - r}{60 + 0.2r} \right) \cdot (1 + 2 \cdot 0.978^{-r}) \qquad (8)$$

where: p_a: atmospheric pressure (101.325kPa)

The proposed equations for Go and Do of the gravel/rubber mixtures of this study are presented in (Figure 3). The extreme values of Do for rubber content 40%, as shown in (Figure 3), are not considered as there are technical restrictions in measurements with resonant column in such a soft material. The equations proposed by (Senetakis, 2012) have been derived by resonant column tests on sand/rubber mixtures with maximum rubber content 35% per weight. In (Nakhaei, 2012) cyclic triaxial tests were performed on sand/rubber mixtures with rubber content up to 14% per weight. In this study the resonant column tests are further complemented by cyclic triaxial tests covering a greater range of rubber content, up to 60% per weight. As it is observed, G_o tends to decrease more rapidly with rubber content ≥40% than estimated by the aforementioned literature (Senetakis et al., 2011; Nakhaei et al., 2012) for sand/rubber mixtures. Moreover it has been observed that

Do increases even for rubber content up to 60% per mixture weight.

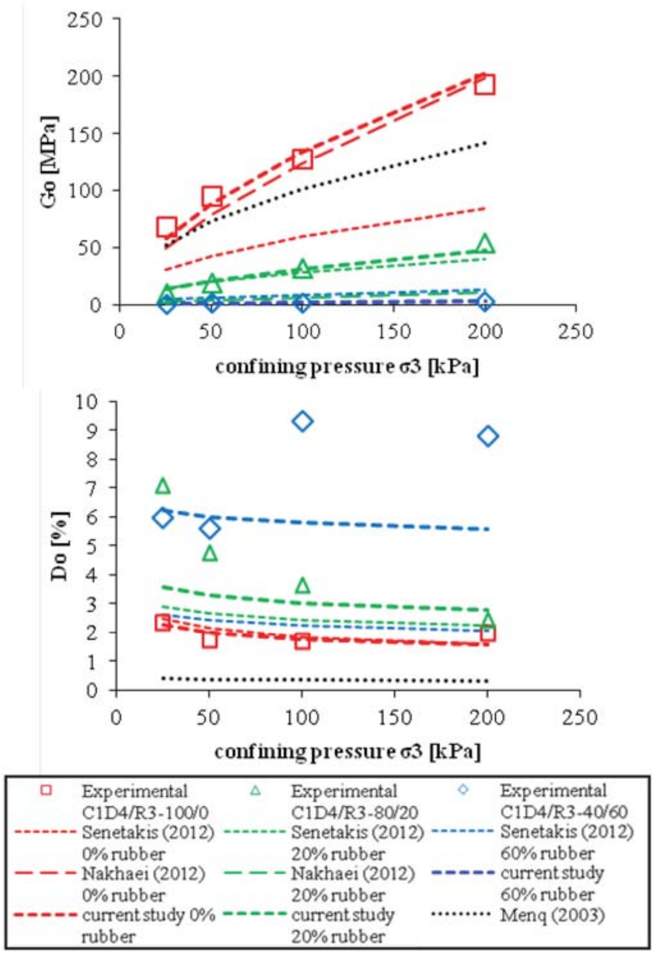

Figure 3. G_o,D_o - Experimental results and proposed equations.

The proposed G/G_o-γ-D/D_o curves are based on modification of the (Darendeli, 2001) equations, accounting for the rubber content of the mixtures as follows.

$$\frac{G}{G_0} = 1 + \left(\frac{\gamma}{\gamma_{ref,r}}\right)^{a_r} \qquad (9)$$

where:

$$\gamma_{ref,r} = \gamma_{ref} \cdot 0.438 \cdot \left(1.079 \cdot \left(\frac{\sigma_m'}{p_a}\right)^{0.0049}\right)^{r} \qquad (10)$$

$$\gamma_{ref} = 0.12 \cdot C_{u,s}^{-0.6} \cdot \left(\frac{\sigma_m'}{p_a}\right)^{0.5C_u^{-0.15}} \qquad (11)$$

$$a_r = a \cdot (5 \cdot 10^{-5} \cdot (r-100)^2 + 0.5) \qquad (12)$$

$$a = 0.86 + 0.1\log\left(\frac{\sigma_m'}{p_a}\right) \qquad (13)$$

Equation (9) for the normalized shear modulus is a function of the modified reference strain, $\gamma_{ref,f}$ [%] and the modified curvature coefficient, ar. Both of them account for the rubber content effects via the parameter r [%]. The D/D_o-γ curve is defined as:

$$D - D_0 = D_{Darendeli} \cdot (1.4 \cdot 1.003^{r} - 0.4 \cdot 10^{-4r}) \qquad (14)$$

where $D_{Darendeli}$ is taken from (Darendeli, 2001):

$$D_{Darendeli} = b \cdot \left(\frac{G}{G_0}\right)^{0.1} D_{Masing,correct} \qquad (15)$$

$$b = 0.6329 - 0.0057 \cdot \ln(N) \qquad (16)$$

$$D_{Masing,correct} = c_1 \cdot D_{Masing} + c_2 \cdot D_{Masing}^2 + c_3 \cdot D_{Masing}^3 \qquad (17)$$

$$D_{Masing} = \frac{100}{\pi} \cdot \left[4 \cdot \frac{\gamma - \gamma_{ref} \cdot \ln\left(\frac{\gamma + \gamma_{ref}}{\gamma_{ref}}\right)}{\frac{\gamma^2}{\gamma + \gamma_{ref}}} - 2\right] \qquad (18)$$

N is the number of loading cycles, while the Massing damping model parameters are calculated as:

$$c_1 = -1.1143 \cdot a^2 + 1.8618 \cdot a + 0.2523$$

$$c_2 = 0.0805 \cdot a^2 - 0.0710 \cdot a - 0.0095$$

$$c_3 = -0.0005 \cdot a^2 + 0.0002 \cdot a + 0.0003$$

Figures 4 and 5 depict the G/G_o-γ and D/D_o-γ curves for the tested materials at σm΄= 50 kPa. The influence of the rubber content in the degradation curve of G/G_o is evident, leading to more linear shape of the curve, as also observed by (Senetakis, 2012). The same behaviour is observed in D/D_o-γ curves, where the rubber inclusion results in limited increase of the initial damping ratio. This trend has been also observed for sand/rubber mixtures by (Pistolas et al., 2014). The granulated rubber acts partially as a granular material in which grains are dislocate although the rubber material itself does not present shear modulus degradation in such a low strain level. This fact leads to greater degradation of G than estimated by equations from the literature.

The divergence of the estimated behaviour of the mixtures, in terms of G/G_o-γ, D/D_o-γ curves, between the proposed model and the literature stems from the fact that in the current study (a) the tested specimens are saturated, (b) the parent material is gravel soil, (c) the proposed model is based on experimental results from both resonant column and cyclic triaxial and (d) the rubber content investigated covers a greater range of shear strains.

As mentioned, in (Nakhaei et al., 2012) the proposed G/G_o-γ curve was based on cyclic triaxial test results on saturated gravel/rubber mixtures with rubber content up to 14% per weight. In (Senetakis et al., 2012) dry sand/rubber mixtures with rubber content up to 35% per mixture weight were tested, using resonant column. In the current study, a greater range of rubber content is tested and the behaviour of the mixtures is investigated for rubber content even up to 60% per mixture weight, allowing for a more comprehensive insight of the cyclic behaviour.

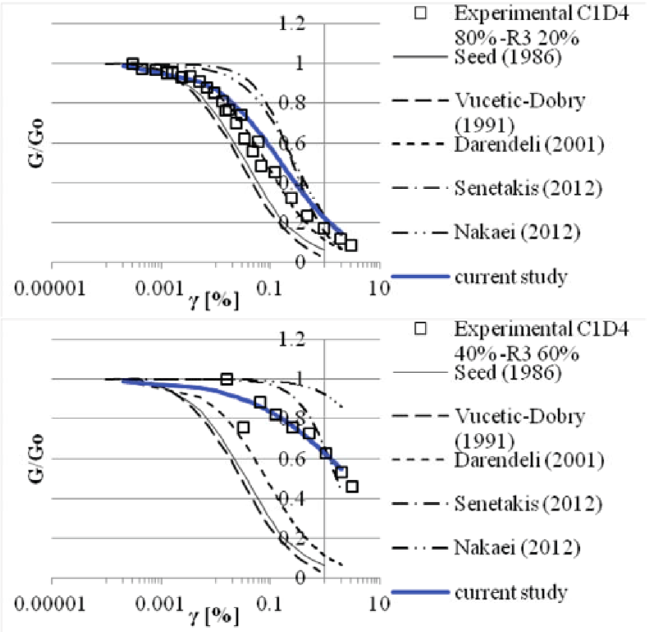

Figure 4. G/G_o-γ: Experimental results and proposed model.

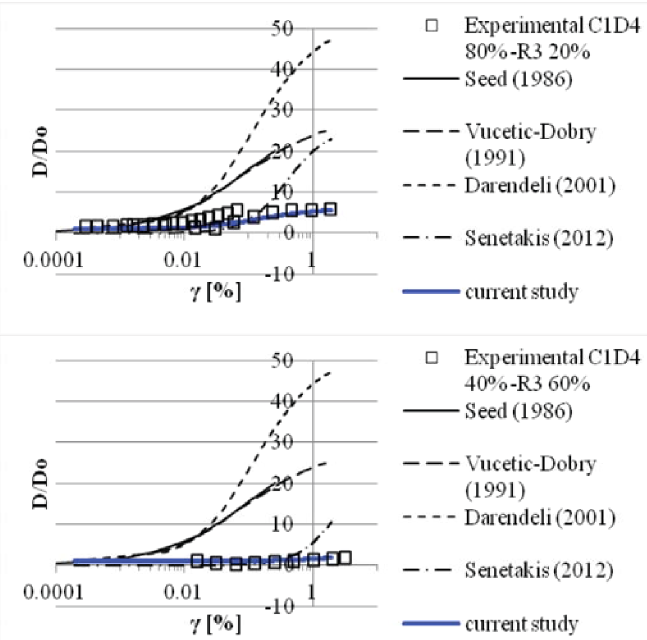

Figure 5. D/D_o-γ: Experimental results and proposed model.

The observed differences between the cyclic triaxial and the resonant column tests at small strain levels is mainly due to the limitation of the two testing methods. The complete set of experimental data of the current study allows for a consistent estimation of the materials' behavior and an accurate adaptation of the exploited model from small strains (γ≤ 5·10-2 %), based on resonant column test data, up to large strains (γ≈ 2%) based on cyclic triaxial test data, for a wide range of rubber content.

4 CONCLUSIONS AND DISCUSSION

In the present study the effect of rubber content on G_o, D_o and G/G_o-γ, D/D_o-γ curves is investigated by means of resonant column and cyclic triaxial tests, considering a wide range of shear strain amplitudes up to 2%. The results show that the increase of rubber content leads to decrease of G_o and increase of D_o. The variation of G/G_o and D/D_o with shear strain γ, is affected by the rubber content, showing a tendency to become more linear when the rubber content increases. Results from cyclic triaxial tests indicate a threshold for the upper value of damping ratio of the mixtures, approximately equal to 20%, for rubber content up to 20%. This threshold is defined by the gravel material of the mixture as the damping mechanism is mainly governed by the gravel grains dislocation.

The observed experimental behaviour is modeled by analytical close form relationships modifying the equations of (Menq, 2003) for G_o and D_o values and those of (Darendeli, 2001) for G/G_o-γ and D/D_o-γ curves. The rubber material is taken into account via the rubber content per mixture weight parameter r [%] and the equivalent void ratio e_{eq} (Feng & Sutter, 2000). The properties of the parent material ($C_{u,s}$ and $D_{50,s}$) affect the results of the normalized shear modulus and damping ratio curves.

REFERENCES

Seed H., Wong R., Idriss I. and Tokimatsu K., (1986). "Moduli and damping factors for dynamic analysis of cohesionless soils", *Journal of Geotechnical Engineering, ASCE*, Vol.112, No.11, pp.1016-1103.

Vucetic M., & Dobry R., (1991). "Effect of soil plasticity on cyclic response", *Journal of Geotechnical Engineering, ASCE*, Vol.117, No.1, pp.89-107.

Z. Feng, K. G. Sutter (2000), "Dynamic Properties of Granulated Rubber/Sand Mixtures," *Geotechnical Testing Journal*, GTJODJ, Vol. 23, No. 3, September 2000, pp. 338–344.

Darendeli M., (2001). "Development of a new family of normalized modulus reduction and material damping curves", *Ph. D. Dissertation,* University of Texas at Austin.

Menq FY (2003) 'Dynamic Properties of Sandy and Gravelly Soils'. Ph.D. Dissertation, University of Texas at Austin, USA.

Zornberg J.G., Carbal A.R., and Viratjandr C., (2004). "Behaviour of tire shred-sand mixtures'', *Can. Geotech. J.*,Vol.41,pp.227-241.

G. Venkatappa Rao, R.K. Dutta (2006) 'Compressibility and strength behaviour of sand–tyre chip mixtures'. *Geotechnical and Geological Engineering* (2006) 24: 711–724.

Kim H., Santamarina J. (2008) 'Sand–rubber mixtures (large rubber chips)'. *Can. Geotech. J.*, Vol.45, pp.1457-1466.

Xiong, W., Tsang, H.-H., Lo, S.H., Shang, S., Wang, H., Zhou, F. (2011)'Geotechnical seismic isolation system-Experimental study'. *Advanced Materials Research*, Vol 163-167,pp 4449-4453.

Anastasiadis A, Senetakis K, Pitilakis K, Gargala C, Karakasi I (2012) 'Dynamic behavior of sand/rubber mixtures, Part I: Effect of rubber content and duration of confinement on small-strain shear modulus and damping ratio'. *ASTM Int* 9(2).

Senetakis K, Anastasiadis A, Pitilakis K, Argiro S (2012) 'Dynamic behavior of sand/rubber mixtures, Part II: Effect of Rubber Content on G/Go-γ-DT Curves and Volumetric Threshold Strain. *J ASTM Int* 9(2).

Nakhaei, S.M.Marandi, S.Sani Kermani, M.H.Bagheripour (2012) 'Dynamic properties of granular soils mixed with granulated rubber'. *J Soil Dynamics and Earthquake Engineering* 43 (2012):124-132.

H. Hazarika, J . Otani and Y. Kikuchi (2012) 'Evaluation of tyre products as ground improving geomaterials'. Ground *Improvement*, Volume 165 Issue GI4: 267-282.

Mohamad, E.T., Latifi, N., Marto, A., Moradim, R., Abad, S.V.A.N.K. (2013) 'Effects of relative density on shear strength characteristics of sand-tire chips mixture'. *Electronic Journal of Geotechnical Engineering Volume* 18 D, pp 623-632.

Pistolas A., Anastasiadis A., Pitilakis K. (2014) 'Cyclic undrained mechanical properties of sand/granulated rubber mixtures'. In: *Proceedings of the 7th National Conference on Geotechnical Mechanics*, Athens, Greece.

Pistolas A., Anastasiadis A., Pitilakis K. (2014) 'Mechanical shear strength properties of sand/granulated rubber mixtures'. In: *Proceedings of the 7th National Conference on Geotechnical Mechanics*, Athens, Greece.

Tsinaris S., Pistolas A., Anastasiadis A., Pitilakis K. (2014) 'Mechanical and dynamical properties of mixtures of volcanic coarse soils with granulated rubber '. In: *Proceedings of the 7th National Conference on Geotechnical Mechanics*, Athens, Greece.

Vulnerability assessment of buildings exposed to co-eismic permanent slope displacements

Evaluation de la vulnérabilité des bâtiments exposes aux mouvements sismiques des pentes

K.D. Pitilakis and S.D. Fotopoulou

ABSTRACT A coherent approach is presented to evaluate the seismic vulnerability of buildings founded on precarious landslide slopes. In the first part a set of new predictive analytical expressions for assessing the coseismic displacements of slopes is presented and compared with existing empirical models generally referred to as Newmark-type models. Advanced statistics of a comprehensive set of numerical results allowed the derivation of analytical predictive expressions of the coseismic slope displacements with the best-correlated scalar and vector intensity measures (IMs) describing seismic hazard and site effects. In the second part of the paper an analytical method for assessing the vulnerability of RC buildings subjected to seismically induced slope displacements is presented. The methodology is based on the derivation of generic probabilistic fragility functions for typical reinforced concrete (RC) buildings considering the slope inclination, the height and the soil material of the precarious slope. The vulnerability is finally assessed through a vulnerability index d_m depending on the estimated probabilistic co-seismic slope displacements. The new predictive analytical expressions can be used in engineering practice while the general methodology for the vulnerability assessment can be extended to any type of building.

1 INTRODUCTION

Strong earthquakes can trigger permanent ground displacements and massive soil movements in landslide prone areas. Their impact on the built environment, the functionality of utility and lifeline systems, and finally to the human lives and economy, may be equal or even higher than the impact of the ground shaking itself. Marano et al. (2010) observed that landslides are both the most abundant and the most deadly earthquake-induced secondary effect, being responsible for 71.1% of the nonshaking deaths. According to Wen et al. (2004), around 20% of the registered landslides are triggered by earthquakes. In particular, many seismically active countries around the world present records of slope failures causing important damages and casualties (e.g. Yin et al. 2009). In landslide seismic risk assessment, it is the extent of permanent ground displacements, and not the factor of safety, that is the most important parameter, since the assessment of landslide potential (e.g. probability of landslide occurrence) on its own is of little relevance if the consequent ground deformations are not expected to cause distress and damage to buildings and infrastructure. In that sense what really matters from economic, societal and human point of view is the evaluation of the damages to buildings and infrastructures for the expected level and amount of ground displacements associated to the earthquake hazard of the area. The real risk is actually quantified with the induced physical damages to various assets. Therefore, what is needed is on the one hand, the evaluation of the performance of natural and artificial slopes during earthquakes in terms of permanent ground displacements and, on the other hand, appropriate fragility relationships of structures (i.e. buildings) and infrastructures (i.e. bridges, tunnels, pipelines, etc.) exposed to the landslide hazard in order to estimate the vulnerability and the risk. This approach is very well developed in earthquake engineering practice (e.g. NIBS 2004) regarding the risk assessment (structural and societal). Inspired from these conceptual considerations, the present work intends to provide the basis for the risk assessment of assets in case of seismically induces landslides. The following graph offers a simplified description of the proposed approach, which is based on the classical probabilistic method widely used in earthquake engineering. Several uncertainties and hypothesis are involved in the different steps of the method (e.g. Pitilakis 2014), which will be only briefly discussed here.

The core of the proposed approach (essentially probabilistic) is the evaluation of the induced ground displacements and the development of adequate fragility curves (Pitilakis et al. 2014) for structures exposed to permanent slope movements triggered from earthquakes. The paper will be concentrated to these two issues. It is basically divided into two main parts. In the first part, we present an overview of the available analytical methods, generally known as "Newmark-type" methods, to estimate co-seismic permanent slope displacements. Emphasis is put on the recently developed analytical method where earthquake-induced slope displacements were calculated using an advanced numerical analysis (Fotopoulou & Pitilakis 2015). The second part presents an analytical method for assessing the vulnerability of low-rise reinforced concrete (RC) buildings subjected to seismically induced slope displacements due to the landslide hazard (Fotopoulou & Pitilakis 2013a). Generic probabilistic fragility functions are proposed based on the parameters, which were found to most significantly contribute to the structure's fragility, namely the slope inclination in conjunction with the slope soil material (Fotopoulou & Pitilakis 2013b). A typical example at the end illustrates the practical use of the proposed methodology.

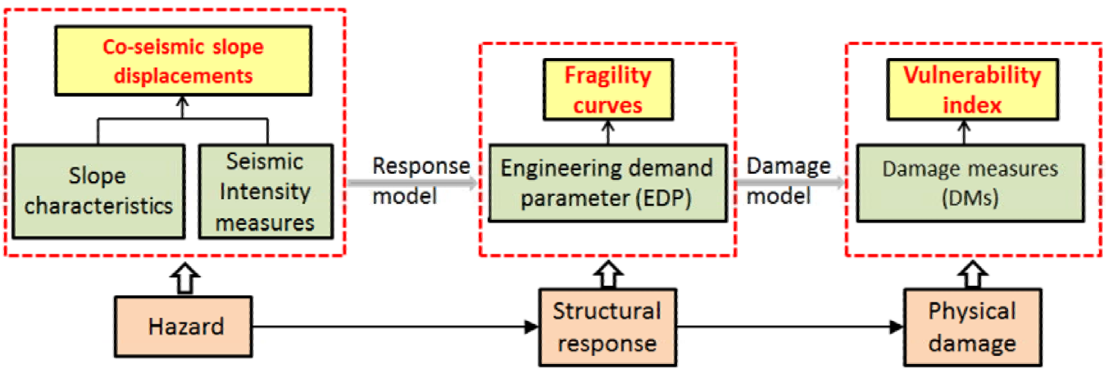

Figure 1. Flowchart of the proposed framework for vulnerability assessment of buildings.

2 PREDICTIVE MODELS FOR CO-SEISMIC SLOPE DISPLACEMENTS

Two different approaches of increased complexity are proposed to assess permanent ground displacements in case of seismically triggered slides: Newmark-type displacement methods and advanced numerical methods. The Newmark-type methods are based on the sliding block assumption first proposed by Newmark (1965) providing an index of the dynamic slope performance in terms of displacements. The advanced numerical analyses based on continuum mechanics (finite element, and finite difference methods) or discontinuum formulations usually incorporating complicated constitutive models are recently becoming attractive, as they can provide approximate solutions to problems which otherwise cannot be solved by conventional methods, e.g. the complex geometry including topographic and basin effects, material anisotropy and non-linear behavior under seismic loading, in situ stresses, pore water pressure built-up, progressive failure of slopes due to strain localization, etc.

Both methodologies depend on the appropriate selection and evaluation of the input motion and the slope characteristics (geometry and soil properties). The input motion characteristics (i.e. amplitude/intensity, frequency content and duration) depend on the seismic hazard and the local site effects, including probably topographic effects as well. Probabilistic (usually) and deterministic methods are applied to evaluate seismic hazard, involving numerous uncertainties (Pitilakis 2014), which may affect seriously the final results. Different parameters describing the input ground motion could be used such as the peak ground acceleration (PGA) and velocity (PGV) and Arias Intensity (I_a) describing mainly the amplitude, or other parameters describing the frequency content (e.g. mean period T_m) and the duration (e.g. significant duration $D_{5\text{-}95}$). A comprehensive overview of the intensity measures (IMs) used in hazard and risk assessment studies may be found in Douglas et al. (2015). The amplitude of ground motion is generally accepted as the dominating parameter providing better correlation with slope displacements and hence it is used in most analytical methods (e.g. Saygili & Rathje 2008; Strenk & Wartman 2013). Additional parameters characterizing either the intensity or the frequency content and duration of the earthquake ground motion are also used, in order to provide more efficient and sufficient estimates of the seismically induced slope displacements (Bray 2007). Recently it has been proved that directivity and fling effects, which are also characterized by long period waves, may be equally important (Garini et al. 2014)

The slope properties associated with the slope geometry, soil strength, stiffness and damping characteristics also play a crucial role in the prediction of seismic slope displacement. In the Newmark-type approaches, a single parameter, i.e. the yield acceleration coefficient, k_y, is commonly used to represent the overall sliding resistance of the slope. It depends primarily on the slope geometry and strength of the material along the critical sliding surface and it may be determined through a pseudostatic analysis or by a simplified empirical relationship (e.g. Bray 2007). Low k_y values (near zero) are indicative of a "weak" slope susceptible to sliding; as k_y increases the strength and the resistance to sliding of the slope increases as well. The stiffness of the slope can be also represented by the initial fundamental period of the slope, T_s. For a stiff nearly rigid slope, T_s approaches zero while for a deformable slope T_s can normally be estimated using a simple analytical expression depending on the shape and the dynamic response characteristics of the potential sliding mass (Bray 2007).

2.1 Newmark-type predictive models

Starting from the pioneer study of Newmark (Newmark 1965), several empirical models are currently available to predict seismically induced displacements of sliding masses. These generally differ with respect to the assumptions and idealizations used to model the mechanism of earthquake induced displacement. They are intended for soil slopes that do not undergo significant strength loss (i.e. liquefaction or flow slides). They are grouped into three main types (Jibson 2011): rigid-block, decoupled, and coupled slopes. The rigid-block model originally proposed by Newmark (1965) treats the potential landslide block as a rigid mass (no internal deformation) that slides in a perfectly plastic manner on an inclined plane. The original Newmark rigid sliding block assumption is employed in many of the available simplified slope displacement procedures (e.g., Sarma 1975; Lin & Whitman 1986; Ambraseys & Menu 1988; Yegian et al. 1991; Jibson 2007; Saygili & Rathje 2008 etc.). Rigid-block analysis is appropriate for analyzing thin, "stiff" landslides but yields quite unconvervative results for deep, "flexible or deformable" slopes. The dynamic site response (ground motion) and the sliding block displacements are computed separately in the 'decoupled' approach (e.g. Makdisi & Seed 1978; Bray & Rathje 1998; Rathje & Antonakos 2011) or simultaneously in the 'coupled' stick-slip analysis (Rathje & Bray 2000; Bray & Travasarou 2007). A comprehensive discussion on the most commonly used methods that account for the soil deformability (both coupled and decoupled) are discussed in Bray (2007). Generally, irrespective of their assumptions to analyze the dynamic slope response, recent approaches (e.g. Watson-Lamprey & Abrahamson 2006; Jibson 2007; Saygili & Rathje 2008; Bray & Travasarou 2007; Rathje & Antonakos 2011) involve larger ground motion datasets and robust mathematical regression techniques and therefore they are expected to yield more reliable estimates of the slope displacement. In the following, four of the most widely used empirical predictive models, namely the conventional analytical Newmark rigid block model (Newmark 1965), the Jibson (2007) rigid block model, the Rathje & Antonakos (2011) decoupled sliding block model and finally the Bray & Travasarou (2007) coupled stick-slip sliding block model, are briefly discussed.

The Newmark conventional analytical rigid block method is used to predict average slope displacements obtained by integrating twice with respect to time the parts of an earthquake acceleration-time history that exceed the critical or yield acceleration, a_c ($k_y \cdot g$) (i.e. threshold acceleration required to overcome shear soil resistance and initiate sliding). The second approach is a simplified rigid block model proposed by Jibson (2007), which predicts slope displacement as a function as Arias intensity (I_a) and critical acceleration ratio (a_c/PGA). This method was selected considering that Arias intensity was found to be the most efficient intensity measure for stiff, weak slopes (Travasarou 2003). The third method is a two-parameter vector (PGA, PGV) model proposed by Rathje & Antonakos (2011). This model is often recommended for use in practice due to its ability to significantly reduce the variability in the displacement prediction (Saygili & Rathje 2008). For flexible sliding, k_{max} (e.g. peak value of the average acceleration time history within the sliding mass) is used in lieu of PGA and k–vel$_{max}$ (e.g. peak value of the k-vel time history provided by numerical integration of the k-time history) is used to replace PGV. The last one is the Bray & Travasarou (2007) model. In this model cumulative displacements are calculated using the nonlinear fully coupled stick-slip deformable sliding block model proposed by Rathje & Bray (2000) to capture the dynamic response of the sliding mass. They use a single intensity parameter to characterize the equivalent seismic loading on the sliding mass, i.e. the ground motion's spectral acceleration Sa at a degraded period equal to $1.5T_s$, which was found to be the optimal one in terms of efficiency and sufficiency (Bray 2007).

It is noted that Newmark method is an analytical rigid block approach whereas Jibson (2007), Rathje & Antonakos (2011) and Bray & Travasarou (2007) models are essentially regression models of the analytical form of the rigid-block, decoupled and coupled methods respectively. As such, Newmark analytical method uses the entire time history to characterize the seismic loading as opposed to the simplified methods of Jibson (2007), Bray & Travasarou (2007) and Rathje & Antonakos (2011) that use one (I_a, Sa(1.5 T_s)) and two (PGA, PGV) intensity parameters respectively. In this way, uncertainties (and potential biases) associated to the selection of the ground motion intensity parameters are limited in the Newmark conventional analytical approach. Table 1 summarizes the functional form of the three simplified sliding block models. The herein models yield mean (Jibson 2007) or median (Rathje & Antonakos 2011; Bray & Travasarou 2007) values of seismic slope displacement when the standard deviation (the last term in the equations) is ignored.

Table 1. Functional form of the simplified sliding block models used in this study.

Model	Functional form
Jibson (2007)	$\mathrm{Log}(D)=0.561\,\log(I_a)$ $-3.833\,\log(a_c/PGA)-1.474\pm\sigma$ Where D is in cm, I_a in m/s, PGA and a_c in g.
Rathje & Antonakos (2011)	For rigid sliding masses: $\ln(D)=-156-4.58\left(\frac{k_y}{PGA}\right)-20.84\left(\frac{k_y}{PGA}\right)^2$ $+44.75\left(\frac{k_y}{PGA}\right)^3-30.50\left(\frac{k_y}{PGA}\right)^4+$ $-0.64\ln(PGA)+1.55\ln(PGV)+\varepsilon\,\sigma_{\ln D}$ where D is in cm, PGA in g and PGV in cm/s. For flexible sliding masses, k_{max} (in g) and k-vel_{max} (in cm/s) are used to replace PGA and PGV respectively and a term conditioned to T_s is added: $\ln(D_{flexible}) = \ln(D_{PGA,PGV}) + 1.42T_s$ for $T_s \le 0.5$ $\ln(D_{flexible}) = \ln(D_{PGA,PGV}) + 0.71$ for $T_s > 0.5$ where $D_{flexible}$ is in cm and T_s in seconds.
Bray & Travasarou (2007)	For the flexible sliding block case (T_s>0.05): $\ln(D)= -1.10 - 2.83\ln(k_y) - 0.333(\ln(k_y))^2$ $+ 0.566\ln(S_a(1.5T_s)) + 3.04\ln(S_a(1.5T_s))$ - $0.244\,(\ln(S_a(1.5T_s)))^2 + 1.50T_s+0.278(M-7)\pm\varepsilon$ where D is in cm, T_s in seconds and $S_a(1.5T_s)$ in g. For the nearly rigid sliding block case (T_s<0.05): $\ln(D) = -0.22 - 2.83\ln(k_y) - 0.333\,(\ln(k_y))^2$ $+ 0.566\ln(PGA) + 3.04\ln(PGA) - 0.244$ $(\ln(PGA))^2 + 1.50T_s+0.278\,(M-7) \pm \varepsilon$ where D is in cm, T_s in seconds and PGA in g.

2.2 Predictive relationships using numerical analysis results

Recently, Fotopoulou & Pitilakis (2015) proposed new predictive analytical expressions for co-seismic slope displacements, using a comprehensive set of numerical parametric analyses with different slope geometries, soil properties and input motions. Advanced statistical analysis and comparisons with the previous empirical analytical expressions, allowed the development of new expressions to estimate the co-seismic slope displacements using scalar or vector IMs. An overview of the proposed approach is presented in the following subsections.

2.2.1 Parametric numerical analyses

Two dimensional (2D) fully non-linear numerical analyses are performed for idealized step-like slope configurations applying the finite difference code FLAC2D (Itasca 2011), considering different real acceleration time histories as input motion. Soil resistance and the compliance of the sliding mass, characterized by the yield coefficient, k_y, and the fundamental period of the sliding mass, T_s, respectively, are also varying among rational limits i.e. k_y=0.05-0.3 and T_s=0.05s-0.69s. In particular, 12 typical slope soil models are analyzed with varying geometrical characteristics, material properties of the surface layer as well as strength and stiffness of the potential sliding surface. Regarding the soil strength parameters we properly selected pairs of the angle of friction φ (varying from 18° to 44°) and the cohesion c (varying from 0.5KPa to 30KPa). Figure 2 describes the layout of the problem under study.

The discretization allows for a maximum frequency of 10Hz to propagate through the grid without distortion. A finer discretization is adopted in the slope area, whereas towards the lateral boundaries of the model the mesh is coarser. Free field absorbing boundaries are applied along the lateral boundaries whereas quiet boundaries are applied along the bottom of the dynamic model to minimize the effect of trapped energy and artificially reflected waves. The soil materials are modeled using an elastoplastic constitutive model with the Mohr-Coulomb failure criterion (shear yield) with tension cutoff (tension yield function), assuming a zero dilatancy non-associated flow rule for shear failure and an associated rule for tension failure (Itasca 2011). Generic soil properties are considered based on the available literature and engineering judgment. These are selected to vary for the surface layer (see Figure 2) while they are kept constant for the intermediate clayed layer (V_s=500m/s, c=50KPa, φ=27°) and the elastic bedrock (V_s=850m/s).

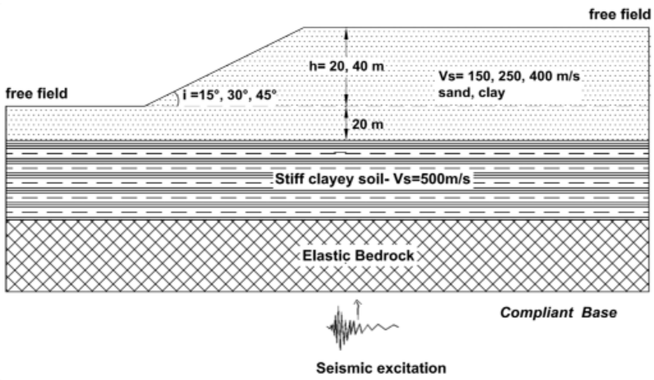

Figure 2. Layout of the cases analyzed.

The fundamental period of the sliding mass (T_s) is estimated using the simplified expression: T_s = 4H/V_s, where H is the depth and V_s the average shear wave velocity of the potential sliding mass. The depth of the sliding surface as well as the horizontal yield coefficient, k_y, are evaluated by means (e.g. no liquefaction or strain softening). of pseudostatic slope stability analyses utilizing the Bishop's simplified method for the critical sliding surface. k_y is calculated assuming that no significant strength loss is anticipated in the slope soil material (e.g. no liquefaction or strain softening).

The dynamic input motion consists of SV waves vertically propagating from the rock basement. 40 real acceleration time histories were used all recorded on rock outcrop or very stiff soil (soil classes A and B according to EC8) derived from the SHARE database (Seismic Hazard Harmonization in Europe, www.share-eu.org). The moment magnitudes, M_w, of the records are varying from 5 to 7.62 and the epicentral distances, R, vary from 3.4 to 71.4 km. The peak ground acceleration (PGA) values range from 0.065g to 0.91g, the peak ground velocity (PGV) from 3.1cm/s to 78.5cm/s and the mean period T_m ranges from 0.16s to 1.14s. To obtain the appropriate input motion at the base of the FLAC2D model, the selected time histories are first subjected to baseline correction and filtering (f_1=0.25Hz, f_2=10 Hz) to assure accurate representation of wave transmission through the model.

Prior to the dynamic analyses, a static analysis is carried out to establish the initial effective stress field throughout the model. It is noticed that only the cases that result to nonzero displacement (≥0.001m) due to seismic loading are addressed. Thus, the number of dynamic analyses performed for each model depends on the considered k_y value in relation to the PGA values of the selected input motions. In total 285 analyses were carried out.

2.2.2 Comparison of the numerical approach with empirical methods

Prior to the statistical analysis of the numerical results, in terms of horizontal permanent displacements of the slope, a comparison is made with the existing analytical expressions. In all cases compatible idealized step-like slopes were used, characterized by different flexibility and resistance of the potential sliding surface. Figure 3 presents the distribution of the computed "effective" horizontal displacements within the sliding mass in log space that vary from very small values (smaller than 0.01m) to large ones (>1m).

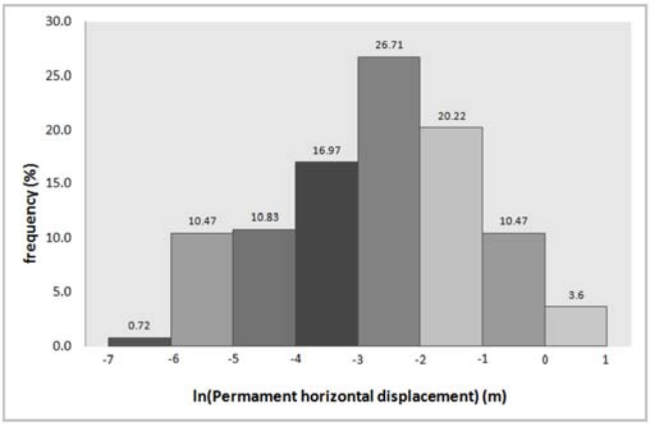

Figure 3. Histogram of the computed numerical horizontal displacements (for all models, N=285).

In total, 285 nonzero permanent horizontal displacements are calculated and compared with the slope displacement (D) predicted with most well known analytical expressions (described in Section 2.1) i.e. the Newmark rigid block model (Newmark 1965), Jibson (2007) rigid block model, Rathje & Antonakos (2011) decoupled sliding block model and Bray & Travasarou (2007) coupled stick-slip sliding block model.

It is noted that Newmark-type methods capture the part of seismically induced displacement attributed to the deviatoric induced deformation while the corresponding part attributed to the volumetric compression is not accounted for. This displacement due to deviatoric deformation is largely horizontal (Bray & Travasarou 2007) justifying the use of the horizontal (instead of the vector) numerical displacement for the comparison.

To derive the appropriate inputs for the Newmark-type methods that include the effect of soil conditions, and to allow a direct comparison with the numerical results, the acceleration time histories and the corresponding IMs at the depth of the sliding surface are computed through a onedimensional (1D) non-linear site response analysis using FLAC 2D considering the same soil properties as in the 2D dynamic analysis. The "average" 1D soil profile is located at the section that approximately corresponds to the maximum slide mass thickness H of the potential sliding surface. The maximum slide mass thickness H (or otherwise the maximum depth of the sliding surface), calculated by means of pseudostatic slope stability analysis, varies between 2 and 26 m for the different analyzed slope cases.

In Figure 4 the horizontal displacements calculated from the full dynamic numerical analyses are compared with the displacements calculated with the analytical Newmark's (1965), Jibson (2007), Bray & Travasarou (2007) and Rathje & Antonakos (2011) expressions. It is observed that numerical displacements generally are not inconsistent with the predicted Newmark-type displacements enhancing the reliability and robustness of the dynamic analysis results. The following general remarks can be deduced: (i) Newmark method generally predicts smaller displacements compared to the numerical model; (ii) Jibson (2007) model tends to underpredict small displacements and overpredict large displacements; (iii) Rathje & Antonakos (2011) model is well compared to the numerical analysis, except for a group of under-predicted displacements at the small displacement range; finally (iv) Bray & Travasarou (2007) model is generally in good agreement with the numerical analysis although its ability to predict very small displacements cannot be assessed as it cannot predict displacements smaller than 0.01m.

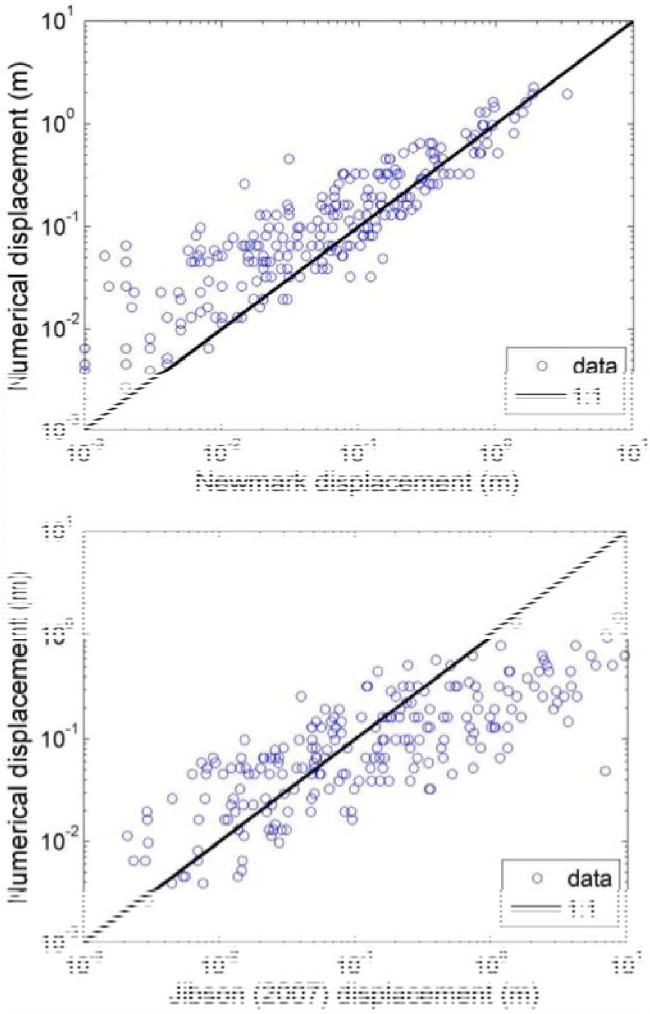

Figure 4. Numerically versus empirically calculated displacements.

However a relatively large dispersion in the displacement estimation is shown. This dispersion is also displayed in Figure 5, which presents the cumulative distribution of the relative difference between the numerical and empirical slope displacements for each of the empirical sliding block model

Relative difference (%)=[($D_{numerical}$ - $D_{empirical}$)/$D_{numerical}$].100%

It is noted that for positive values of the *relative difference* the empirical methods underpredict the displacements derived from the numerical analysis and vice versa. By examining the cumulative distribution functions it is seen that the rigid block Newmark model and the decoupled Rathje & Antonakos (2011) model generally tend to predict smaller displacements compared to the numerically derived ones. In particular, positive values of the *relative difference* in the displacement prediction are presented for cumulative frequencies from around 20÷30% to 100%. On the other hand, Bray & Travasarou (2007) coupled model may either overpredict or underpredict the numerical displacements yielding positive values of the *relative difference* in the displacement prediction for cumulative frequencies from around 49% to 100%. This is in line with the inherent coupled stick-slip assumption adopted in the method that offers a conceptual improvement over the rigid block and decoupled approaches for modeling the physical mechanism of earthquake induced slope displacement. Finally, Jibson (2007) simplified rigid block model tends to predict larger displacements compared the numerical ones dominated by negative predictions of the *relative difference* for cumulative frequencies up to 65%. The latter model is also associated with a very large dispersion in the median displacement estimation with respect to the numerical analysis compared to the former ones. This dispersion is obvious in the cumulative distribution of the *relative difference* diagram resulting to *relative differences* greater than - 500% for cumulative frequencies up to 20%. This observation confirms the author's statement regarding the avoidance of using his regression equations for site-specific applications where accurate estimates of displacement are required (e.g. for design purposes).

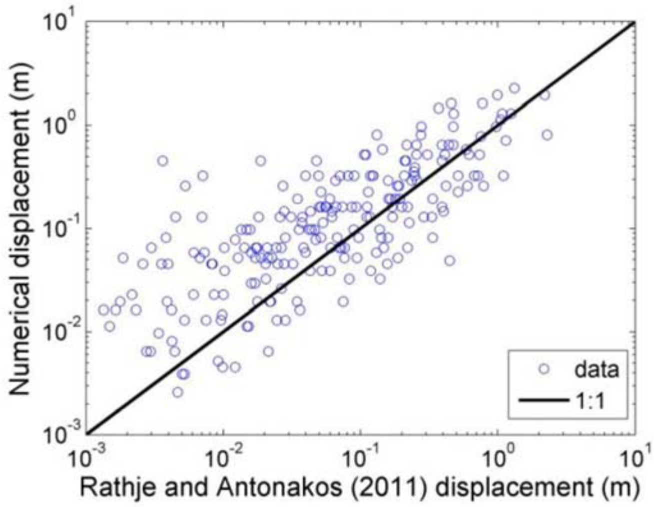

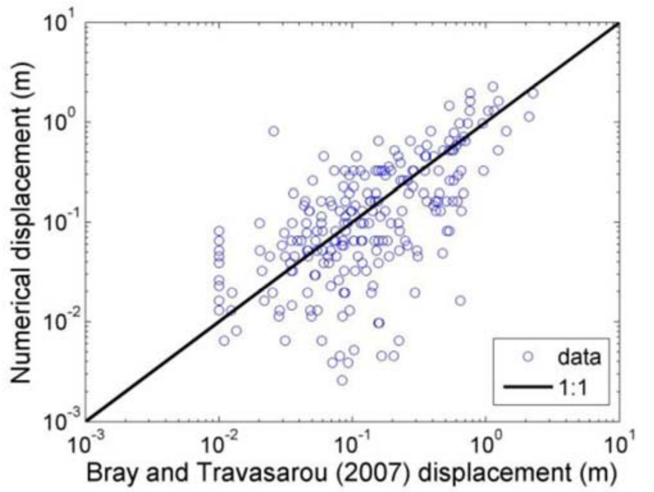

Figure 4. Numerically versus empirically calculated displacements (continued).

As a final remark, among the four models, Newmark's analytical approach presents the minimum dispersion. This trend may prove the superiority of the analytical over the simplified approaches as the latter are "models of models" that are subjected to additional assumptions associated with reducing the analytical approach into a simplified mathematical equation.

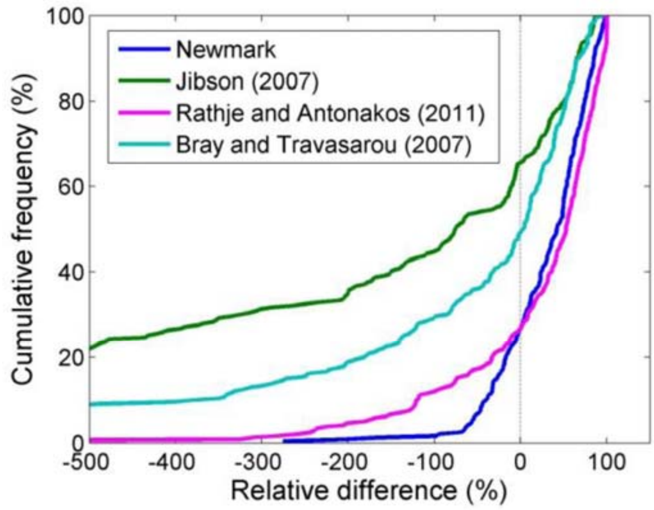

Figure 5. Cumulative distribution of the *Relative difference* (%) between numerical and empirical slope displacements for each of the empirical sliding block model.

2.2.3 Development of regression models using optimal scalar intensity measures

Uncertainty in the ground motion characterization is the greatest source of uncertainty in calculating earthquake seismic risk (Pitilakis 2014) and in the present cases the induced seismic slope displacements (Bray 2007). Thus, the selection of appropriate IMs is important to increase the accuracy of the predictive analytical relationships of seismic permanent displacement. The selection of the proposed IMs is also important to reduce the overall computation effort, as fewer ground motions are required to achieve the desired accuracy. This fact is the basic motivation to develop a new set of predicting expressions for co-seismic permanent slope displacements.

The optimal IM is identified through regression analyses correlating the numerical seismic slope displacements (D) and various IMs, namely PGA, PGV, I_a, T_m, $S_a(1.5T_s)$. As said before these are some of the most frequently used IMs in earthquake engineering practice representing different aspects of the ground motion characteristics (i.e. intensity, frequency content and duration). In particular, PGA characterizes the earthquake ground motion peak amplitude (amplitude/intensity), PGV the intensity and frequency content of the earthquake motion, I_a the intensity and implicitly the duration of the ground motion, Tm the earthquake frequency content and finally $S_a(1.5T_s)$ is related to both the ground motion intensity and the frequency characteristics of the sliding mass. It is noted that the ratio k_y/PGA is also used as an IM as it provides a direct assessment of whether the displacement will be greater than zero (i.e. for PGA>k_y, D>0 and 0 otherwise) (Saygili & Rathje 2008). It is also worth mentioning that the estimated IMs at the depth of the sliding surface estimated via the 1D dynamic analyses (Section 2.2.2), which account for the of site conditions (soil classes B, C and D according to EC8), are used in the regressions. Considering the fact that seismic motions are essentially recorded at the ground surface, IMs at the free-field ground surface are suggested in practice without any depth modification. This is in line with previous studies (e.g. Bray & Travasarou 2007; Rathje & Antonakos 2011) and as discussed in Bray &Travasarou (2007) is considered a relatively “conservative” hypothesis. In cases, however, where the IMs for soil conditions cannot be accurately estimated or for more generic applications, simplified relationships that yield the IMs for soil conditions (e.g. at the depth of the sliding surface) given the corresponding IMs at the rock outcrop may be proposed (see Fotopoulou & Pitilakis 2015).

IMs were rated based on two different criteria: *proficiency* (i.e. a composite measure of efficiency and practicality) (Padgett et al. 2007) and *sufficiency* (Luco & Cornell 2007). Proficiency serves as the primary factor in the selection process for an optimal IM while sufficiency is a secondary factor, which further supports the selection of appropriate IMs.

A power model is first used to describe the relationship between the seismic slope displacement D and the various IMs:

$$D=a\cdot IM^{b} \quad (1)$$

where a and b are coefficients defined by the regression. This can be rearranged to perform a linear regression of the logarithms of the IMs and the response quantity (seismic slope displacement) to establish a demand model of the following form:

$$In(D) = b\cdot ln(IM)+In(a)+\varepsilon\cdot\sigma \quad (2)$$

where D is the seismically induced slope displacement (in m), ε is the standard normal variant with zero mean and unit standard deviation. The dispersion term sigma (σ) represents the conditional standard deviation of the regression (in natural log units) and is a metric of the efficiency of the IM with respect to the demand parameter (seismic slope displacement). Lower σ values yields less dispersion about the estimated median in the results indicating a more efficient IM. The regression parameter b in Eq. 2 is a metric of the practicality of the IM. Practicality describes the dependence of the level of the slope displacement upon the level of the IM. When this parameter approaches zero the IM term contributes negligibly to the demand estimate and thus a lower b value implies a less practical IM (Padgett et al. 2007).

For an optimal IM selection, the term proficiency is introduced (Padgett et al. 2007), which measures the composite effect of efficiency and practicality. A more proficient IM is characterized by a lower modified dispersion ζ and is estimated as follows:

$$\zeta = sigma/b \quad (3)$$

Figure 6 presents representative correlations between the slope displacements and the PGV along with the curve fit using Eq. 2. Similar correlations have been performed for the other IMs.

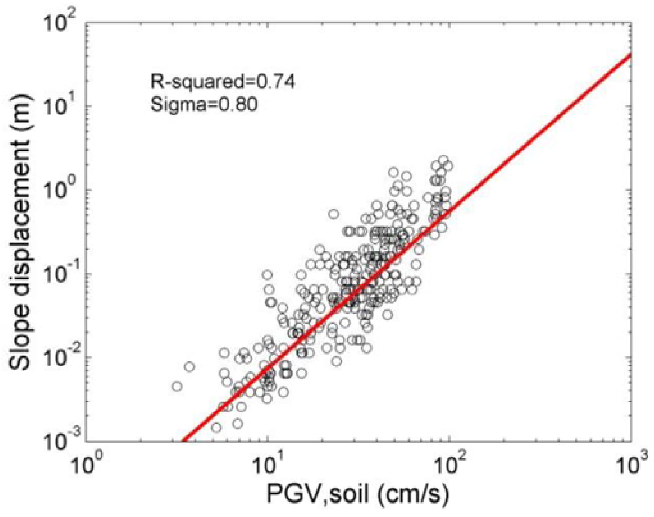

Figure 6. Regression of seismic slope displacement for quantifying the efficiency and practicality of PGV as IM.

Table 2 lists the parameters of the demand models from Eq. 2 as well as their proficiency. As shown in the table, PGV and I_a are the most efficient IMs whereas PGV is the most proficient one followed by PGA and k_y/PGA (shown in bold in Table 2). Thus, although I_a is an efficient IM, it is not practical (low b value) and therefore it should not be considered an optimal IM.

Table 2. Demand models and their efficiency, practicality and proficiency for the different considered IMs.

IM	ln(a)	b	sigma	ζ
PGA (g)	-0.428	2.127	0.93	**0.44**
PGV (cm/s)	-8.892	1.873	080	**0.43**
T_m (s)	-1.455	1.717	1.46	0.85
I_a (m/s)	-2.944	0.993	0.82	0.82
S_a ($1.5T_s$)	-1.716	1.588	1.21	0.76
k_y/PGA	-4.770	-2.165	1.01	**0.46**

A sufficient IM is conditionally statistically independent of ground motion characteristics, such as magnitude (M) and epicentral distance (R) (Luco & Cornell 2007). In this study, the sufficiency is evaluated by performing a regression analysis on the residuals, ε|IM, from the calculated seismic slope displacements relative to the ground motion characteristic, *M* or *R*. A small *p*-value for the linear regression of the residuals on *M* or *R* is indicative of an insufficient IM, in which the coefficient of the regression estimate is statistically significant. The cutoff for an insufficient IM is assumed to be a *p*-value of 0.10. In Figure 7 representative plots examining the sufficiency of PGA with respect to magnitude and epicentral distance respectively are shown.

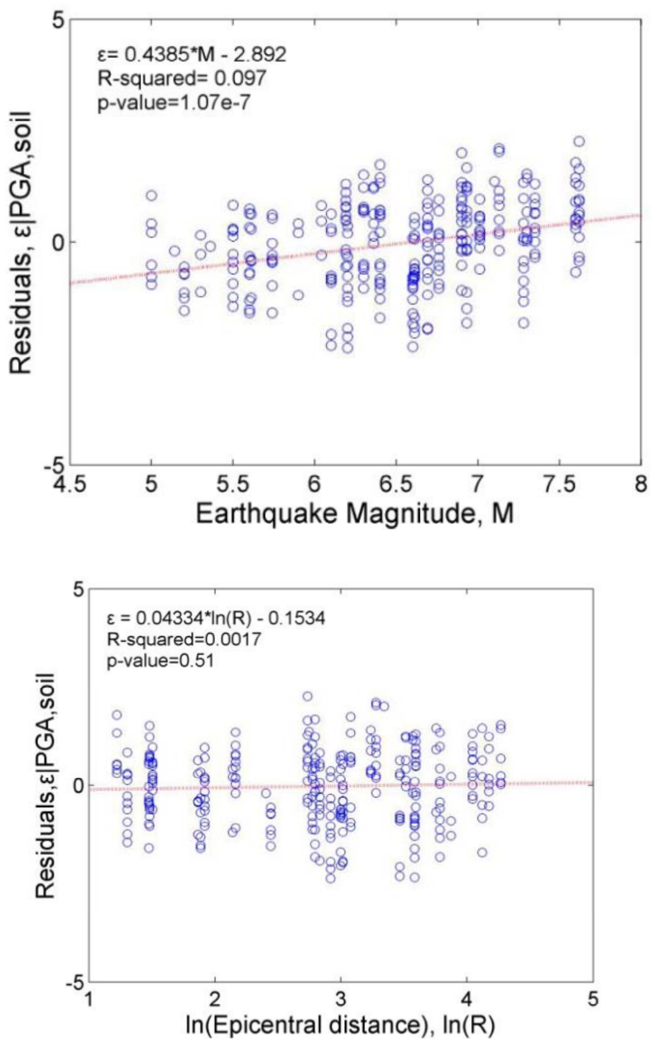

Figure 7. Sufficiency of PGA as IM by examining the conditional statistical independence from magnitude (top) and epicentral distance (bottom).

Similar plots have been constructed for the other IMs. For PGA, PGV, $S_a(1.5T_s)$ and k_y/PGA, the mean residuals do not vary with distance (p-value>0.10), but they increase with increasing magnitude (p-value~0). On the other hand, I_a is statistically independent from magnitude (p-value=0.70) but it depends on epicentral distance (p-value<0.10) while T_m is dependent both on magnitude and epicentral distance (p-value~0). These trends indicate that none of the selected IMs satisfies the sufficiency criterion with respect to magnitude and epicentral distance in a rigorous way.

However, as shown by Shome (1999), the error in the prediction of the demand parameter (seismic slope displacement in our case) using a hazard decoupling assumption with an insufficient IM can be as small as ±10%. Considering this remark, scalar IMs are proposed to assess slope displacement based only on the proficiency criterion. In particular, the most proficient IMs, i.e. PGV, PGA and k_y/PGA, are suggested to correlate to slope displacements using the functional form described in Eq. 2.

The yield coefficient k_y, which represents the overall dynamic resistance of the slope, has been always used in sliding block procedures due to its important effect on seismically induced slope displacement (Bray 2007). In this respect, k_y is also added to the regression equation where a linear dependence of the residuals for the considered IMs on k_y is taken into account:

$$\ln(D)=b\cdot\ln(IM)+\ln(a)+c\cdot k_y+\varepsilon\cdot\sigma \quad (4)$$

The proposed regression parameters for the most proficient IMs, i.e. PGV, PGA and k_y/PGA are presented in Table 3. It is seen that the models display significantly less variability when considering k_y term in the regression.

Table 3. Demand models for the most proficient IMs when considering k_y in the regression equation.

IM	ln(a)	b	c	sigma
PGA (g)	0.529	2.127	-6.583	0.80
PGV (cm/s)	-8.028	1.873	-5.964	0.68
k_y/PGA	-5.965	-2.165	7.844	0.82

Finally, taking into account the dependence of the residuals for almost all considered IMs (i.e. PGV, PGA, k_y/PGA, T_m and $S_a(1.5T_s)$) on magnitude, magnitude term is also added to the regression equation to eliminate bias due to magnitude:

$$\ln(D)=b\cdot\ln(IM)+\ln(a)+ c\cdot k_y +d\cdot M+\varepsilon\cdot\sigma \quad (5)$$

A linear dependence of the residuals for the IMs on magnitude is considered as shown in Eq. 5. It is worth noting that the inclusion of magnitude term in Eq. 4 captures in part the influence of the duration of the seismic motion in the seismically induced slope displacement estimation. The proposed regression parameters for the most proficient IMs, i.e. PGV, PGA and k_y/PGA, when considering also the magnitude dependence are presented in Table 4. As shown in the table, the efficiency of the demand models is further improved when considering the magnitude term.

Table 4. Demand models for the most proficient IMs when considering both the k_y and the magnitude term in the regression equation.

IM	ln(a)	b	c	d	sigma
PGA (g)	-2.965	2.127	-6.583	0.535	0.72
PGV (cm/s)	-9.891	1.873	-5.964	0.285	0.65
k_y/PGA	-10.246	-2.165	7.844	0.654	0.75

Based on the above considerations, these scalar models (Eq. 5 and Table 4) are recommended for use in engineering applications. The demand models that do not include the magnitude term (Eq. 4 and Table 3) could also be applied at projects where the inclusion of magnitude causes some complication.

2.2.4 Development of regression models using optimal vector intensity measures

The use of vector IMs enables the model to capture additional significant features of the ground motion (related to its amplitude, frequency content or duration), which affect the magnitude of the seismic slope displacement. Vector IMs were selected based on the proficiency (i.e. efficiency and practicality) of the scalar IMs, the correlation coefficient $\rho_{IMi,IMj}$ between them as well as the overall efficiency of the vector model. Correlation coefficients were estimated using the methodology outlined by Baker & Cornell (2006). IMs with smaller correlation coefficients were selected as a smaller value of $\rho_{IMi,IMj}$ indicates that the two IMs cover more complementary information about the ground motion parameters leading to a smaller standard deviation in the displacement prediction (Saygili & Rathje 2008). PGV is the first component of the vector as it is the most proficient IM. Table 5 presents correlation coefficients between PGV and the remaining IMs. It is seen that the combination of PGV and k_y/PGA yields the lowest correlation coefficient. The functional form used for the regression on a vector of IMs is described as:

$$\ln(D)= \ln(a)+ b\cdot\ln(IM_1)+ e\cdot\ln(IM_2) +\varepsilon\cdot\sigma \quad (6)$$

where D is the seismically induced slope displacement (in m), IM_1 is the peak ground velocity (in cm/sec), IM_2 is the second intensity measure and a, b , and e are regression coefficients. Equation 6 was selected based on the observation that the residuals of the regression on PGV had only a linear dependence on the logarithm of the remaining IMs when plotted against them.

Table 5. Correlation coefficients between PGV and the remaining IMs.

	$\rho_{IM1,IM2}$				
IM_1/IM_2	PGA	T_m	I_a	$S_a(1.5T_s)$	k_y/PGA
PGV	0.75	0.57	0.67	0.59	0.15

Table 6. Demand models and their associated efficiency for the different considered vector IMs.

IM1	IM2	ln(a)	b	e	sigma
PGV(cm/s)	k_y/PGA	-9.524	1.873	-0.634	**0.70**
PGV	T_m (s)	-9.250	1.873	-0.444	0.79
PGV	I_a (m/s)	-8.940	1.873	0.072	**0.80**
PGV	PGA (g)	-8.897	1.873	0.025	0.80
PGV	$S_a(1.5T_s)$(g)	-8.912	1.873	0.018	0.80
PGV	k_y/PGA	-9.524	1.873	-0.634	**0.70**

Table 6 presents the derived vector models along with their overall efficiency (defined by their sigma values). As shown in the table, among the considered vector IMs, PGV- I_a and PGV- k_y/PGA are the most efficient ones (shown in bold in Table 6). It is seen that the efficiency of the vector IMs is improved compared to the corresponding scalar IMs (lower sigma values) (see Table 2). However, it is up to the engineer to decide on a project basis whether this improvement in efficiency by the use of a vector IM offsets the complexities in the vector seismic hazard evaluation associated with the computation of the joint annual probability of occurrence of the pairs of ground motion parameters (Travasarou & Bray 2003).

The sufficiency criterion is addressed by considering the magnitude and distance dependence of the residuals for each pair of IMs. For all considered pairs of IMs, the mean residuals do not vary with distance (p-value≥0.10). However, only PGVk$_y$/PGA and PGV-I$_a$ pairs are statistically independent from magnitude (p-value≥0.10) and therefore only these IMs cover the sufficiency criterion. Thus the vectors IMs that may sufficiently predict seismic slope displacement are PGV-k$_y$/PGA and PGVI$_a$. However, PGV- k$_y$/PGA pair has a correlation coefficient 0.15 that is indicative of intensity parameters that provide considerable complementary information about the ground motion as opposed to PGV-I$_a$ pair that distinguishes a quite higher correlation coefficient (equal to 0.67) (see Table 5). In addition, PGV and k$_y$/PGA represent the most proficient scalar IMs; consequently the PGV- k$_y$/PGA pair is proposed as the most appropriate one to correlate to seismic slope displacements.

Finally, k$_y$ term is also incorporated in Eq. 6 considering its importance in seismic slope displacement estimation. Thus the functional form for the regression on a vector of IMs becomes:

$$\ln(D)= \ln(a)+ b\cdot\ln(IM1)+ e\cdot\ln(IM2) + c\cdot k_y +\varepsilon\cdot\sigma \quad (7)$$

Table 7 presents the proposed regression parameters and the associated standard deviations of the vector IMs when k$_y$ is also considered in the models. It is seen that combination of PGV with I$_a$, PGA and k$_y$/PGA yields the most efficient vector models. From these vector models only PGV- I$_a$ and PGVk$_y$/PGA (shown in bold in Table 7) cover the sufficiency criterion and thus they are recommended for use. However, between the two vector models, PGV- k$_y$/PGA model should be preferred taking into account the increased proficiency of k$_y$/PGA compared to I$_a$. As in the scalar IMs, a considerable increase in efficiency is observed when k$_y$ term is added in the regression equation.

Table 7. Demand models and their associated efficiency for the different considered vector IMs when considering the k$_y$ term in the regression equation.

IM1	IM2	ln(a)	b	c	e	sigma
PGV(cm/s)	k$_y$/PGA	-8.36	1.87	-5.96	-0.35	**0.64**
PGV	T$_m$ (s)	-8.31	1.87	-5.96	-0.38	0.66
PGV	I$_a$ (m/s)	-8.06	1.87	-5.96	0.20	**0.61**
PGV	PGA (g)	-7.67	1.87	-5.96	0.33	0.64
PGV	S$_a$(1.5T$_s$)(g)	-7.91	1.87	-5.96	0.19	0.66
PGV	k$_y$/PGA	-8.36	1.87	-5.96	-0.35	**0.64**

2.2.5 Suggested scalar and vector predictive models

Based on the optimally selected scalar and vector IMs, equations 8 to 12 summarize the proposed scalar (Eq. 8-10) and vector (Eq. 11-12) predictive models for assessing the seismically induced slope displacement that are recommended for use in practice:

$$\ln(D)= -9.891+ 1.873\cdot\ln(PGV) - 5.964\cdot ky + 0.285\cdot M \pm \varepsilon\cdot 0.65 \quad (8)$$

$$\ln(D)= -2.965 + 2.127\cdot\ln(PGA) - 6.583\cdot ky + 0.535\cdot M \pm \varepsilon\cdot 0.72 \quad (9)$$

$$\ln(D)= -10.246 - 2.165\cdot\ln(k_y/PGA) + 7.844\cdot ky + 0.654\cdot M \pm \varepsilon\cdot 0.75 \quad (10)$$

$$\ln(D)= -8.076 + 1.873\cdot\ln(PGV) + 0.200\cdot\ln(I_a) - 5.964\cdot k_y \pm \varepsilon\cdot 0.61 \quad (11)$$

$$\ln(D)= -8.360 + 1.873\cdot\ln(PGV) - 0.347\cdot\ln(k_y/PGA) - 5.964\cdot k_y \pm \varepsilon\cdot 0.64 \quad (12)$$

where D is in m, PGA in g, PGV in cm/s and I$_a$ in m/s.

The free field ground surface intensity parameters (i.e. PGA, PGV, I$_a$) estimated through a conventional seismic hazard analysis that account for site effects could be used in the above equations without any modification with depth. Otherwise, one could estimate the IMs for soil conditions (e.g. at the depth of the sliding surface) given the corresponding IMs at the rock outcrop using the simplified expressions proposed in this study (see Fotopoulou & Pitilakis 2015 for details).

2.2.6 Example application

A typical application of the proposed scalar and vector regression models is presented to exemplify the proposed analytical expressions to assess the coseismic slope displacement providing also a comparison with Newmark-type methods. A natural step-like slope is considered with a yield coefficient k$_y$ equal to 0.1. The elastic fundamental period of the slide mass T$_s$ is estimated as 0.2s assuming a maximum depth of the sliding mass and an average V$_s$ equal to 15m and 300m/s respectively. The scenario earthquake is represented by a real ground motion derived from the SHARE database (Seismic Hazard Harmonization in Europe, www.share-eu.org) that is recorded on soil conditions (soil class C according to EC8) with moment magnitude M$_w$=6.93 and epicentral distance R=30 km.

Table 8 presents the main characteristics of the recorded ground motion while Table 9 depicts the estimated ground motion intensity parameters that will be used for the given example application. The median (or mean) and the median (or mean) ±1 σ predictions for the proposed scalar and vector models (see Section 2.2.5) as well as the corresponding predictions of the empirical Newmark-type models applied in this study are presented in Table 10 for the given earthquake event and slope properties.

Table 8. Characteristics of the selected scenario earthquake.

Earthquake	M$_w$	R (km)	Preferred FS	Vs$_{,30}$ (m/s)	Database Code
Loma Prieta 1989, USA	6.93	30	Reverse-Oblique	302	NGA_766

Table 9. Estimated ground motion intensity parameters of the given earthquake event.

PGA (g)	PGV(cm/s)	T$_m$ (s)	I$_a$ (m/s)	S$_a$(1.5T$_s$) (g)
0.363	32.87	0.526	1.197	0.715

Table 10. Seismic slope displacement predictions for the proposed scalar and vector models and the Newmark-type empirical methods for the given slope properties and earthquake event.

		Seismic slope displacement (m)		
		Median (or mean)	Median (or mean) + 1σ	Median (or mean) -1σ
Scalar models	PGV- M	0.140	0.267	0.073
	PGA-M	0.126	0.259	0.061
	k$_y$/PGA-M	0.118	0.249	0.056
Vector models	PGV- I$_a$	0.123	0.226	0.067
	PGV-k$_y$/PGA	0.140	0.241	0.074
Newmark		0.088	-	-
Jibson 2007		0.355	0.657	0.192
Rathje & Antonakos 2011		0.148	0.240	0.091
Bray& Travasarou 2007		0.259	0.499	0.134

It is seen that the proposed models predict consistent displacement for the considered earthquake scenario and slope properties. The estimated median values vary from 0.118 to 0.140m, resulting at a maximum difference in the prediction on the order of 15%. In particular, the scalar k_y/PGA- M model predicts the smallest displacement (0.118m) while the largest one is predicted by both the scalar PGVM and the vector PGV- k_y/PGA models. Differences of this order are not important taking also into account the considerable aleatory variability associated to both the characteristics of the slope and the ground motion intensity parameters. As shown in the table, for the scalar predictive models the estimated median+1σ and median-1σ displacements are about two times and half the median value respectively. Considering that the vector models are shown to display smaller σ values, the estimated range of the median±1σ displacements is even more converged for the proposed two-parameter vector models.

A comparison between the slope displacements estimated by the models recommended for use in this study and the corresponding displacements predicted by the Newmark-type or empirical models is also performed (see Table 10). It is observed that Newmark analytical rigid block method predicts an average displacement that is 25-37% smaller than the median displacements estimated by the proposed new models, while the remaining simplified models overpredict the corresponding displacements. In particular, Jibson (2007), Rathje & Antonakos (2011) and Bray & Travasarou (2007) present respectively 150-200%, 6-25% and 85-120% larger displacements. These findings that are generally in line with the observations presented in Section 2.2.2 indicate the significant uncertainties (both aleatory and epistemic) associated with the modeling assumptions as well as with the selection of the intensity parameters and slope properties in the different approaches highlighting the need for a probabilistic assessment of the seismically induced slope displacements (e.g. Rathje et al. 2014).

3 VULNERABILITY ASSESSMENT OF RC BUILDINGS TO CO-SEISMIC SLOPE DISPLACEMENT

3.1 Vulnerability assessment method

The physical or structural vulnerability of a building is defined as the degree of loss, in terms of percentage of structural damage, to a given element or set of elements subjected to a landslide hazard (e.g. Corominas et al. 2014). In the present paper we deal with the seismically triggered landslides and in particular with the co-seismic slope ground movements in the absence of flow-type massive landslides or lateral spreading after liquefaction. The landslide hazard is expressed in terms of permanent ground displacements (PGD or D according to the previous chapter). While PGD is a deterministic quantity, the parameters used for its calculation are probabilistic quantities depending on the seismic hazard. So PGD is also of probabilistic nature.

The way we propose herein to evaluate the seismic vulnerability of buildings, and finally the risk, is inspired from the relevant and well-developed approach used in earthquake engineering. The difference is that while in earthquake engineering the vulnerability and the structural losses are due to the ground shaking, in our case the vulnerability will depend on the co-seismic permanent slope displacements The essential of the methodology has been developed in the framework of the EU research project called SAFELAND (http://www.safeland-fp7.eu) and has been recently published in a series of papers (e.g. Fotopoulou & Pitilakis 2013a; 2013b; Mavrouli et al. 2014).

According to the proposed methodology the key element is the construction of the so-called probabilistic fragility curves, which are describing the probability for a structure of a given typology of exceeding a certain limit state of the building given a measure of the landslide intensity, which in the present case is the PGD. Four damage limit states (LS1, LS2, LS3, LS4) are defined with respect to the building classification and its structural characteristics in terms of threshold values of building's material strain based on the work of Crowley et al. (2004), Bird et al. (2005); (2006), Negulescu & Foerster (2010) and proper engineering judgment. They describe the exceedance of minor, moderate, extensive and complete structural damage of the building. Different limit state values are adopted for buildings of different typology, e.g. masonry or RC, low-rise or high-rise, high code frame RC buildings etc. An extensive presentation of these issues may be found in Pitilakis et al. (2014). Figure 8 presents a typical set of fragility curves of a low rise RC building for the four damage states subjected to permanent ground displacements (PGD).

Once the fragility curves of any building type subjected to slope co-seismic displacements are available, a single vulnerability curve can be constructed (see Figure 9), which provides a unique damage or vulnerability index d_m for each level of PGD. It can be mathematically expressed as follows:

$$d_{mj} = \sum_{i=1}^{4} P_{ij} \cdot d_i \quad (13)$$

where d_{mj} is the damage index (taking values from 0: no damage to 1: complete damage) corresponding to landslide intensity level *j*, P_{ij} is the discrete damage probability for each damage state and d_i stands for the damage index at each of the four damage states (taken for this generic application as 0.25, 0.50, 0.75 and 1.0 for the LS_1, LS_2, LS_3 and LS_4 respectively).

The damage index d_m is a convenient measure to quantify the structural losses and finally to assess the risk at building or community level when properly aggregated. It may be quantified in cost terms as the ratio of cost of repair to cost of replacement taking values from 0: no damage (cost of repair equals 0) to 1: complete damage (cost of repair equals the cost of replacement).

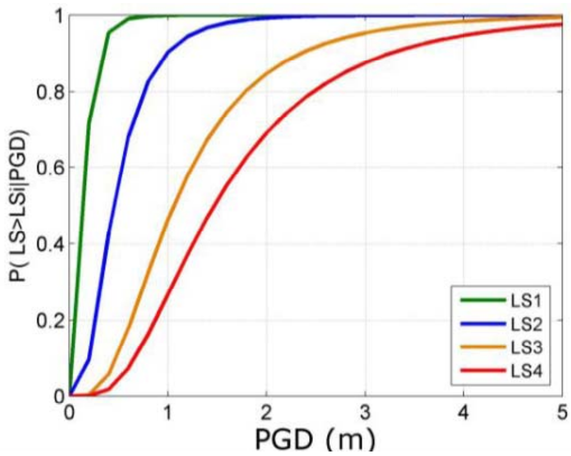

Figure 8. Typical set of fragility curves.

In the following paragraphs we will briefly present the methodology used to derive fragility curves for bay-single story RC buildings located next to the ridge of a potentially unstable slope. Contrary to earthquake engineering where the structure is subjected to ground shaking now it is subjected to forced differential displacement due to the earthquake-triggered landslide and subsequently to structural distress and damage. Figure 10 illustrates the parameters of the problem under study.

The method is principally based on a two-step numerical approach and adequate statistical analysis First, the total and differential permanent displacements are estimated considering the actual stiffness and weight of the building and its foundation, using a plane strain FLAC2D (Itasca

2011) finite difference, non-linear dynamic slope model. The same numerical tool has been used for the development of the analytical expressions of permanent coseismic slope displacements presented in previous paragraphs. The width and the height of the model are selected in a way that the effects of artificial wave reflections from the boundaries near the slope are sufficiently reduced. For the same purpose, free field and quiet boundaries are applied along the lateral boundaries and the bottom of the dynamic model respectively.

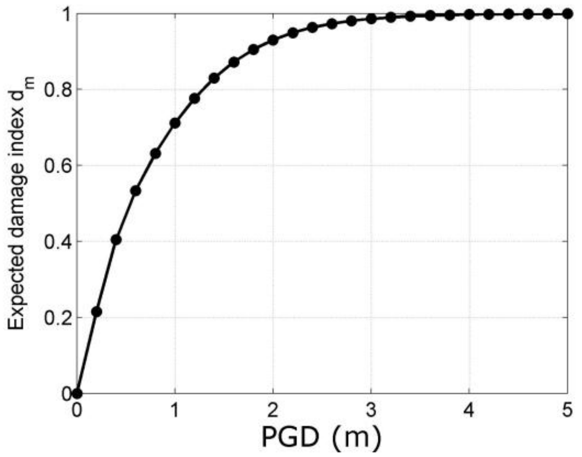

Figure 9. Vulnerability curve and vulnerability index (d_m).

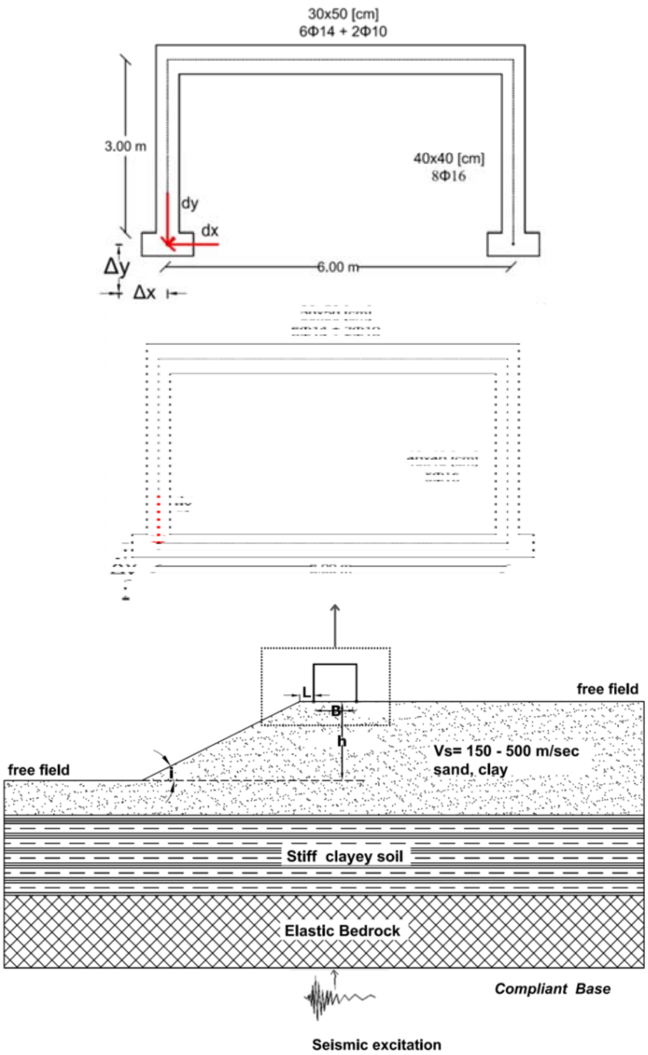

Figure 10. Idealized single bay-single storey RC frame building with flexible (left) and stiff (right) foundation system and displacement loading pattern considered for the non-linear quasi-static analysis.

The soil materials (sandy or clayey) are modeled using the same elastoplastic constitutive model used in Section 2.2.1 to estimate the seismic slope displacements. It is noticed that the sliding surface is not predefined but "emerges" naturally, following the elastoplastic constitutive law.

To illustrate the methodology an idealized structure, representative of typical RC frame buildings, is assumed to be located next to the slope's crest (Figure 10). Shallow foundation systems of different stiffness characteristics are considered: isolated footings and/or a uniform loaded continuous slab foundation. In the first case, the foundation is simulated with concentrated loads at the footings' links assuming no relative slip and/or separation between foundation and subsoil. In the second case, the foundation system is modeled as a deformable elastic beam connected to the soil elements' grid through appropriate interface elements that can approximate the potential Coulomb sliding and/or tensile separation of the beam.

The seismic input applied along the base of the model consists of a sufficient number of gradually increasing acceleration time histories recorded on rock outcrop (Fotopoulou & Pitilakis 2013a; 2013b). The output of the full dynamic analyses consists of the vectors of the permanent displacements at the level of the foundation system.

Then, non-linear static time history analyses of the building are performed to assess the building's response to the differential ground deformation computed in the previous step. The analyses are conducted using the finite element code Seismo-Struct (Seismosoft 2011) for progressively increasing levels of differential displacements provided by the computed dynamic stress strain analysis for increasing amplitudes of input acceleration time histories. The derived differential displacements at the foundation level are imposed quasi-statically at one of the RC building supports (footings).

The studied building is a low-rise RC bare frame structure with flexible or stiff foundation system designed with "low" or "high" seismic code prescriptions. Both local (beam-column effect) and global (large displacements/rotations effects) sources of geometric nonlinearity are automatically taken into account. Nonlinear constitutive models are used to simulate the behavior of RC materials since cracking and irreversible deformations are normally expected to govern the building's response. The "fiber approach" is used to represent the cross-section behaviour, where each fiber is associated with a uniaxial stress-strain relationship. More specifically, a uniaxial nonlinear constant confinement model considering a constant confining pressure throughout the entire stress-strain range is used for the concrete material (Mander et al. 1988) whereas a uniaxial bilinear stress-strain model with kinematic strain hardening is utilized for the reinforcement. Structural response data in terms of maximum material strain are then statistically correlated to the corresponding limit damage states and the landslide intensity parameters to estimate structure's performance and fragility.

The next step is the derivation of the fragility curves for the four damage states LS_1, LS_2, LS_3 and LS_4. A two-parameter lognormal distribution function is adopted to represent a fragility curve *F(IM)* for a predefined damage/limit state:

$$F(IM) = \Phi\left[\frac{1}{\beta} ln\left(\frac{IM}{IM_i}\right)\right] \quad (14)$$

where IM is the intensity measure, Φ[·] is the standard normal cumulative distribution function, IM_i is the median value of the specified intensity parameter at which the building reaches the limit state i, β is the standard deviation of the natural logarithm of the specified intensity parameter.

The landslide intensity may be expressed in terms of PGA at the seismic bedrock, which is the initial triggering force of the slow-moving slide. Alternatively, the permanent ground displacement (PGD) at the slope area (i.e. a product of PGA) may be used as an intensity parameter. The latter is generally better correlated to structural deformation and damage (Fotopoulou 2012) and it is used in the next. The proposed predictive relationships presented in Section 2.2 which correlate the numerically calculated seismically induced permanent slope displacements with optimal scalar and vectors IMs should be used for the direct estimation of the PGD used throughout this paper as IM.

Different procedures can be applied to estimate the log-normally distributed fragility parameters (median and log-standard deviation) given the simulated damage data. A purely statistical approach, i.e. the Maximum Likelihood Method (Shinozuka et al. 2000) is implemented in this study. A common log-standard deviation, which forces the fragility curves not to intersect, is assumed for all limit states. More information regarding the adopted optimization procedure is given in Fotopoulou & Pitilakis (2013b).

3.2 Derivation of fragility curves

In order to construct an abacus of fragility curves applicable to low-rise RC frames for various soil conditions and slope configurations, an extensive parametric investigation is performed based on the proposed method. The main parameters selected to vary are associated to (see Figure 10): the geometry of the finite slope (slope height h=20, 40 m, slope inclination i=15°, 30°, 45°), the soil properties of the slope material (soft to stiff clayey and sand soils corresponding to soil categories B, C and D of EC8 with Vs,30 values varying from 150m/s to 500m/s) as well as the relative position of the building with respect to the slope crest (L=3, 5 m). Six simplified – yet realistic– step-like slope configurations are considered. For each geometry, 4 different models are developed that vary on the soil conditions (sand, clay) of the surface layer and the relative location of the building to the slope crest (L=3, 5 m). It is noticed that the soil properties of the slope materials are consistent with the considered inclination angles to ensure static slope stability. Thus, it does not make any sense to analyze steep slopes with soft soil, as the slope would be already unstable in static conditions. It is also worth noting that only the cases that result to the highest susceptibility to landsliding are modeled. For instance, slopes with small inclination (i=15°) on stiff soil are not investigated as the resulting permanent deformation and consequently the building expected damage would be negligible and thus out of the scope of this study. More details regarding the assumed properties for the soil materials and the elastic bedrock can be found in Fotopoulou & Pitilakis (2013b).

The seismic excitation applied at the base of the model consists of a suite of 7 real acceleration time histories from different earthquakes worldwide recorded on rock outcropping conditions (see Fotopoulou & Pitilakis 2013b for details) and scaled at different levels of PGA i.e. 0.3g, 0.5g, 0.7g and 0.9g. Some additional analyses for lower levels of PGA (e.g. 0.1) were deemed necessary for certain models in order to obtain reliable results for all damage states.

The herein studied building (Figure 10; left) is a single bay-single storey RC bare frame structure with flexible foundation system. The building's height and length are 3.0 m and 6.0 m respectively. All columns and beams have rectangular cross sections (beam: 0.30x0.50 m, column: 0.40x0.40 m). The structure has been designed according to the provisions of the Greek Seismic Code (EAK 2000), for a design acceleration Ad = 0.36 g, and a behavior factor q = 3.5. The specified yield stress of reinforcing steel and the compressive strength of concrete are 400MPa and 20MPa respectively. The adopted dead and live loads (g = 1.3 kN/m^2 and q = 2 kN/m^2) are typical values for residential buildings. The longitudinal section reinforcement degree used is 1% for the columns and 0.75% for the beams.

Limit states (LS) are defined in terms of threshold values of steel and concrete material strain. The first limit state is specified as steel bar yielding whereas for the rest, mean values of post-yield limit strains for steel reinforcement and concrete material are suggested for both "low" and "high" code designed RC buildings, as shown in Table 11.

Table 11. Definition of limit states for "low" and "high" code design RC buildings.

LS	Limit strains –"low" code		Limit strains –"high" code	
	Steel strain(ε^s)	Concrete strain (ε_c)	Steel strain (ε^s)	Concrete strain (ε_c)
1	yielding	-	yielding	-
2	0.0125	0.0045	0.0125	0.005
3	0.025	0.006	0.04	0.010
4	0.045	-	0.06	-

The parametric analysis results to the construction of fragility curves as a function of the PGD at the slope area for the different investigated models. The log-normal parameters (median and log standard deviation) of the fragility relationships were obtained with the aid of Maximum Likelihood Method. The derived fragility curves can be used to assess the vulnerability of low-rise, "high-code" RC buildings on isolated footings subjected to seismically induced slope displacements for a variety of slope configurations and site conditions. Similar curves, generally associated with a more rapid transition from slight damage to collapse could be derived for "low-code" RC frame structures.

Figures 11 to 14 illustrate some representative results of fragility curves using PGD as IM. In particular Figure 11 presents the fragility curves for extensive damages (LS$_3$) for a 20m high sandy slope with three different inclinations (15°, 30° and 45°). Figure 12 presents the fragility curves for the four damage states when the building is located at the ridge of a sandy slope (with inclination of 30°) of different heights (20m and 40m). Figure 13 presents the differences between sandy and clayey slopes with an inclination of 30° and a height of 20m. Finally Figures 14a and 14b illustrate the fragility curves for the four damage states according to the distance of the building from the crest of the slope (sandy or clayey with a height of 20m and an inclination of 30°).

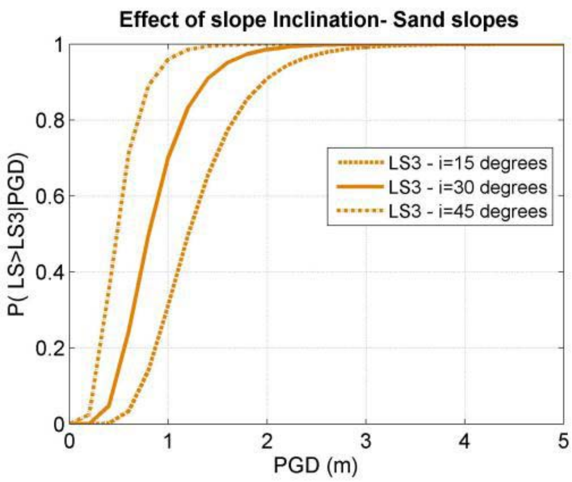

Figure 11. Fragility curves for extensive damage as a function of PGD when varying slope inclination for sand slope soil material.

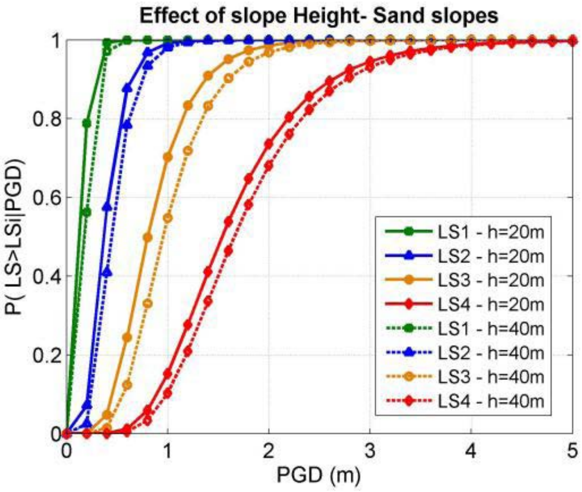

Figure 12. Fragility curves as a function of PGD when varying slope height (h= 20, 40m) for 30° inclined sand slopes.

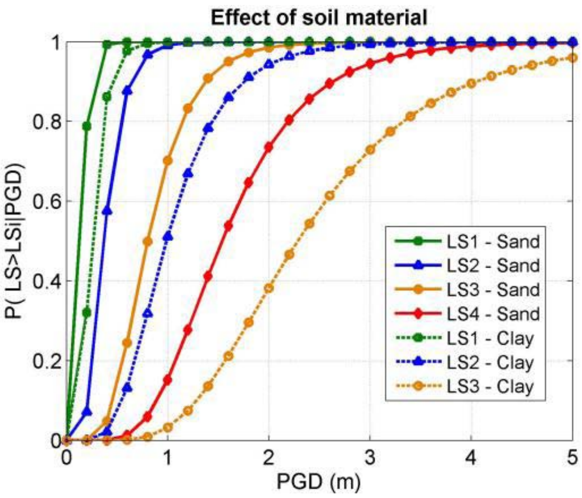

Figure 13. Fragility curves as a function and PGD when varying the slope soil properties (sand, clay) for 30° inclined slopes.

From these representative examples it is observed that the structure's vulnerability may vary significantly with respect to the various considered features. It is shown that, as it was expected, the slope inclination plays a fundamental role in the fragility analysis of the building standing next to the slope's crest. However, it should be regarded in conjunction to the slope soil properties to obtain meaningful conclusions. Thus, for the sand slope, the building would suffer more damage as the slope inclination increases. On the contrary, for the clayey slope, the building is expected to sustain less structural damage when standing on the 45° inclined slope compared to the gentler ones, due to the stiff cohesive soil conditions assumed for the steep slope configuration.

The soil material is certainly a significant parameter in assessing building's vulnerability standing near the crest of a potentially precarious slope. Slopes consisting of clay material generally demonstrate better performance compared to sands when subjected to differential permanent ground displacements, resulting to lower vulnerability levels for the building. This is largely due to the inherent cohesive behavior of clay soil material that is associated to the formation of larger and deeper sliding surfaces. Thus, the considered one-bay building located at a close distance (i.e. 3m) from the slope's crest would be practically within the sliding mass and therefore it is primarily expected to move uniformly with the landslide mass, rather than to distort differentially. The above observation is more noticeable as the slope inclination increases, i.e. for the stiffer clayey soil materials.

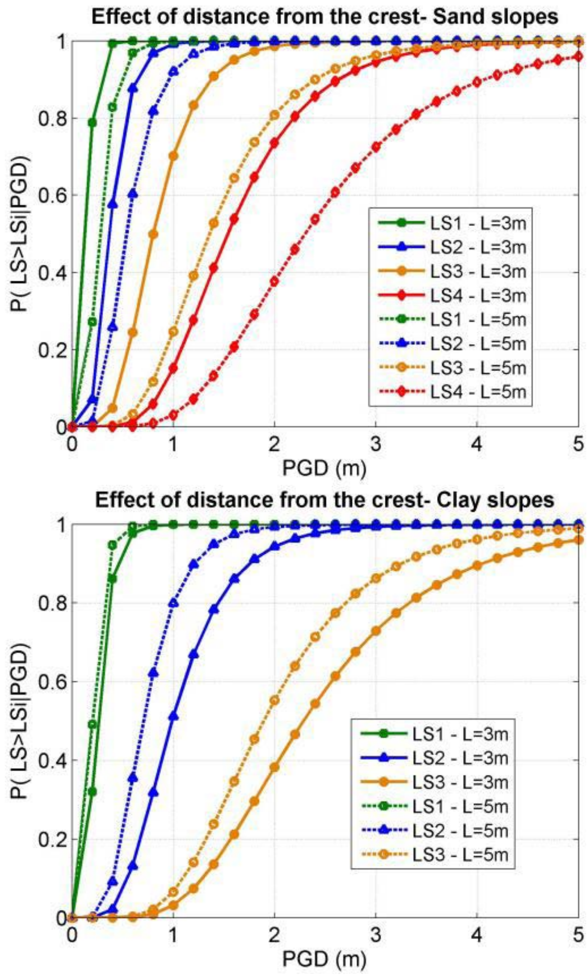

Figure 14. Fragility curves as a function of PGD for sand (top) and clayey (bottom) slopes when varying the distance from the crest (L= 3, 5m).

The slope height can moderately affect the structure's fragility. However, apart from some exceptions, lower vulnerability values of the building were observed with increased slope heights. A plausible explanation of the latter is that in the case of higher slopes the mobilized sliding mass is larger and thus it affects more the building located close to the crest in terms of total displacements, which are larger, while the differential displacement demand on the building, which really affects the damages, is reduced.

The distance of the building from the crest of the slope may also considerably influence its vulnerability to the permanent slope displacement. For sand slopes, the building is expected to suffer less damage as the distance from the crest increases. On the contrary, for the clayey slopes, the more distant building from the crest would be more vulnerable. This differentiation lies again on the nature of the slope soil materials involved, which are associated to the formation of sliding surfaces that may vary for very small and shallow for sands brittle slopes to large and deep for clayey deformable slopes. Thus, the assumed one-bay building standing at 3m from the crest of the clayey slope is basically within the landslide mass and moves rather uniformly as a rigid body whereas for increasing distances from the crest (5m) the building shifts (partially) outside the landslide mass and therefore it exhibits higher differential (rather than uniform) ground displacements and hence more structural damage. On the other hand, the building located at the closest distance from the crest (i.e. 3m) of the sand slope is outside the landslide mass and consequently it is subjected to extensive differential deformation demand that is gradually decayed as the distance from the crest increases.

3.3 Generic fragility curves

Seven sets of fragility curves in terms of PGD are proposed herein that could be used for engineering applications based on the main features that proved to be the most influential in assessing the vulnerability of the building to the differential permanent deformation due to the landslide hazard. These are principally the slope inclination and the soil material of the slope, which are highly correlated. The slope height is also proved to be a significant contributor to the building's fragility for the steep sand slope configurations. Thus, for the 45° inclined sand slopes fragility curves are also differentiated with respect to the considered slope height (h=20, 40 m). It is noted that the proposed curves have been constructed considering the most adverse position of the building with respect to the landslide zone that was found to be different for sand and clay slopes. It is also important to note that the curves presented herein refer to "high-code", adequately confined RC frame structures. Table 12 presents the median and the dispersions of the suggested curves. As already shown, the building founded close to the crest of sand slopes is expected to demonstrate a greater damaging potential than the respective clayey ones. The corresponding fragility curves referring to sand slopes are generally shifted to the left compared to clays and they are associated with a more rapid transition from slight to complete damage limits. These differences are becoming more pronounced as the slope inclination increases. The dispersion of the suggested curves is found to vary from 0.40 to 0.50. Larger β values are expected for the 45° slope configurations and for clayey soil materials.

Table 12. Parameters of the proposed fragility functions in terms PGD.

Perametric models	Median PGD (m)				Dispersion β
	LS1	LS2	LS3	LS4	
sand_i30	0.15	0.39	0.87	1.64	0.43
clay_i30	0.22	0.67	1.70	3.43	0.43
sand_i15	0.24	0.60	1.29	2.19	0.40
clay_i15	0.28	0.94	2.31	-	0.43
sand_i45_h20	0.09	0.18	0.47	0.91	0.43
sand_i45_h40	0.04	0.16	0.45	0.67	0.50
clay_i45	0.77	1.72	-	-	0.47

4 ILLUSTRATIVE EXAMPLE

An illustrative application of the proposed vulnerability model and of the derived fragility functions is presented herein. A 30° inclined sand slope is considered with a yield coefficient k_y equal to 0.1. A low-rise RC frame building with flexible foundations standing next to the slope's crown (i.e. 3m) is considered impacted by the seismically induced slope displacements due to the landslide hazard. Based on the proposed generic fragility curves (presented in Section 3.3), Figure 15 presents the appropriate set of fragility curves for the given structure, soil conditions and slope configuration while Figure 16 shows the corresponding vulnerability curve.

We consider the same scenario earthquake as in Section 2.2.6 represented by a real ground motion derived from the SHARE database. The main characteristics of the recorded ground motion and the estimated ground motion intensity parameters have been presented in Tables 8 and 9 respectively while the median ±1 σ predictions for the proposed scalar and vector models have been depicted in Table 10 for the considered earthquake scenario and slope properties. As shown in the table, the estimated median slope displacement values vary from 0.118 to 0.140m for the different proposed simplified expressions. Thus, for the maximum calculated level of PGD (i.e. 0.14m), the probability of exceeding LS_1 is estimated as 0.4 (see Figure 14) whereas the expected damage index d_m is calculated as 0.1 (see Figure 15). Hence, for the estimated level of PGD, rather slight damages are expected for the building.

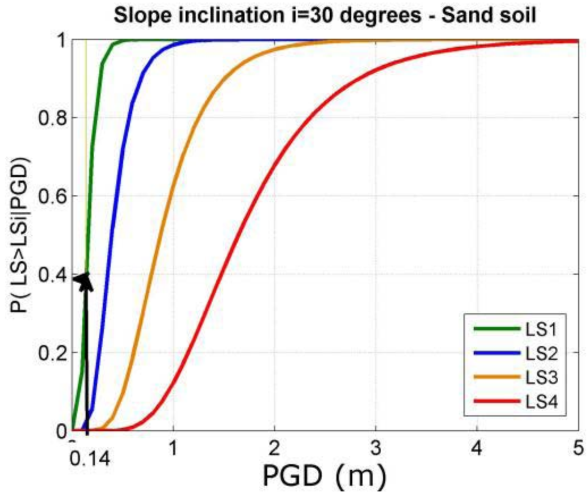

Figure 15. Fragility curves as a function of PGD for the given slope configuration and soil properties.

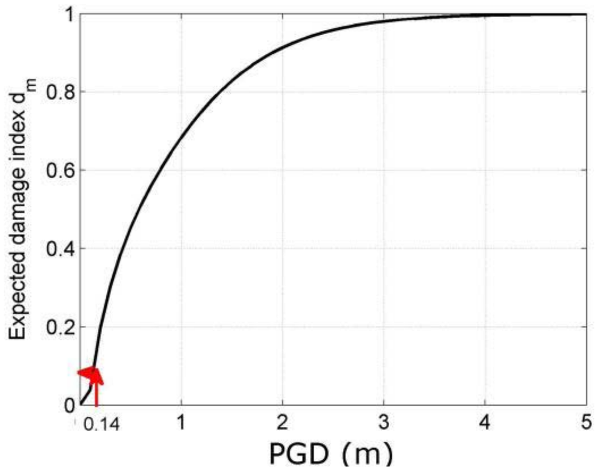

Figure 16. Vulnerability curve as a function of PGD for the given slope configuration and soil properties.

5 CONCLUSIONS

A coherent approach is presented to evaluate the vulnerability of buildings founded close to the crest of precarious landslide slopes after a strong earthquake.

In the first part a set of new predictive models and analytical expressions for assessing the coseismic displacements of slopes is presented and compared with existing empirical models generally referred as Newmark-type models. The new analytical expressions are based on a comprehensive set of numerical analyses of representative slope geometries and soil conditions. Advance statistics of the numerous results of the numerical computations, allowed the derivation of the analytical predictive expressions of co-seismic slope displacements to be used in earthquake engineering practice. The proposed expressions relate the co-seismic slope displacement with the best-correlated scalar and vector intensity parameters describing seismic hazard and site effects.

In the second part of the paper an analytical method for assessing the vulnerability of low-rise RC buildings subjected to seismically induced slope displacements is shortly described. Generic probabilistic fragility functions were proposed based on the features that have proved to affect more drastically the vulnerability of the building, i.e. slope inclination and height as well as soil material of the slope. The proposed fragility curves can be applied to evaluate the physical (structural) vulnerability of low-rise RC buildings subjected to earthquake induced slope displacements. The analytical expressions proposed in the first part of the paper for the co-seismic slope displacements (PGD or D) can be used as IM. The methodology can be extended to any type of building. An example given at the end illustrates the whole approach.

REFERENCES

Ambraseys, N.N. & Menu, J.M. 1988. Earthquake-induced ground displacements, *Journal of Earthquake Eng*ineering **16**, 985–1006.

Baker, J.W. & Cornell, C.A. 2006. Correlation of Response Spectral Values of Multicomponent Ground Motions, *Bulletin of the Seismological Society of America* **96**(1), 215-227.

Bird, J.F., Bommer, J.J., Crowley, H. & Pinho, R. 2006. Modelling liquefaction-induced building damage in earthquake loss estimation, *Soil dynamics and Earthquake Engineering* **26**, 15-30.

Bird, J.F., Crowley, H., Pinho, R. & Bommer, J.J. 2005. Assessment of building response to liquefaction induced differential ground deformation, *Bul of the New Zealand Society for Earthquake Engineering* **38**, 215-234.

Bray, J.D. & Rathje, E.R. 1998. Earthquake-induced displacements of solid-waste landfills. *Journal of Geotechnical and Geoenvironmental Engineering* ASCE **124**(3), 242–253.

Bray, J.D. & Travasarou, T. 2007. Simplified procedure for estimating earthquake-induced deviatoric slope displacements, *Journal of Geotechnical and Geoenvironmental Engineering* ASCE **133**(4), 381-392.

Bray, J.D. 2007. *Simplified seismic slope displacement procedures. Earthquake Geotechnical Engineering*. K. D. Pitilakis, Editor, 2007 Springer.

Corominas, J., Van Westen, C., Frattini, P., Cascini, L., Malet, J.-P., Fotopoulou, S., Catani, F., Van Den Eeckhaut, M., Mavrouli, O., Agliardi, F., Pitilakis, K., Winter, M. G., Pastor, M., Ferlisi, S., Tofani, V., Hervás, J. & Smith, J. T. 2014. Recommendations for the quantitative assessment of landslide risk, *Bull Eng Geol Environ* **73**, 209–263.

Crowley, H., Pinho, R. & Bommer, J.J. 2004. A probabilistic displacement-based vulnerability assessment procedure for earthquake loss estimation, *Bulletin of Earthquake Engineering* **2**, 173-219.

Douglas, J., Seyedi, D., Ulrich, T., Modaressi, H., Foerster, E., Pitilakis, K., Pitilakis, D., Karatzetzou, A., Gazetas, G., Garini, E. & Loli, M. 2015. Evaluation of seismic hazard for the assessment of historical elements at risk: description of input and selection of intensity measures, *Bulletin of Earthquake Engineering* **13**(1), 49-65.

EAK2000, Greek Seismic Code, Organization of Seismic Planning and Protection, 2000.

Fotopoulou, S. 2012. *Seismic vulnerability of reinforced concrete buildings in sliding slopes*, PhD thesis, Dept. of Civil Engineering, Aristotle University of Thessaloniki, Greece.

Fotopoulou, S. & Pitilakis, K. 2013a. Vulnerability assessment of reinforced concrete buildings subjected to seismically triggered slow-moving earth slides, *Landslides* **10**(5), pp 563-582.

Fotopoulou S., Pitilakis K. 2013b. Fragility curves for reinforced concrete buildings to seismically triggered slow-moving slides, *Soil Dynamics and Earthquake Engineering* **48**, 143–161.

Fotopoulou, S. & Pitilakis, K. 2015. Predictive relationships for seismically induced slope displacements using numerical analysis results, *Bulletin of Earthquake Engineering* (under review).

Garini, E., Makris, N. & Gazetas, G. 2014. Elastic and inelastic systems under near-fault seismic shaking: acceleration records versus optimally-fitted wavelets, *Bulletin of Earthquake Engineering,* DOI 10.1007/s10518-014-9631-z.

Itasca Consulting Group 2011. Inc. FLAC (Fast Lagrangian Analysis of Continua), ver. 7.0. Itasca Consulting Group, Inc., Minneapolis.

Jibson, R.W. 2007. Regression models for estimating co seismic landslide displacement. *Engineering Geology* **91**, 209–218.

Jibson, R.W. 2011. Methods for assessing the stability of slopes during earthquakes: A retrospective. *Engineering Geology* **122**(1-1):43-50

Lin, J.S. & Whitman, R. 1986. Earthquake induced displacements of sliding blocks, *Journal of Geotechnical Engineering* **112**(1), 44–59.

Luco, N. & Cornell, A.C. 2007. Structure-Specific Scalar Intensity Measures for Near-Source and Ordinary Earthquake Ground Motions, *Earthquake Spectra* **23**(2), 357–392.

Makdisi F. & Seed H. 1978. Simplified procedure for estimating dam and embankment earthquake induced deformations, *Journal of Geotechnical Engineering* **104**(7), 849–867.

Mander, J.B., Priestley, M.J.N. & Park, R. 1988. Theoretical stress-strain model for confined concrete, *Journal of Structural Engineering* **114**, 1804-1826.

Marano, K.D., Wald, D.J. & Allen, T.I. 2010. Global earthquake casualties due to secondary effects: a quantitative analysis for improving rapid loss analyses, *Nat Hazards* **52**, 319–328.

Mavrouli, O., Fotopoulou, S., Pitilakis, K., Zuccaro, G., Corominas, J., Santo, A., Cacace, F., De Gregorio, D., Di Crescenzo, G., Foerster, E. & Ulrich, T. 2014. Vulnerability assessment for reinforced concrete buildings exposed to landslides, *Bull Eng Geol Environ* **73**, 265–289.

Negulescu, C. & Foerster, E., Parametric studies and quantitative assessment of the vulnerability of a RC frame building exposed to differential settlements, N*atural Hazards and Earth System Sciences* **10**, 1781-1792.

Newmark, N.M. 1965. Effects of earthquakes on dams and embankments, *Geotechnique* **15** (2):139–159.

Padgett, J.E., Nielson, B.G. & DesRoches, R. 2008. Selection of optimal intensity measures in probabilistic seismic demand models of highway bridge portfolios, *Earthquake Engineering and Structural Dynamics* **37**, 711–725.

Pitilakis, K. 2014. Keynote lecture: Earthquake risk assessment: Certitudes, fallacies, uncertainties and the quest for soundness, *Second European Conference on Earthquake Engineering and Seismology*, Istanbul.

Pitilakis, K., Crowley, H. & Kaynia, A. (Eds) 2014. SYNER-G: Typology Definition and Fragility Functions for Physical Elements at Seismic Risk, Series: Geotechnical, Geological and

Earthquake Engineering, Vol. 27, Springer, ISBN 978-94-007-7872-6.

Rathje, E.M. & Antonakos, G. 2011. A unified model for predicting earthquake-induced sliding displacements of rigid and flexible slopes, *Engineering Geology* **122**(1-2), 51-60.

Rathje, E.M. & Bray, J.D. 2000. Nonlinear coupled seismic sliding analysis of earth structures, *Journal of Geotechnical and Geoenvironmental Engineering* ASCE **126**(11), 1002–1014.

Rathje, E.M., Wang, Y., Stafford, P., Antonakos, G. & Saygili, G. 2014. Probabilistic assessment of the seismic performance of earth slopes, *Bulletin of Earthquake Engineering* **12**, 1071–1090.

Sarma, S.K. 1975 Stability analysis of embankments and slopes, *Geotechnique* **25**(4): 743-761.

Saygili, G. & Rathje, E.M. 2008. Empirical Predictive Models for Earthquake-Induced Sliding Displacements of Slopes, *Journal of Geotechnical and Geoenvironmental Engineering* ASCE **134**(6), 790-803.

SeismoSoft, SeismoStruct, 2011. *A computer program for static and dynamic nonlinear analysis of framed structures*, Available from URL: www.seismosoft.com.

Shinozuka, M., Feng, M.Q., Lee, J. & Naganuma, T. Statistical analysis of fragility curves, *J. Eng. Mech.*-ASCE **126**, 1224–1231.

Shome, N. 1999. *Probabilistic seismic demand analysis of nonlinear structures*, Ph.D Thesis, Stanford University.

Strenk, P.M. & Wartman, J. 2013. Influence of Ground Motion Variability on Seismic Displacement Uncertainty. *Proceedings of the 18th International Conference on Soil Mechanics and Geotechnical Engineering*, Paris 2013.

Travasarou, T. & Bray, J.D. 2003. Optimal ground motion intensity measures for assessment of seismic slope displacements. *2003 Pacific Conf. on Earthquake Engineering*, Christchurch, New Zealand.

Travasarou, T. 2003. *Optimal ground motion intensity measures for probabilistic assessment of seismic slope displacements*, Ph.D. Dissertation, U.C. Berkeley.

Watson-Lamprey, J., Abrahamson, N. 2006. Selection of ground motion time series and limits on scaling, *Soil Dyn. Earthquake Eng.* **26**(5), 477–482.

Wen, B., Wang, S., Wang, E. & Zhang, J. 2004. Characteristics of rapid giant landslides in China, *Landslides* **1**(4), 247-261.

Yegian, M., Marciano, E. & Ghahraman, V. 1991. Seismic risk analysis for earth dams. *J. Geotech. Engrg*. **117**(1), 18–34.

Yin, Y., Wang, F. & Sun, P. 2009. Landslide hazards triggered by the 2008 Wenchuan earthquake, Sichuan, China. *Landslides* **6**(2), 139-152.

Το άρθρο αυτό παρουσιάστηκε ως προσκεκλημένη ομιλία του πρώτου εκ των συγγραφέων στο συνέδριο.

ΠΡΟΣΕΧΕΙΣ ΓΕΩΤΕΧΝΙΚΕΣ ΕΚΔΗΛΩΣΕΙΣ

Για τις παλαιότερες καταχωρήσεις περισσότερες πληροφορίες μπορούν να αναζητηθούν στα προηγούμενα τεύχη του «περιοδικού» και στις παρατιθέμενες ιστοσελίδες.

3rd ICTG – 3rd International Conference on Transportation Geotechnics 4 - 7 September 2016, Guimaraes, Portugal, www.civil.uminho.pt/3rd-ICTG2016

IAS'5 5th International Conference on Geotechnical and Geophysical Site Characterisation, 5-9 September 2016, Gold Coast, Queensland, Australia, http://www.isc5.com.au

Urban Underground Space & Tunneling Asia Summit 2016, September 6-9, 2016, Singapore, www.equip-global.com/urban-underground-space-and-tunnelling-asia-summit-2016

The World Multidisciplinary Earth Sciences Symposium– WMESS 2016, 5-9 September 2016, Prague, Czech Republic www.mess-earth.org

3rd European Conference on Unsaturated Soils E-UNSAT 2016, 12-14 September 2016, Paris, France, http://eunsat2016.sciencesconf.org

ACCUUS 2016 15th World Conference Underground Urbanisation as a Prerequisite for Sustainable Development, September 12-15, 2016, http://acuus2016.com

SAHC 2016 - 10th international Conference on Structural Analysis of Historical Constructions 13-15 September 2016, Leuven, Belgium, www.sahc2016.be

Hydropower Development Europe 2016 - Flexible hydropower and pump storage generation for a safe renewable electricity system, 14 – 15 September 2016, Lyon, France, http://www.wplgroup.com/aci/event/hydropower-development-europe-2016

13 Baltic States Geotechnical Conference Historical Experiences and Challenges of Geotechnical Problems in Baltic Sea Region, 15 - 17 September 2016, Vilnius, Lithuania, http://www.13bsgc.lt

Dam Surveillance Practice - 3rd Experts Seminar, 18 - 23 Sep 2016, Landeck, Tyrol, Austria, www.atcold.at/de/home-1/41-2016-veranstaltungen/155-dam-surveillance-practice-2016

ACE 2016 12th International Congress on Advances in Civil Engineering, 21-23 September 2016, Istanbul, Turkey, http://www.ace2016.org

International Geotechnical Engineering Conference on Sustainability in Geotechnical Engineering - Practices and Related Urban Issues, 23-24 September 2016, Powai, Mumbai, India, www.igsmumbaichapter.in

EuroGeo 6 – European Regional Conference on Geosynthetics, 25 – 29 Sep 2016, Istanbul, Turkey, www.eurogeo6.org

8th Nordic Grouting Symposium State of the art – Future Development, 26-27 September 2016, Oslo, Norway, http://nordicgrouting.com

SOFT SOILS 2016 - International Conference on Problematic Soils and Ground Improvement September 26-28th, 2016, Bandung, Indonesia www.softsoils2016.org

5th International Scientific Conference on Industrial and Hazardous Waste Management, 27 - 30 September 2016, Chania, Crete, Greece, http://hwm-conferences.tuc.gr

Basements and Underground Structures 2016, 5-6 October 2016, London, United Kingdom, https://basements.geplus.co.uk

2nd International Specialized Conference on Soft Rocks – ISRM 2016 Understanding and interpreting the engineering behavior of Soft Rocks, 6-7 October 2016, Cartagena, Colombia, www.scg.org.co/?p=1634

GEO-EXPO 2016

Scientific-Expert Conference
Geotechnics, Ecological Engineering
And Sustainable Development
October 7 - 8, 2016, Banja Luka, Bosnia and Herzegovina
www.geotehnika.ba/en/Home.php

The Geotechnical Society of Bosnia and Herzegovina organizes annual scientific and expert conference GEO-EXPO 2016 in Banja Luka on October 7 - 8, 2016.

The following topics are covered:

- ecological engineering and sustainable development,
- landslides,
- landfills,
- foundations,
- roads,
- underground objects,
- open pits,
- materials and
- infrastructure.

For additional information, please contact us on e-mail address geotehnika@geotenhika.ba

HYDRO 2016 - Achievements, opportunities and challenges 10-12 October 2016, Montreux, Switzerland, www.hydropower-dams.com/hydro-2016.php?c_id=88

The British Tunnelling Society Conference and Exhibition 2016, October 11 – 12, 2016, London, United Kingdom, www.btsconference.com

65th Geomechanics Colloquium 2016, Georg Feder Colloquium, October 13 - 14th, 2016, Salzburg, Austria, www.oegg.at/en/geomechanics-colloquium-3/65th-geomechanics-colloquium-2016-georg-feder-colloquium-79

ARMS 9, 9th Asian Rock Mechanics Symposium, ISRM Regional Symposium, 18-20 October 2016, Bali, Indonesia, http://arms9.com

SFGE 2016 Shaping the Future of Geotechnical Education International Conference on Geo-Engineering Education 20 - 22 October 2016, Minascentro, Belo Horizonte, MG, Brazil, http://cobramseg2016.com.br/index.php/sfge-sobre/?lang=en

10th ICOLD European Club Symposium & Exhibition, 25-30 October 2016, Antalya, Turkey, http://trcold.com

1st International Symposium on Seismic Rehabilitation of Heritage Structures 30-31 October 2016, Tehran, Iran, www.srhs.ir

NEMO International Conference Probing the Santorini volcano for 150 years / Διεθνές συνέδριο NEMO 150 χρόνια μελέτης ηφαιστείου της Σαντορίνης, 3-5 November 2016, Santorini, Greece, http://nemo.conferences.gr

GeoAsia 6 - 6th Asian Regional Conference on Geosynthetics 8-11 November 2016, New Delhi, India, http://seags.ait.asia/news-announcements/11704

3rd Annual Underground Infrastructure & Deep Foundations UAE, 13 - 15 November 2016, Dubai, United Arab Emirates, www.undergrounduae.com

Risk Management in Underground Construction, November 14-16, 2016, Florida University, USA, http://undergroundriskmanagement.com/agenda

5th International Conference on Geotechnical Engineering and Soil Mechanics, 14-16 November 2016, Tehran, Iran, www.icgesm2016.ir

RARE 2016 Recent Advances in Rock Engineering 16-18 November 2016, Bangalore, India, www.rare2016.in

TBM DiGs Istanbul 2016 2nd International conference on "TBM DiGs in difficult grounds", 16-18 November 2016, Istanbul, Turkey, www.tbmdigsturkey.org

International Seminar on Roads, Bridges and Tunnels, 18-24 November 2016, Thessaloniki, Greece, http://isrbt2016.civil.auth.gr

GEOTEC HANOI 2016, The 3rd International Conference on Geotechnics for Sustainable Infrastructure Development, 24-25 November, Hanoi, Vietnam, www.geotechn.vn

TUNNELLING SUMMIT - Pinpointing project opportunities and exploring innovation in tunnelling, 7-8 December 2016, London, U.K., https://tunnelling.newcivilengineer.com

5th International Conference on Forensic Geotechnical Engineering, 8-10 December 2016, Bangalore, Karnataka, India, http://5icfge.com

International Symposium on Submerged Floating Tunnels and Underwater Tunnel Structures (SUFTUS-2016), 16—18 December 2016, Chongqing, China, www.cmct.cn/suftus

International Workshop on "Advances in Multiphysical Testing of Soils and Shales", 18-20 January 2017, Villars, Switzerland, http://atmss.epfl.ch

ICNCGE-2017 International Conference on New Challenges in Geotechnical Engineering, 23 January 2017, Lahore, Pakistan, www.pges-pak.org/home/icncge-2017

4th Arabian Tunnelling Conference & 20th Gulf Engineering Forum - Advancing Underground Space, 21-22 February 2017, Dubai, UAE, www.atcita.com

AFRICA 2017 - Water Storage and Hydropower Development for Africa, 14-16 March 2017, Marrakech, Morocco, www.hydropower-dams.com/AFRICA-2017.php?c_id=89

2nd International Conference on Geotechnical Research and Engineering (ICGRE'17), April 3 - 4, 2017, Barcelona, Spain, http://icgre.org

9th International Symposium on Geotechnical Aspects of Underground Construction in Soft Ground, IS - São Paulo 2017
April 4 and 5, 2017 - São Paulo - Brazil

www.is-saopaulo.com

On behalf of the Brazilian Association for Soil Mechanics and Geotechnical Engineering (ABMS) and the Brazilian Tunneling Committee (CBT), we are pleased to invite you to participate in the 9th International Symposium on Geotechnical Aspects of Underground Construction in Soft Ground, IS - São Paulo 2017.

The TC-204 Symposia have been traditionally high-level events, where specialists from around the world join to present and discuss their contributions and experiences in underground construction in soft ground.

Contact us

Organization and Sales
MCI São Paulo
Rua George Ohm, 230 – Torre A, 19º Andar
04576-020 - São Paulo - SP
Fone / Fax: 55 11 3056-6000
atendimento@mci-group.com
helpdeskbrasil@mci-group.com

EURO:TUN 2017 IV International Conference on Computational Methods in Tunneling and Subsurface Engineering, 18 – 20 April 2017, Innsbruck, Austria, www.eurotun2017.com

TechnoHeritage 2017 3rd International Congress Science and Technology for the Conservation of Cultural Heritage, May 20-23, 2017, Cádiz, Spain, http://technoheritage2017.uca.es

EPS'17 5th International Conference on the Use of EPS Geofoam Blocks in Construction Applications, 22-24 May 2017, Istanbul, Turkey, www.geofoam2017.org

Rapid Excavation and Tunneling Conferrence, June 4-7, 2017, San Diego, USA, www.retc.org

EurAsian Geotextiles Symposium 2017
07 - 08 June 2017, Beijing, China
www.edana.org/education-events/conferences-and-symposia/event-detail/eurasia-geotextiles-symposium-2017

Organised under the auspices of IGS, the EurAsian Geotextiles Symposium (EAGS) will take place in Beijing on 7-8 June 2017. The first event of its kind, the EAGS is a two-day conference and exhibition covering markets, products and technology for geotextiles. Featuring a conference and an exhibition, the EAGS is designed to cover both nonwoven and woven geotextiles and to encompass the entire value chain, from raw materials to buyers and users of geotextiles, in Greater Europe and Asia.

The Symposium's programme will include the following themes:

· Best practice in specifications of geotextiles
· Improved understanding of the market for geotextiles
· Identification of new opportunities for growth

This event will be co-organised by CNITA, the China Nonwovens & Industrial Textiles Association, and EDANA, the leading global association serving the nonwovens and related industries. The Symposium is focussed on geotextiles in Eurasia and aimed at supporting the growth of the geotextiles market in China and in Asia as a whole and helping companies access this dynamic market.

The EAGS is designed to offer extensive networking opportunities, attracting leading decision makers from across the geotextiles supply chain. Top level speakers will give presentations on recent and upcoming developments of 2 relevance for geotextiles markets in Europe and Asia and the table top exhibition will provide a unique opportunity for companies to meet new and existing business partners and promote their products and services.

Further information

Is available at:
http://www.edana.org/educationevents/conferences-and-symposia/event-detail/eurasia-geotextiles-symposium-2017
eva.fabbri@edana.org

World Tunnel Congress 2017 Surface challenges – Underground solutions, 9 to 16 June 2017, Bergen, Norway, www.wtc2017.no

EUROCK 2017 Human Activity in Rock Masses, 20-22 June 2017, Ostrava, Czech Republic, www.eurock2017.com

BCRRA 2017 Tenth International Conference on the Bearing Capacity of Roads, Railways and Airfields, 28th to 30th June 2017, Athens, Greece, www.bcrra2017.com

GeoMEast2017, 15 - 19 July 2017, Sharm El-Sheik, Egypt, www.geomeast2017.org

3rd International Conference on Performance-based Design in Earthquake Geotechnical Engineering (PBD-III), July 16 - 19, 2017, Vancouver, Canada, http://pbdiiivancouver.com

19th International Conference on Soil Mechanics and Geotechnical Engineering, 17 - 22 September 2017, Seoul, Korea, www.icsmge2017.org

AfriRock 2017, 1st African Regional Rock Mechanics Symposium, 2 – 7 October 2017, Cape Town, South Africa, www.saimm.co.za/saimm-events/upcoming-events/afrirock-2017

Geotechnique Symposium in Print 2017 Tunnelling in the Urban Environment, http://www.icevirtuallibrary.com/pb-assets/Call%20for%20Papers/Geo-Symposium-CFA-AW.pdf

GeoAfrica 2017
3rd African Regional Conference on Geosynthetics
9 – 13 October 2017, Morocco

PARIS 2017 AFTES International Congress "The value is Underground", 13-16 November 2017, Paris, France, www.aftes2017.com

World Tunnel Congress 2018
20-26 April 2018, Dubai, United Arab Emirates

EUROCK 2018
22-26 May 2018, Saint Petersburg, Russia

Contact Person: Prof. Vladimir Trushko
Address: 21-st line V.O., 2
199106 St. Petersburg
Russia
Telephone: +7 (812) 328 86 71

Fax: +7 (812) 328 86 76
E-mail: trushko@spmi.ru

16th European Conference on Earthquake Engineering (16thECEE), 18-21 June 2018, Thessaloniki, Greece, www.16ecee.org

CPT'18 4th International Symposium on Cone Penetration Testing, 21-22 June 2018, Delft, Netherlands, www.cpt18.org

UNSAT2018 The 7th International Conference on Unsaturated Soils, 3 - 5 August 2018, Hong Kong, China, www.unsat2018.org

11th International Conference on Geosynthetics (11ICG), 16 - 20 Sep 2018, Seoul, South Korea, www.11icg-seoul.org

ARMS10
10th Asian Rock Mechanics Symposium
ISRM Regional Symposium
October 2018, Singapore
www.arms10.org

Contact Person: Prof. Yingxin Zhou
Address: 1 Liang Seah Street
#02-11 Liang Seah Place
SINGAPORE 189022
Telephone: (+65) 637 65363
Fax: (+65) 627 35754
E-mail: zyingxin@dsta.gov.sg

14th ISRM International Congress
2019, Foz de Iguaçu, Brazil

Contact Person: Prof. Sergio A. B. da Fontoura
E-mail: fontoura@puc-rio.b

ISDCG 2019
7th International Symposium on Deformation Characteristics of Geomaterials
26-28 June 2019, Strathclyde, Scotland, UK,

Organizer: TC101

The 17th European Conference on Soil Mechanics and Geotechnical Engineering
1st - 6th September 2019, Reykjavik Iceland
www.ecsmge-2019.com

The theme of the conference embraces all aspects of geotechnical engineering. Geotechnical engineering is the foundation of current as well as future societies, which both rely on complex civil engineering infrastructures, and call for mitigation of potential geodangers posing threat to these. Geotechnical means and solutions are required to ensure infrastructure safety and sustainable development. Those means are rooted in past experiences enhanced by research and technology of today.

At great events such as the European Geotechnical Conference we should: Spread our knowledge and experience to our colleagues; Introduce innovations, research and development of techniques and equipment; Report on successful geotechnical constructions and application of geotechnical design methods, as well as, on mitigation and assessment of geohazards and more.

Such events also provide an opportunity to draw the attention of others outside the field of geotechnical engineering to the importance of what we are doing, particularly to those who, directly or indirectly, rely on our services, knowledge and experience. Investment in quality geotechnical work is required for successful and safe design, construction and operation of any infrastructure. Geotechnical engineering is the key to a safe and sustainable infrastructure and of importance for the society, economy and the environment. This must be emphasized and reported upon.

ΕΝΔΙΑΦΕΡΟΝΤΑ ΓΕΩΤΕΧΝΙΚΑ ΝΕΑ

Οι καταρράκτες του Νιαγάρα χωρίς νερό

Το καλοκαίρι του 1969 μια ομάδα μηχανικών του αμερικανικού στρατού διέκοψε τη ροή στους καταρράκτες του Νιαγάρα προκειμένου να πραγματοποιήσει γεωλογικές έρευνες μετά από κατολισθήσεις που είχαν σημειωθεί . Για σχεδόν έξι μήνες οι καταρράκτες που βρίσκονται στην αμερικανική πλευρά, έμειναν χωρίς νερό μετά από 12 .000 χρόνια συνεχούς ροής. Για το έργο οι Αμερικανοί έφτιαξαν ένα τεράστιο φράγμα 182 μέτρων στον ποταμό εκτρέποντας τη ροή προς τη μεριά του Καναδά. Οι μηχανικοί μελέτησαν την κοίτη του ποταμού ώστε να εντοπίσουν τυχόν προβλήματα που θα μπορούσαν να προκαλέσουν διάβρωση του εδάφους.

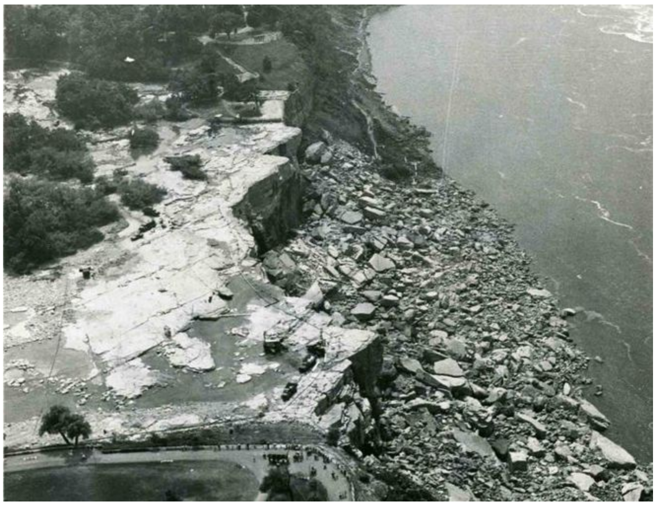

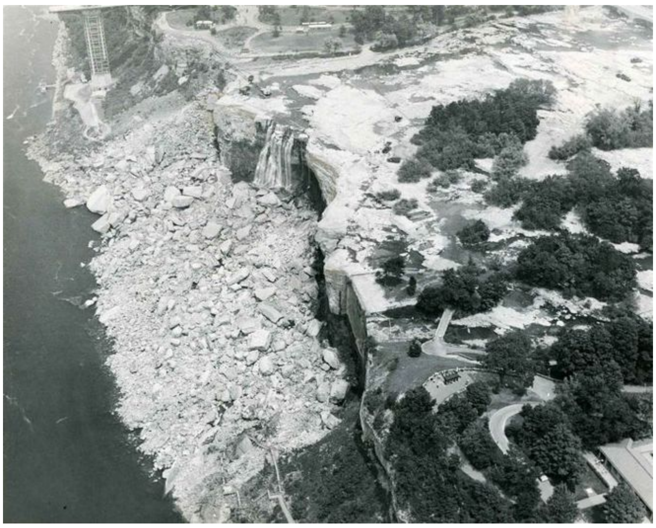

Όσο οι μηχανικοί εξέταζαν τον ποταμό δημιουργήθηκε ένας προσωρινός διάδρομος που επέτρεπε στους επισκέπτες να δουν το απρόσιτο και σκληρό τοπίο. Στην αρχή τους φάνηκε παράξενο και απογοητευτικό το θέαμα. Στη συνέχεια όμως ολοένα και περισσότεροι επισκέπτονταν την περιοχή για να δουν από κοντά τους στεγνούς καταρράκτες. Κατά το χρονικό διάστημα που οι καταρράκτες έμειναν στεγνοί ανακαλύφθηκαν δύο πτώματα, ενός άνδρα και μίας γυναίκας.

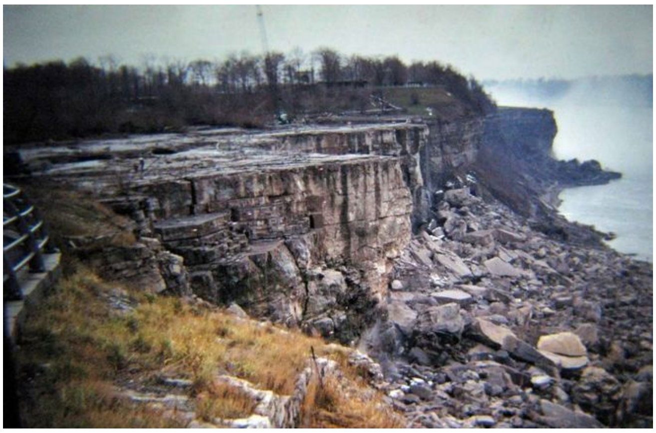

Τον Νοέμβριο του 1969 μπροστά σε 2.650 θεατές συνεργεία ανατίναξαν το φράγμα και η ροή αποκαταστάθηκε. Οι καταρράκτες του Νιαγάρα είναι σύμπλεγμα του ποταμού Νιαγάρα, στα διεθνή σύνορα μεταξύ του Οντάριο στον Καναδά και της πολιτείας της Νέας Υόρκης. Αποτελούνται από δύο μεγάλα τμήματα που χωρίζονται από το νησί Goat : οι καταρράκτες Horseshoe, η πλειονότητα των οποίων βρίσκεται στην Καναδική πλευρά των συνόρων και των Americans Falls στην Αμερικανική πλευρά. Οι μικρότεροι Bridal Veil Falls βρίσκονται στην αμερικανική πλευρά, αλλά διαχωρίζονται από τους άλλους με το νησί Luna. Ακόμα και μετά τι εργασίες των μηχανικών το νησί Luna έμεινε κλειστό για το κοινό καθώς υπήρχε ο φόβος της αστάθειας.

Οι καταρράκτες του Νιαγάρα έχουν μεγάλο πλάτος. Περισσότερο από 6 εκατομμύρια κυβικά πόδια νερού πέφτουν κάθε λεπτό κατά την περίοδο της υψηλής ροής και σχεδόν 4 εκατομμύρια κυβικά πόδια κατά μέσο όρο. Είναι οι πιο ισχυροί καταρράκτες στη Βόρεια Αμερική.

Πηγή:mixanitouxronou.gr

(30 Αυγούστου 2016)

ΕΝΔΙΑΦΕΡΟΝΤΑ - ΣΕΙΣΜΟΙ

Σουβενίρ από την Γκοντβάνα
Ανάμεσα στην Κύπρο και την Κρήτη, ο αρχαιότερος βυθός του κόσμου

Η Μεσόγειος θεωρείται απομεινάρι του αρχαίου ωκεανού της Τηθύος

Με τα ηφαίστεια να φέρνουν μάγμα από τα βάθη και τις τεκτονικές πλάκες να κινούνται αέναα, ο γήινος φλοιός ανανεώνεται συνεχώς και σχεδόν κανένα τμήμα του δεν μένει ίδιο. Φαίνεται όμως ότι υπάρχει μια εξαίρεση: ένα κομμάτι φλοιού στην Ανατολική Μεσόγειο που δείχνει να έχει ηλικία 340 εκατομμυρίων ετών, και δεν αποκλείεται να είναι απομεινάρι από την εποχή της υπερηπείρου Γκοντβάνα.

Μελέτη στην επιθεώρηση Nature Geoscience εξετάζει τη Λεκάνη του Ηροδότου, μια βαθιά περιοχή της Μεσογείου ανάμεσα στην Κύπρο, την Κρήτη και την Ρόδο. Σε δύο αποστολές το 2012 και το 2014, το ισραηλινό ερευνητικό πλοίο RV Mediterranean Explorer πόντισε ένα ευαίσθητο μαγνητόμετρο και το έσυρε σε συνολική απόσταση 7.000 χιλιομέτρων, κινούμενο σε παράλληλες γραμμές.

Το ισραηλινό ωκεανογραφικό σκάφος RV Mediterranean Explorer πραγματοποίησε δύο αποστολές στην περιοχή

Αυτό επέτρεψε στους ερευνητές να διαβάσουν τη μαγνητική υπογραφή του υποκείμενου φλοιού, η οποία εξαρτάται από τον προσανατολισμό του γήινου μαγνητικού πεδίου την εποχή που σχηματίστηκε το συγκεκριμένο τμήμα φλοιού από τη στερεοποίηση μάγματος.

Αυτό που είδε η ερευνητική ομάδα είναι ότι το μαγνητικό πεδίο της Γης αντιστράφηκε πολλές φορές όσο σχηματιζόταν ο φλοιός, κάτι που άφησε ένα αποτύπωμα από εναλλασσόμενες μαγνητικές λωρίδες στα πετρώματα.

Οι ίδιες λωρίδες, εξάλλου, σημαδεύουν τον φρέσκο ωκεάνιο φλοιό που σχηματίζεται ακόμα και σήμερα από την άνοδο μάγματος στη μέση του Ατλαντικού και του Ειρηνικού Ωκεανού.

Η μέτρηση του αριθμού των μαγνητικών λωρίδων, σε συνδυασμό με προηγούμενες παρατηρήσεις, οδηγεί στην εκτίμηση ότι ο φλοιός της Λεκάνης του Ηροδότου έχει ηλικία 315 έως 265 εκατομμυρίων ετών.

Αυτό, λένε οι συντάκτες της μελέτης, αφήνει ανοιχτό το ενδεχόμενο να πρόκειται για τμήμα του ωκεάνιου φλοιού της Τηθύος, ενός ωκεανού που χώριζε κάποτε τις υπερηπείρους της Γκοντβάνα και της Λαυρασίας. Η Μεσόγειος και η Ερυθρά Θάλασσα θεωρούνται τμήματα αυτού του αρχαίου ωκεανού.

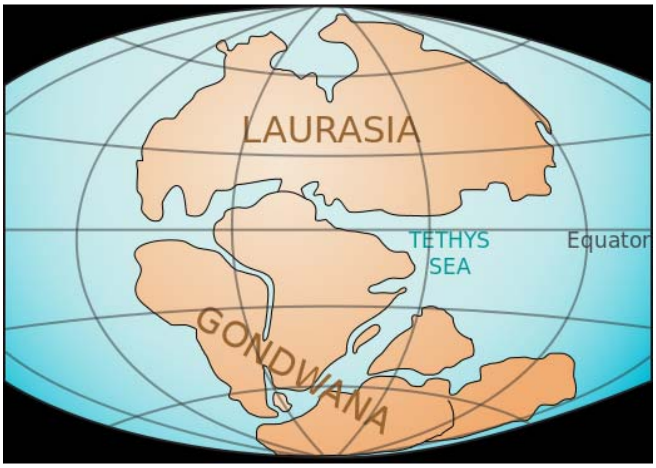

Ο ωκεανός (ή θάλασσα) της Τηθύος χώριζε κάποτε δύο υπερ-ηπείρους (CC BY-SA 3.0)

Αν οι ερευνητές έχουν δίκιο, ο φλοιός ανάμεσα στην Κύπρο και την Κρήτη είναι ο αρχαιότερος γνωστός ωκεάνιος φλοιός.

Θα ήταν πάντως δύσκολο να συλλεχθούν δείγματα, καθώς σήμερα είναι θαμμένος από ένα στρώμα ιζημάτων που φτάνει σε βάθος το εντυπωσιακό νούμερο των 15 χιλιομέτρων.

(Βαγγέλης Πρατικάκης / Newsroom ΔΟΛ, 16 Αυγούστου 2016, http://news.in.gr/science-technology/article/?aid=1500095797)

Palaeozoic oceanic crust preserved beneath the eastern Mediterranean

[Roi Granot](#)

Subduction of oceanic crust into the mantle results in the relatively young Mesozoic–Cenozoic age of the current oceanic basins[1], thus, hindering our knowledge of ancient oceanic lithospheres. Believed to be an exception, the eastern Mediterranean Sea (containing the Herodotus and Levant basins) preserves the southern margin of the Neotethyan, or older, ocean. An exceptionally thick sedimentary cover and a lack of accurate magnetic anomaly data have led to contradicting views about its crustal nature and age. Here I analyse total and vector magnetic anomaly data from the Herodotus Basin. I identify a long sequence of lineated magnetic anomalies, which imply that the crust is oceanic. I use the shape, or skewness, of these magnetic anomalies to constrain the timing of crustal formation and find that it formed about 340 million years ago. I suggest that this oceanic crust formed either along the Tethys spreading system, implying the Neotethys Ocean came into being earlier than previously thought, or during the amalgamation of the Pangaea Supercontinent. Finally, the transition from the rather weak and stretched continental crust found in the Levant Basin to the relatively strong oceanic Herodotus crust seems to guide the present-day seismicity pattern as well as the plate kinematic evolution of the region.

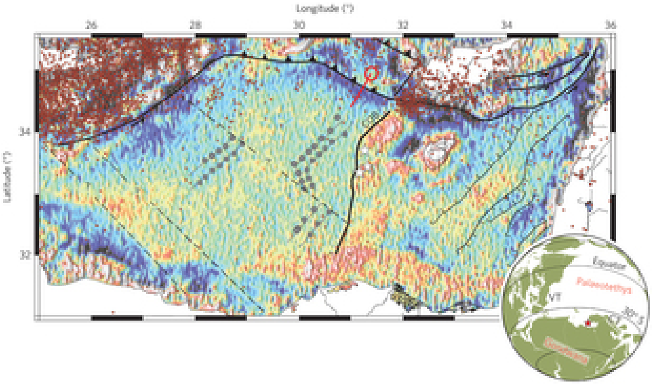

Figure 4: Tectonic map of the eastern Mediterranean.

(Nature Geoscience, 15 August 2016, http://www.nature.com/ngeo/journal/vaop/ncurrent/full/ngeo2784.html)

EPA links oil and gas drilling to Texas quakes

Federal regulators have tied a string of earthquakes in north Texas to oil and gas drilling operations in the state.

An Environmental Protection Agency (EPA) report filed with the Texas Railroad Commission this month concluded that the frequency of earthquakes in the state correlates to the number and location of injection or disposal wells for hydraulic fracturing wastewater there.

"In light of findings from several researchers, its own analysis of some cases and the fact that earthquakes diminished in some areas following shut-in or reduced injection volume of targeted wells, EPA believes there is a significant possibility that North Texas earthquake activity is associated with disposal wells," said the report, via The Texas Tribune (https://www.texastribune.org/2016/08/22/epa-north-takes-quakes-likely-linked-oil-and-gas-a).

The EPA said it's concerned about the seismic activity around the Dallas/Fort Worth area because of the "potential impact on public health and the environment, including underground drinking water."

It recommended more monitoring of injection wells and analysis of seismic activity in the state. It also "commended" state regulators on the Texas Railroad Commission for establishing earthquake-related regulations for drilling operations there, though the commission has not yet connected wastewater injection to seismic activity in the state, the Tribune reported.

The EPA report is the latest from scientists and regulators to find a link between wastewater injection and earthquakes.

Oklahoma was in the spotlight last year when state scientists concluded that injection wells were behind an explosion of small earthquakes there, though the state has seen (http://thehill.com/policy/energy-environment/291114-oklahoma-earthquakes-decline-amid-new-regulations) the number of quakes decline since stiffening regulations on wastewater disposal.

Federal officials in March concluded that 7 million Americans live in areas threatened by earthquakes induced by human activity (http://thehill.com/policy/energy-environment/274471-feds-7-million-people-at-risk-of-man-made-earthquakes).

(Devin Henry / THE HILL, 08.22.2016, http://thehill.com/policy/energy-environment/292248-epa-drilling-operations-behind-texas-quakes)

Latest Italian quake is history repeated

The 6.2 magnitude earthquake that devastated parts of central Italy on Wednesday is the eighth major quake to hit the country in the past 40 years. Located near the meeting point of the Eurasian and African plates, the region has long been known as a seismic hotspot. Indeed, it was only in 2009 that over 300 people lost their lives in the nearby L'Aquila earthquake. As I write, the death toll from this quake stands at 268, and will inevitably continue to rise as rescue workers sift through the destruction and the region is rocked by strong aftershocks.

Aftermath of the 2009 L'Aquila earthquake

Similarities with the L'Aquila disaster are striking. Just an hour's drive south of Amatrice (the worst hit town, where at least 200 people are known to have died so far), the L'Aquila quake measured 6.3. The Richter Scale is base-10 logarithmic, making the L'Aquila quake twice as strong as the 6.2 that hit this week. Both quakes struck at a shallow depth of around 10km beneath the surface, contributing to the intensity of the vibrations. But questions must be asked about the extent of the damage, as the lessons of history appear to go unheeded.

It's been widely reported that experts estimate 70 per cent of Italy's buildings are not built to seismic standards. In a first-world country prone to earthquakes, that figure is simply unacceptable. Naturally, in 12th century towns there will always be historical buildings not built to today's standards, and where it can be difficult to retrospectively put mitigating measures in place. What is difficult to understand is why modern buildings are not built to modern standards.

"Hospitals, police stations, schools and barracks in Amatrice and Accumuli completely collapsed during the earthquake – with the exception of a gym that is now being used to house displaced residents," said Prof Giulio Di Toro, Geology Chair at Manchester University's School of Earth and Environmental Sciences, who was conducting research in central Italy this week when the earthquake struck.

"The village of Norcia, which was rebuilt adhering to the construction codes after the 1979 earthquake (5.8 magnitude, five casualties), suffered little damage and no casualties despite being located in the epicentral area."

Reports from Amatrice indicate that investigators are examining the town's Romolo Capranica school. The building was restored in 2012 using funds provided in the aftermath of the L'Aquila quake, but on Wednesday it almost completely collapsed. The town's clock tower, built in the 13th century, remained standing.

The town of Norcia was relatively unscathed this week, having been rebuilt to codes after a 1979 quake

"In a country where in the past 40 years there have been at least eight devastating earthquakes … the only lesson we have learned is how to save lives after the fact," columnist Sergio Rizzo wrote in Thursday's Corriere della Sera, one of Italy's leading newspapers. "We are far, far behind in the other lessons."

Italy is a proud nation with a fabled history, and what can often be an admirable streak of stubbornness. But this week's tragic events are a wake-up call, and the lessons from L'Aquila have clearly not been learned. The Italian government must now look at the systems other countries have put in place to protect their citizens from the dangers of earthquakes.

Damage following the 2011 Japanese quake

Japan is, of course, a leader in this regard, as indeed it must be. Lying in one of the most seismically active regions in the world, the country has seen its fair share of devastation from earthquakes and tsunamis. The 9.0 quake that struck off the coast in 2011 caused huge tremors across the country, but the vast majority of casualties were caused by the resulting tsunami rather than the quake itself. In Japan, building codes are strict, citizens are prepared for the inevitable, and countless lives are saved when catastrophe does strike. It's time for Italy to follow suit.

(Andrew Wade / the engineer, 26th August 2016, https://www.theengineer.co.uk/latest-italian-quake-is-history-repeated/?cmpid=tenews_2578111)

ΕΝΔΙΑΦΕΡΟΝΤΑ - ΠΕΡΙΒΑΛΛΟΝ

Σκηνή εγκλήματος
Ούρμια, η λίμνη που έγινε κατακόκκινη από τη θλίψη

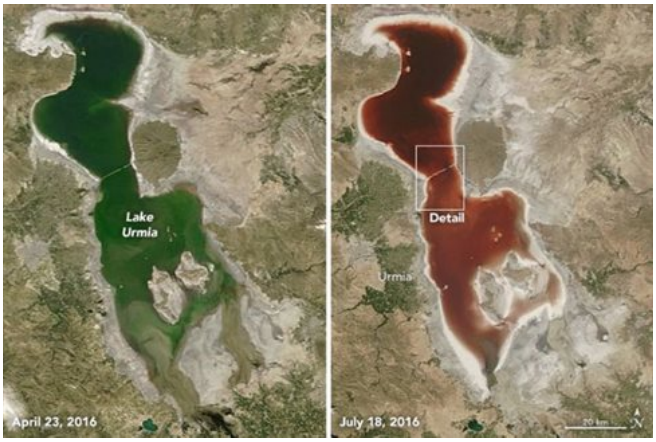

Πριν και μετά: το χρώμα της λίμνης είναι τελείως διαφορετικό σε εικόνες που τραβήχτηκαν τον Απρίλιο και τον Ιούλιο (Φωτογραφία: NASA)

Η λίμνη Ούρμια στο Ιράν, κάποτε η μεγαλύτερη λίμνη της Μέσης Ανατολής και μια από τις μεγαλύτερες του κόσμου, έχασε το πράσινο χρώμα της και μοιάζει πια με απέραντη σκηνή εγκλήματος.

Στα τέλη Απριλίου, η λίμνη φαινόταν καταπράσινη σε εικόνα του δορυφόρου Aqua της NASA. Μέχρι τα μέσα Ιουλίου, τα νερά είχαν αποκτήσει ένα βαθύ κόκκινο χρώμα σαν κρασί.

Η αλλαγή χρώματος στη λίμνη κοντά στα σύνορα με την Τουρκία έχει γίνει σύνηθες φαινόμενο τα καλοκαίρια, όταν η εισροή νερού περιορίζεται και η αλατότητα αυξάνεται λόγω έντονης εξάτμισης.

Η αύξηση της συγκέντρωσης αλατιού ευνοεί τον πολλαπλασιασμό κόκκινων μικροοργανισμών, εξηγεί η NASA σε ανακοίνωσή της.

Μια γέφυρα για οχήματα χωρίζει στα δύο τη λίμνη Ούρμια (NASA)

Η ταυτοποίηση των μικροβίων αυτών θα απαιτούσε λήψη δειγμάτων, ωστόσο οι υποψίες στρέφονται σε δύο ομάδες μονοκύτταρων οργανισμών. Η πρώτη είναι τα φύκη του γένους Dunanelia, τα οποία είναι πράσινα υπό κανονικές συνθήκες, αλλάζουν όμως χρώμα σε συνθήκες υψηλής αλατότητας και έντονου φωτισμού.

«Τα φύκια γίνονται κόκκινα λόγω της παραγωγής προστατευτικών καροτενοειδών μέσα στα κύτταρα» εξηγεί ο Μοχάμαντ Τούριαν, ερευνητής του Πανεπιστημίου της Στουτγάρδης. Σε καροτενοειδή οφείλεται εξάλλου και το χρώμα του καρότου.

Η δεύτερη ομάδα είναι αρχαιοβακτήρια της οικογένειας Halobacteriaceae, τα οποία προτιμούν νερά κορεσμένα σε αλάτι. Οι «πρωτόγονοι» αυτοί οργανισμοί παράγουν την κόκκινη χρωστική ουσία βακτηριοροδοψίνη, μέσω της οποίας απορροφούν την ηλιακή ενέργεια για να παράγουν σάκχαρα μέσω φωτοσύνθεσης.

Η λίμνη Ούρμια έχει αλλάξει από πράσινη σε κόκκινη και το αντίστροφο αρκετές φορές στο παρελθόν. Συνήθως ξαναγίνεται πράσινη την άνοιξη, όταν τα χιόνια λιώνουν στα γειτονικά βουνά και ανεβάζουν και πάλι τη στάθμη.

Παρόλα αυτά, η λίμνη είναι σήμερα σκιά του παλιού εαυτού της: κάποτε έφτασε σε έκταση τα 5.200 τετραγωνικά χιλιόμετρα, σχεδόν μιάμιση φορά η έκταση της Εύβοιας.

Λόγω της ξηρασίας και της χρήσης του νερού για άρδευση, η μέση στάθμη πέφτει έως και κατά ένα μέτρο το χρόνο, και πλέον η λίμνη έχει συρρικνωθεί μόλις στο 10% της αρχικής της έκτασης.

Όπως είχε προειδοποιήσει στο Scientific American (http://blogs.scientificamerican.com/guest-blog/saving-iran-s-precious-lake-urmia) ο Χουσεΐν Ακάνι, βιολόγος του Πανεπιστημίου της Τεχεράνης, χωρίς τη λήψη δραστικών μέτρων η οριστική εξαφάνιση της Ούρμιας πρέπει να θεωρείται βέβαιη.

(Βαγγέλης Πρατικάκης / Newsroom ΔΟΛ, 03 Αυγ. 2016, http://news.in.gr/science-technology/article/?aid=1500093877)

Οι πιο ιδιαίτερες εκκλησίες του κόσμου

Οι εκκλησίες σε όλο τον κόσμο αποτελούν εδώ και χρόνια τουριστικό πόλο έλξης για τους ταξιδιώτες όχι μόνο για θρησκευτικούς λόγους, αλλά και για την απίστευτη αρχιτεκτονική τους και τις ασυνήθιστες τοποθεσίες που έχουν κατασκευαστεί.

Μπορεί να τις βρει κανείς κάτω από το έδαφος ή στην άκρη ενός γκρεμού, ενώ μερικοί ναοί βρίσκονται ανάμεσα ακόμα και από δύο χώρες. Η Daily Mail δημοσιεύει μερικές από τις πιο ιδιαίτερες που υπάρχουν στον κόσμο σήμερα…

1. St Samaan El Kharaz, Μοκατάμ, Αίγυπτος

Η συγκεκριμένη εκκλησία σε σπήλαιο είναι κρυμμένη στο ίσως λιγότερο τουριστικό μέρος της Αιγύπτου, σε μια περιοχή όπου οι οικογένειες ζουν από τη συλλογή σκουπιδιών.

Υπάρχει μια πρόσοψη από πέτρα που χρησιμεύει ως είσοδος του ναού, αλλά το υπόλοιπο μέρος του κτιρίου είναι ουσιαστικά μια σειρά από σπηλιές. Η μεγαλύτερη από αυτές έχει τη μορφή ενός αμφιθέατρου, χωρίς πόρτες, όπου μπορούν να καθίσουν μέχρι και 10.000 άτομα.

2. St Michel d'Aiguilhe, Γαλλία

Σκαρφαλωμένο στην κορυφή ενός ψηλού ηφαιστειακού πετρώματος, το παρεκκλήσι St Michel d'Aiguilhe, χρονολογείται από τον 10ο αιώνα. Είναι προσβάσιμη μόνο από τα πέτρινα σκαλοπάτια που τυλίγονται γύρω από το βράχο.

3. Temppeliaukio Church, Ελσίνκι, Φινλανδία

Είναι γνωστή συχνά και ως η βραχώδης εκκλησία του Ελσίνκι καθώς πρόκειται για ένα λαξευμένο σπήλαιο.

Το εσωτερικό αποτελείται από μια τραχιά επιφάνεια βράχου έχοντας επίσης μια θεαματική οροφή από χαλκό. Η ακουστική του ναού είναι τόσο καλή στο εσωτερικό, ώστε μερικές φορές χρησιμοποιείται για συναυλίες.

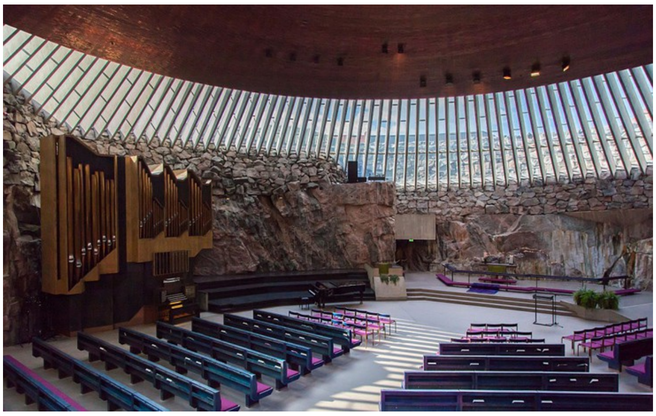

4. Chapel of the Holy Cross, Αριζόνα, ΗΠΑ

Αυτός ο καθεδρικός ναός βρίσκεται μέσα στον κόκκινο βράχο της Σεντόνα σε ένα πολύ ψηλό σημείο, με θέα την πεδιάδα. Το σχήμα του ναού είναι πολύ απλό και ιδιαίτερο, ενώ χαρακτηριστικός είναι ο σταυρός που διακρίνεται.

5. Εκκλησία του Αγίου Γεωργίου, Αιθιοπία

Πρόκειται για μία από τις 11 διαφορετικές εκκλησίες σκαλισμένες σε βράχους, στην καρδιά της Αιθιοπίας και ίσως η ωραιότερη από το σύνολο. Ένας τεράστιος σταυρός κόπηκε από ένα κομμάτι του βράχου και στη συνέχεια το εσωτερικό δημιουργήθηκε σκάβοντας το βράχο.

6. Παναγία Παραπορτιανή, Μύκονος

Στη λίστα της, η Daily Mail περιλαμβάνει και μια εκκλησία στην Ελλάδα, την Παναγία Παραπορτιανή. Την αναφέρει ως την πιο πολυφωτογραφημένη στο νησί.

Στην πραγματικότητα, πρόκειται όχι για μια απλή εκκλησία, αλλά για ένα διώροφο συγκρότημα, που περιλαμβάνει τέσσερις ισόγειους ναΐσκους και την ανώγεια, υπερυψωμένη Παναγία Παραπορτιανή.

(30 Αυγούστου 2016)

ΕΝΔΙΑΦΕΡΟΝΤΑ - ΛΟΙΠΑ

Augmented Reality Could Speed Up Construction Projects

Builders are experimenting with Microsoft's HoloLens to visualize projects and avoid expensive mistakes.

Employees at Gilbane Building Company, a commercial construction firm based in Rhode Island, usually work off paper blueprints or with digital models that they view on computers or iPads. But Gilbane senior manager John Myers now gets a closer look by putting Microsoft's augmented-reality computer, HoloLens, on his head.

When Myers recently put on HoloLens to look at a mockup of a project, he could see that steel frames the company planned to order to support the building's walls were too long to fit the design. Having spotted the issue ahead of time, the company can now ask the supplier to cut the frames shorter in his shop rather than make workers adjust dozens of tracks that would hold the frames in place. Myers estimates that the move will save Gilbane about $5,000 in labor costs.

Construction is one of the least automated industries around, and it will be for a long time. But augmented reality might begin to change that. Tools like HoloLens, which places holographic images in its user's physical environment, could help this $10 trillion business increase efficiency so that fewer projects run over budget and behind schedule. Gilbane is one of many early testers of the technology. The engineering firm AECOM, the design and architecture firm Gensler, and the China State Construction Engineering Corporation have also announced they are experimenting with HoloLens.

Gilbane's John Myers uses HoloLens to review a virtual 3-D model of Boston's Dearborn STEM Academy.

Gilbane says the $3,000 HoloLens, which it received in mid-June, has already shown its value. It was while viewing life-size 3-D models of Dearborn STEM Academy, a $70 million, 120,000-square-foot school Gilbane is constructing in Boston, that Myers spotted the frame-length issue. "That one catch paid for the HoloLens," he says.

Gilbane vice president Sue Klawans says HoloLens could also be used before a building is constructed to detect flaws in the way ducts and pipes are laid out in office ceilings—a complicated process that often takes up more room than anticipated—and in building designs that feature glass "curtain" walls, which sometimes require more than 10 different contractors to fabricate.

I tried Gilbane's HoloLens at the Dearborn STEM Academy site. After strapping on and adjusting the headset (which required another person's assistance), I pinched my fingers in the air to move a 3-D image of the school's mechanical room from its virtual perch on a table to the floor. Then I tapped a button on a virtual control panel to increase the model's size to 100 percent. That let me walk inside it and look at details of the construction as if it were actually built. Using a virtual control panel, I could also toggle different views on and off to see either a simple architectural image of the room, a more detailed structural image, or one that just showed its mechanical, electrical, and plumbing systems.

All the features I tried were easy to navigate and seemed useful. But the HoloLens image stuttered at times, and the life-size model didn't quite look like a real room, partly because the headset's lenses don't cover your peripheral view.

Amar Hanspal, a senior vice president at the software company Autodesk, which supplies the building visualization data necessary for the system to work, says that eventually, builders could wear HoloLens at construction sites "and see in real time, 'Here's what the building should be and here's what it actually looks like.'"

First, though, builders have to figure out how to wear HoloLens along with their safety gear and keep it from being a dangerous distraction. HoloLens wraps around the middle part of your head, like a bulky pair of goggles, which makes it difficult to wear a hard hat at the same time. Another problem: its lenses aren't as rugged as construction safety glasses, which are typically heat-resistant and shatter-proof. There's also a possibility that the holographic images could divert your attention and cause you to take a wrong step—a potentially fatal move on a multistory construction site. For now, Gilbane employees are mostly using HoloLens inside a mobile office trailer parked on the side of the school construction site.

Reviewing construction models via HoloLens would be more useful if people could make notes directly on the 3-D images they were viewing. Trimble, a technology company that sells the popular 3-D modeling software SketchUp, lets people do that in its HoloLens app. Users can mark problem areas on SketchUp building models with circular virtual icons and record short audio clips explaining why they highlighted particular spots. Eventually, they might be able to use their hands to move an element within a virtual mockup and immediately see how the change affected the design, says Aviad Almagor, who leads Trimble's HoloLens business.

"We're going to want to see HoloLens improve [as a construction aid]," says Klawans, the Gilbane executive. "But it's a leap over what we were doing before. It's not just a new toy."

(Elizabeth Woyke, Business Editor / MIT Technology Review, August 10, 2016, https://www.technologyreview.com/s/602124/augmented-reality-could-speed-up-construction-projects)

Ανύψωση αντικειμένων με τη «δύναμη» του ήχου

Μία τεχνική που υπόσχεται πως στο μέλλον θα μπορεί να διατηρεί στον αέρα αντικείμενα τα οποία δεν θα έρχονται σε επαφή με οποιοδήποτε άλλο σώμα, ανέπτυξαν επιστήμονες από το πανεπιστήμιο του Σάο Πάολο της Βραζιλίας.

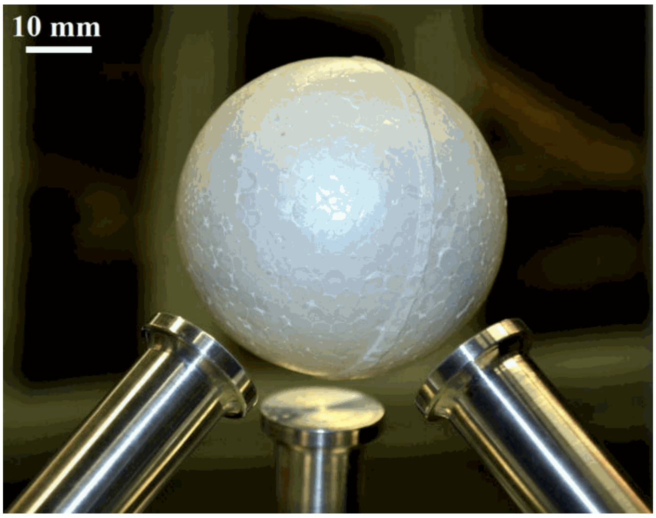

Η τεχνική αυτή βασίζεται σε ακτίνες υπερήχων, χάρη στις οποίες ένα αντικείμενο μπορεί να αιωρείται σαν να «αψηφά» τη βαρύτητα. Σε πρόσφατη δοκιμή, οι επιστήμονες κατάφεραν με αυτό τον τρόπο να ανυψώσουν μία μπίλια διαμέτρου 5 εκατοστών από πολυστυρένιο (Appl. Phys. Lett. **109**, 044101 (2016); http://dx.doi.org/10.1063/1.4959862).

Πριν από τους Βραζιλιάνους επιστήμονες, και άλλες ερευνητικές ομάδες έχουν ασχοληθεί με την ακουστική αιώρηση, όπως ονομάζεται το φαινόμενο, «επιστρατεύοντας» κι αυτές ηχητικά κύματα για να ανυψώσουν μικρά αντικείμενα, όπως σταγόνες νερού.

Για παράδειγμα, τον περασμένο Οκτώβριο επιστήμονες του πανεπιστημίου του Σάσεξ στην Αγγλία ανακοίνωσαν πως δημιούργησαν ελκτικές ακτίνες υπερήχων, με τις οποίες μπορούν να ανυψώσουν και να μετακινήσουν αντικείμενα.

Ωστόσο, η μπίλια που χρησιμοποίησαν οι ερευνητές από το Σάο Πάολο είναι από τα μεγαλύτερα σώματα που έχουν ανυψωθεί με αυτό τον τρόπο, ενώ μάλιστα η τεχνική ακουστική αιώρησης που έχουν αναπτύξει μπορεί να βελτιωθεί για να κρατά στον αέρα ακόμη μεγαλύτερα σώματα και σε μεγαλύτερο ύψος.

Μέχρι σήμερα, οι περισσότερες μέθοδοι ακουστικής αιώρησης βασίζονταν σε δύο ηχητικά κύματα που διαδίδονταν σε αντίθετες κατευθύνσεις, δημιουργώντας έτσι ένα στάσιμο κύμα. Σε αυτή την περίπτωση, αν ένα αντικείμενο βρεθεί σε ένα σημείο του στάσιμου κύματος με σταθερή πίεση («δεσμός»), τότε το αμέσως χαμηλότερο σημείο μέγιστης αυξομείωσης της πίεσης («κοιλία») προκαλεί μία ανοδική δύναμη – λειτουργώντας περίπου σαν μια «αόρατη» ρακέτα του πινκ-πονκ, πάνω στην οποία αναπηδά συνεχώς το αντικείμενο.

Ωστόσο, οι μέθοδοι αυτές φαίνεται πως έχουν ένα μέγιστο όριο στο μέγεθος των αντικειμένων που μπορούν να ανυψώσουν, το οποίο αγγίζει τα 4 χιλιοστά σε διάμετρο. Μία τιμή που ήδη υπερδεκαπλασίασαν οι επιστήμονες από το Σάο Πάολο με την τεχνική τους.

Ο λόγος είναι πως η συγκεκριμένη τεχνική βασίζεται στη συμβολή τριών αυτή τη φορά, και όχι δύο, ηχητικών κυμάτων. Μάλιστα, παρόλο που η μάζα της σφαίρας ήταν περίπου 1,5 γραμμάρια και το ύψος αιώρησης 7 χιλιοστά, οι ερευνητές υποστηρίζουν πως στο μέλλον θα μπορούν να βελτιώσουν τις επιδόσεις της τεχνικής τους.

Επιπλέον, αν και προς το παρόν η σφαίρα μπορεί απλώς να αιωρείται σε ένα σταθερό σημείο, η ομάδα σχεδιάζει να αναπτύξει νέες συσκευές, χάρη στις οποίες θα μπορεί να (μετακινήσει) αντικείμενα στον αέρα, αλλάζοντας τους θέση.

(Κώστας Δεληγιάννης / naftemporiki.gr, Τρίτη, 16 Αυγούστου 2016, http://www.naftemporiki.gr/story/1137563/anupsosi-antikeimenon-me-ti-dunami-tou-ixou)

A Fifth Force of Nature - We'll Try to Explain

There may be a new 'force of nature' to add to our list of forces that control the universe, energy and matter.

If you remember any of the physics you learned in school, it's possible you may remember that there are four fundamental forces of nature.

They are in no particular order gravity, electromagnetism, the weak nuclear force and the strong nuclear force.

Fifth? Am I supposed to know the other four?

Gravity is fairly easy to understand: any two things that have mass (atoms, people, planets, stars) are drawn towards each other. The bigger the mass the stronger the pull. Easy peasy.

Electromagnetism? Well that's simple, it's electricity and magnetism mashed up. Yes, but that doesn't really explain how it works. The Electromagnetic force explains how things that are electrically charged (positively or negatively) interact with each other. One of the big takeaways, a magnetic charge can create an electric charge, and vice versa. Those interactions are responsible for electric power generation which is kind of a big deal. Electromagnetism and how it pushes and pulls objects is responsible for the energy in things like batteries and magnets, but it also includes light, which is just waves of electromagnetic radiation.

The other two are the weak and the strong nuclear forces and while they're both stronger than gravity they only act in the tiny spaces between atoms, and the even smaller spaces where quantum physics starts making everything really weird.

The strong nuclear force in fact is the strongest of the four known forces and basically the glue that binds everything together. It is responsible for keeping protons and neutrons (which along with electrons make up atoms) stable and then allows those to bind into atomic nuclei. The weak force on the other hand is responsible for radioactive decay, the opposite of the strong force, it is what controls how things on a nuclear level fall apart. Oh and by the way it's responsible for fission, and keeps our sun bright and warm.

That's what the four forces are, without getting too into the weeds on how these things work.

So what about a fifth force?

But, we do need to get into the weeds a bit, because we need to know what makes gravity or any of the other forces actually do their thing.

Does one body with mass, just magically start moving towards another massive thing? Nope, it's made possible by things called force carrier particles. Force carriers are the particles that carry information between things and tell them how to behave. Think of force carriers as little pocket constitutions for each of the four fundamental forces. They lay out not only all the rules for how to behave but also force the forces (ha) to act by those rules.

The force carriers for gravity are hypothetical things called gravitons, for electromagnetism they're the photons.

For the weak nuclear force the carriers are called W and Z particles, and for the strong nuclear force, gluons. These force carries are all classified as examples of bosons.

But last year, a group of physicists at the Hungarian Academy of Sciences saw what the University of California at Irvine (UCI) physics department called "puzzling anomalies in their experimental data." The Hungarians weren't sure what the anomalies were but they pointed to the existence of a new kind of light particle. That's about as far as they got. They were unable to figure out if this new particle had mass, or if it was a new kind of boson with no mass, like a photon.

Unfortunately, to paraphrase Abraham Lincoln, the world "little noted nor long remembered" the Hungarian scientists' work.

Except for a team of physicists led by Jonathan Feng, UCI professor of physics and astronomy. Along with his team, Feng took a look at the Hungarians' work, pulled together a host of other similar experiments and decided that the Hungarians may in fact have found a new kind of force carrier boson.

"Sometimes," Feng says, "we also just call it the X boson, where X means unknown." If they're right, a new force carrier particle means there must be a new force, a fifth fundamental force.

The teams' work was just published in the journal *Physical Review Letters*. “If true, it’s revolutionary,” Feng said. “For decades, we’ve known of four fundamental forces...this discovery of a possible fifth force would completely change our understanding of the universe, with consequences for the unification of forces and dark matter.”

And no, we're not even going to get into dark matter at this point.

So where has this force been hiding? Feng says that it's simply been overlooked in the past. "Its interactions are very feeble," says Feng.

But he adds, "There are many experimental groups working in small labs around the world that can follow up the initial claims, now that they know where to look.”

So what does it do, and what does it mean?

This new force is very similar to the electromagnetism, but, according to Tim Tait who co-authored the "while the normal electric force acts on electrons and protons, this newfound boson interacts only with electrons and neutrons – and at an extremely limited range."

But more research is needed to determine exactly what THAT means when it comes to how the physical world works.

So, If this new force is confirmed, what would it do for our understanding of the world? Not even Feng knows yet. But there's no shortage of speculation. It could play a role in helping scientists find the Holy Grail of Physics, the Grand Unified Theory. This fifth force might help unify the effects of the electromagnetic, weak and strong nuclear forces, “manifestations," Feng says, "of one grander, more fundamental force.”

It's long been the dream of physicists to figure out if or how electromagnetism, and the strong and weak nuclear forces work together, and this new force could be a big piece of that that puzzle.

If we can prove the existence of this fifth force it might bring us one stop closer to making real sense of how our universe works.

Got it?

(Kevin Enochs / EIN News, August 20, 2016, http://world.einnews.com/article/340988066/OAnxcttBTSGI5nUE)

Το Μουσείο του Αύριο μόλις άνοιξε στο Ρίο ντε Τζανέιρο

Δεν υπάρχει περιοδικό αρχιτεκτονικής που δεν ασχολείται αυτές τις μέρες με το νέο έργο του Σαντιάγκο Καλατράβα στο Ρίο ντε Τζανέιρο.

Το Μουσείο του Αύριο, καταλαμβάνει 5.000 τ.μ. και περιβάλλεται από μια δημόσια πλατεία 7.600 τ.μ. στο Guanabara Bay. Το έργο αποτελεί μέρος ενός μεγάλου σχεδίου αναβάθμισης της περιοχής Maravilha κοντά στην θάλασσα.

Ο Καλατράβα δήλωσε ότι *«η πόλη του Ρίο ντε Τζανέιρο δίνει το παράδειγμα στον κόσμο για το πώς να ανακτήσει την ποιότητα των αστικών χώρων με δραστικές παρεμβάσεις και τη δημιουργία πολιτιστικών εγκαταστάσεων όπως το Μουσείο του Αύριο".*

Η προσθήκη της μεγάλης πλατείας έξω από το μουσείο έγινε για να υπάρχει συνοχή του μουσείου με τον αστικό χώρο πράγμα που θα αντανακλά θετικά στην γειτονιά. Το κτίριο είναι προσανατολισμένο κάθετα προς τον κόλπο ενώ η στέγη είναι καλυμμένη με ηλιακούς συλλέκτες που κινούνται με τη θέση του ήλιου.

Τα αγαπημένα λευκά στέγαστρα του Καλατράβα πρωταγωνιστούν και εδώ, ενώ το νερό από τον κόλπο τροφοδοτεί τα μηχανήματα κλιματισμού του κτιρίου και τροφοδοτεί τις δυο μεγάλες λίμνες που υπάρχουν γύρω από αυτό και στη συνέχεια ανακυκλώνεται.

Στο εσωτερικό, το μουσείο περιλαμβάνει προσωρινούς και μόνιμους εκθεσιακούς χώρους, ένα αμφιθέατρο 400 θέσεων, ένα εκπαιδευτικό κέντρο, καφετέρια και κατάστημα με είδη δώρων.

Το επιστημονικό αυτό μουσείο θα διερευνά θέματα όπως η κλιματική αλλαγή και η αύξηση του πληθυσμού, οι αλλαγές στη βιοποικιλότητα, η γενετική μηχανική και η βιοηθική, οι νέες εξελίξεις στην τεχνολογία.

Το έργο χρηματοδοτήθηκε από την πόλη του Ρίο ντε Τζανέιρο, το Ίδρυμα Roberto Marinho, Banco Santander, και την κυβέρνηση της Βραζιλίας. Το Ρίο ετοιμάζεται να φιλοξενήσει τους Ολυμπιακούς του 2016 που θα πραγματοποιηθούν μέσα σε 15 αθλητικές εγκαταστάσεις σε μια λιμνοθάλασσα.

(http://www.thetoc.gr/politismos/article/to-mouseio-tou-aurio-molis-anoikse-sto-rio)

(σ.ε. Σχεδόν σε κάθε πόλη, όπου διεξάγονται Ολυμπιακοί Αγώνες, και ένα νέο έργο του Καλατράβα...)

ΝΕΕΣ ΕΚΔΟΣΕΙΣ ΣΤΙΣ ΓΕΩΤΕΧΝΙΚΕΣ ΕΠΙΣΤΗΜΕΣ

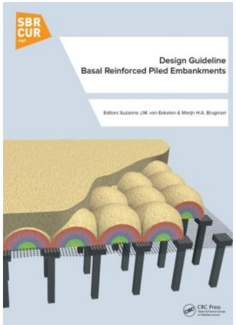

Design Guideline Basal Reinforced Piled Embankments

Suzanne J.M. van Eekelen, Marijn H.A. Brugman

A basal reinforced piled embankment consists of a reinforced embankment on a pile foundation. The reinforcement consists of one or more horizontal layers of geosynthetic reinforcement installed at the base of the embankment.

A basal reinforced piled embankment can be used for the construction of a road or a railway when a traditional construction method would require too much construction time, affect vulnerable objects nearby or give too much residual settlement, making frequent maintenance necessary.

This publication is a guideline (CUR226) for the design of basal reinforced piled embankments. The guideline covers the following subjects: a survey of the requirements and the basic principles for the structure as a whole; some instructions for the pile foundation and the pile caps; design rules for the embankment with the basal geosynthetic reinforcement; extensive calculation examples; finite element calculations; construction details and management and maintenance of the piled embankment. The guideline includes many practical tips. The design guideline is based on state-of-the-art Dutch re-search, which was conducted in cooperation with many researchers from different countries.

(July 4, 2016 by CRC Press)

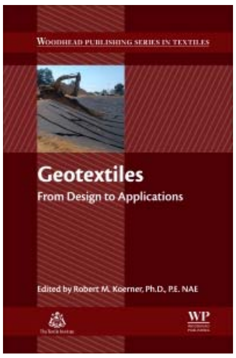

Geotextiles, 1st Edition
From Design to Applications

R. Koerner

As a comprehensive review of the manufacture, functions, properties, designs, and applications of geotextiles, this book presents valuable information on the high performance fabrics used in soil separation, drainage, filtration, reinforcement, and cushioning, also covering their use as solutions for geoengineering and other civil engineering specialties due to their advanced physical, mechanical, hydraulic, and endurance properties.

Geotextiles: From Design to Applications presents valuable information on the high performance fabrics used in soil separation, drainage, filtration, reinforcement, and cushioning. These polymeric materials offer solutions for geoengineering and other civil engineering specialties due to their advanced physical, mechanical, hydraulic, and endurance properties.

This important book offers comprehensive coverage of the manufacture, functions, properties, designs, and applications of geotextiles. Part One begins with a chapter on the history of geotextiles, followed by chapters giving detailed reviews of the types of fabrics and their manufacturing processes, from resin type, to fiber extrusion, to textile fabrication. Part Two covers the properties, behavior, and testing of geotextiles, with Part Three focusing on applications dealing with the specific primary functions of geotextiles. In Part Four, chapters offer numerous general applications of geotextiles, including those in waste containment, marine engineering, walls/slopes, agriculture, and erosion control. Finally, the chapters of Part Five address quality control and assurance for geotextiles, and the increasingly important topic of sustainability.

(03 Mar 2016, Woodhead Publishing)

ΗΛΕΚΤΡΟΝΙΚΑ ΠΕΡΙΟΔΙΚΑ

http://files.constantcontact.com/15018a1b201/8ed9a591-b6cd-46c7-b218-c00b2ae4eeb0.pdf

Κυκλοφόρησε το Τεύχος 2 του Τόμου 32, των IGS NEWS με τα παρακάτω περιεχόμενα:

General Information for IGS Members

- Summary of 2015 IGS Chapter Activities

Conference Reports

- A Capsule Summary of GeoAmericas 2016

Announcements of Regional Conferences of IGS

- EuroGeo6 6th European Regional Conference on Geosynthetics
- GeoAsia6 6th Asian Regional Conference on Geosynthetics

Announcements of Conferences under the Auspices of IGS

- 3rd International Conference on Transportation Geotechnics (3rd ICTG 2016)
- Geotechnical Frontiers 2017
- EurAsian Geotextiles Symposium (EAGS)

News from the IGS Chapters and the Membership

- Iranian Chapter of IGS Report of the 1st Board for the 2013 - 2016
- Prof. Dennes T. Bergado honored as Professor Emeritus at the Asian Institute of Technology
- Hellenic Geosynthetics Society (HGS)
- Viennese Tradition – Austrian Chapter of IGS is established
- Honduran IGS Chapter
- 11th Slovak Seminar on Geosynthetics
- "The Third Youth of Flood Defence"
- International Course on Basal Reinforced Piled Embankments
- Design Guideline Basal Reinforced Piled Embankments
- New handbook by Bob Koerner: "Geotextiles: From Design to Applications"
- Conference in Honour of Michele Maugeri
- 12th International Symposium on Landslides (ISL)
- Meeting of ISO/TC 221 'Geosynthetics'
- News from the Portuguese IGS Chapter
- IGS Objectives embraced at ICOLD 2016
- MAXConference held the 1st International Conference "Geosynthetics in Road Construction"
- Geosynthetic Institute Announces 2016 – 2017
- Fellowships

List of IGS Chapters

Official Journals of the IGS

- Geosynthetics International
- Geotextiles & Geomembranes
- Geotextiles and Geomembranes: Best papers in 2015

Corporate Membership

- Long term IGS Corporate Membership: 20 years of for PRESTO GEOSYSTEMS and 30 years for GEOSYNTHETIC MATERIALS ASSOCIATION
- Case studies – use the chance!
- Rock Fall Protection System (SCCP) on the Slopes of critical Highways, Costa Verde, Lima-Peru
- Beneficial Reuse: From Landfill to a Country Park
- Potash Mining - High Temperature Liners Withstand the Elevated Temperatures of Mine Processing Operations
- Economical Solution to Kusile Ash Dump
- Emergency Slope Stabilisation, Savièse, Switzerland
- Geobag® Coffer Dam Structure for the Panama Canal
- 45 m high reinforced soil slope in award winning Shillong Bypass Project, Meghalaya
- Cityringen, Denmark, Ourkiss Dam, Algeria, Aughinish Alumina, Ireland
- Corporate Members of the IGS

IGS News Publisher, Editor and Chapter Correspondents

IGS Council

IGS Officers

IGS Membership Application

Calendar of Events

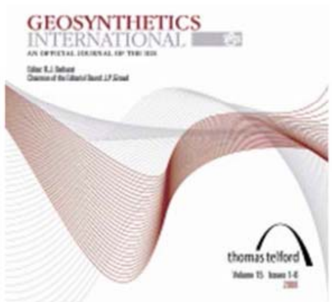

Content of Volume: 23, Issue: 2 (April 2016)

Laboratory study on the use of EPS-block geofoam for embankment widening, A. T. Özer

Water vapour adsorption and desorption in GCLs, M. A. Rouf, A. Bouazza, R. M. Singh, W. P. Gates, R. K. Rowe

Effects of geogrid encasement on lateral and vertical deformations of stone columns in model tests, M. Gu, M. Zhao, L. Zhang, J. Han

Shear-induced changes in smooth geomembrane surface topography at different ambient temperatures, J. D. Frost, T. Karademir

Cyclic and post-cyclic behaviour from sand–geogrid interface large-scale direct shear tests, F.-Y. Liu, P. Wang, X. Geng, J. Wang, X. Lin

Scaled model tests on influence factors of full geosynthetic-reinforced pile-supported embankments, C. Xu, S. Song, J. Han

Content of Volume: 23, Issue: 3 (June 2016)

Service-state behavior of reinforced soil walls supporting spread footings: a parametric study using finite-element analysis

S. Ambauen, B. Leshchinsky, Y. Xie, D. Rayamajhi

Effect of fibre type on the compressive and tensile strength of a soft soil chemically stabilised

P. J. Venda Oliveira, A. A. S. Correia, J. M. N. P. C. Teles, D. G. Custódio

Mechanical response of flexible pavements enhanced with geogrid-reinforced asphalt overlays

N. S. Correia, J. G. Zornberg

Geogrid pullout behaviour according to the experimental evaluation of the active length

G. Cardile, N. Moraci, L. S. Calvarano

Effects of coir fibres modified with Ca(OH)2 and Mg(OH)2 nanoparticles on mechanical properties of lime-treated marine clay

V. Anggraini, A. Asadi, N. Farzadnia, H. Jahangirian, B. B. K. Huat

Modelling deformation during the construction of wrapped geogrid-reinforced structures

I. Scotland, N. Dixon, M. Frost, G. Fowmes, G. Horgan

Content of Volume: 23, Issue: 4 (August 2016)

Model tests and parametric studies of two-layer geomembrane tubes, W. Guo, J. Chu

Settlement of footings at the crest of reinforced slopes subjected to toe unloading, C. C. Huang

Effect of geomembrane colour and cover soil on solar-driven down-slope bentonite erosion from a GCL, A. K. Rentz, W. A. Take, R. W. I. Brachman, R. K. Rowe

Geogrid pullout load–strain behaviour and modelling using a transparent granular soil, R. J. Bathurst, F. M. Ezzein

Numerical investigation of earth pressure reduction on buried pipes using EPS geofoam compressible inclusions, A. F. Witthoeft, H. Kim

Reliability analysis of geosynthetic-reinforced steep slopes, F. B. Ferreira, A. Topa Gomes, C. S. Vieira, M. L. Lopes

Please find the download of the articles at:
http://www.icevirtuallibrary.com/content/issue/gein/23/2
http://www.icevirtuallibrary.com/content/issue/gein/23/3
http://www.icevirtuallibrary.com/content/issue/gein/23/4
For the IGS members to have FREE access to the papers they MUST log in through the IGS website.

Geotextiles and Geomembranes: Best papers in 2015

Following the Editorial Board meeting held in Yokohama in September 2006 it was decided that it would be desirable to recognise some of the best papers published in *Geotextiles and Geomembranes*. We started with Volume 23 and have selected the Best paper in each subsequent year. This year the Editorial Board were charged with selecting what they considered to be the "Best Paper" published in *Geotextiles and Geomembranes* in 2015. Papers were considered for their contribution to the discipline in terms of providing significant new insights and/or of being of high potential impact on the discipline. All Technical Articles, except those co-authored by the Editor, were eligible. The selection of wining papers was decided based on a vote of the Editorial Board members (excluding the Editor).

Following a rigorous review of the papers I am pleased announce that the winner for the Best Paper for 2015 was:

Lessons learned from geotextile filter failures under challenging field conditions *by* R.M. Koerner and G.R. Koerner, *Geotextiles and Geomembranes*, 43(3):272-281.

Two papers were selected for Honourable Mention

Validation of analytical models for the design of basal reinforced piled embankments *by S.J.M. van Eekelen, A. Bezuijen, & A.F. van Tol*, *Geotextiles and Geomembranes*, 43(1):56-81

and

MSE walls as bridge abutments: Optimal reinforcement density *by Y. Xie & B. Leshchinsky*, *Geotextiles and Geomembranes*, 43(2):128-138.

as runners-up and hence being judged to be amongst the three best papers published in *Geotextiles and Geomembranes* in 2015. Congratulations to all of the authors for their very significant contribution to the geosynthetics discipline.

Content of Volume 44, issue 3 (June 2016)

Performance of a geogrid reinforced soil wall on PVD drained multilayer soft soils, Jian-Feng Chen, Ali Tolooiyan, Jian-Feng Xue, Zhen-Ming Shi

Experimental and DEM investigation of geogrid–soil interaction under pullout loads, Zhijie Wang, Felix Jacobs, Martin Ziegler

Analysis of geomembrane whale due to liquid flow through composite liner, Wei Guo, Jian Chu, Bo Zhou, Liqiang Sun

Effect of particle size of sand and surface asperities of reinforcement on their interface shear behaviour, Prashanth Vangla, Madhavi Latha Gali

Laboratory analysis of encased stone columns, Marina Miranda, Almudena Da Costa

Assessment of friction properties at geotextile encapsulated-sand systems' interfaces used for coastal protection, Andreia Moreira, Castorina Silva Vieira, Luciana das Neves, Maria Lurdes Lopes

Evaluation of the combined effect of toe resistance and facing inclination on the behavior of GRS walls, S.H. Mirmoradi, M. Ehrlich, C. Dieguez

A three-dimensional finite element approach for modeling biaxial geogrid with application to geogrid-reinforced soils, M.G. Hussein, M.A. Meguid

Material point modelling of releasing geocontainers from a barge, Fursan Hamad, Dieter Stolle, Christian Moormann

Electrokinetic strengthening of slopes – Case history, J. Lamont-Black, C.J.F.P. Jones, D. Alder

Modified unit cell approach for modelling geosynthetic-reinforced column-supported embankments, Yan Yu, Richard J. Bathurst, Ivan P. Damians

Reinforcement and mud-pumping benefits of geosynthetics in railway tracks: Numerical analysis, Sowmiya Chawla, J.T. Shahu

Geosynthetic-reinforced soil structures with concave facing profile, Farshid Vahedifard, Shahriar Shahrokhabadi, Dov Leshchinsky

Reinforcement and mud-pumping benefits of geosynthetics in railway tracks: Model tests, Sowmiya Chawla, J.T. Shahu

Load transfer mechanisms in geotextile-reinforced embankments overlying voids: Numerical approach and design, Pascal Villard, Audrey Huckert, Laurent Briançon

Direct shear tests on geosynthetic-encased granular columns, Sunil Ranjan Mohapatra, K. Rajagopal, Jitendra Sharma

Imperial smelting furnace (zinc) slag as a structural fill in reinforced soil structures, P.S. Prasad, G.V. Ramana

Mechanistic-empirical approach to characterizing permanent deformation of reinforced soft soil subgrade, Xiaochao Tang, Shelley M. Stoffels, Angelica M. Palomino

Load transfer mechanisms in geotextile-reinforced embankments overlying voids: Experimental and analytical approaches, Audrey Huckert, Laurent Briançon, Pascal Villard, Patrick Garcin

Performance of the new reinforcement system in the increase of shear strength of typical geogrid interface with soil, M. Mosallanezhad, M.C. Alfaro, N. Hataf, S.H. Sadat Taghavi

Discussion of Palmeira, E. and Tatto, J. (2015). "Behaviour of geotextile filters in armoured slopes subjected to the action of waves." Geotextiles and Geomembranes, 10.1016/j.geotexmem.2014.11.003, 46–55, Xuguang Chen

Reply from authors Palmeira, E. and Tatto, J. (2015). "Behaviour of geotextile filters in armoured slopes subjected to the action of waves." Geotextiles and Geomembranes, 10.1016/j.geotexmem.2014.11.003, 46–55: To Discussion of Chen (G&G2875)

Behavior of cement-stabilized fiber-reinforced pond ash, rice husk ash–soil mixtures, Arvind Kumar, Deepak Gupta

Pullout resistance of bearing reinforcement embedded in marginal lateritic soil at molding water contents, Kampanart Sukmak, Patimapon Sukmak, Suksun Horpibulsuk, Avirut Chinkulkijniwat, Arul Arulrajah, Shui-Long Shen

Geotextiles and Geomembranes: Best papers in 2014, R. Kerry Rowe

Discussion of "Stress–strain behavior of a silty soil reinforced with polyethylene terephthalate (PET)" by E. Botero, A. Ossa, G. Sherwell and E. Ovando-Shelley, Geotextiles and Geomembranes 43 (2015) 363–369, Lei Gao, Guo-hui Hu

Reply to the discussion by Gao, L. and Hu, G., on "Stress-strain behavior of a silty soil reinforced with polyethylene terephthalate (PET)" [Geotextiles and Geomembranes 43 (4), 2015, pp. 363–369], E. Botero, A. Ossa

Content of Volume 44, issue 4 (August 2016)

Modelling of geocell-reinforced subballast subjected to cyclic loading, M. Mahdi Biabani, Buddhima Indraratna, Ngoc Trung Ngo

Limit analysis of reinforced embankments on soft soil, Colin C. Smith, Alireza Tatari

Performance of geotextile filters after 18 years' service in drainage trenches, Guillaume Veylon, Guillaume Stoltz, Patrice Mériaux, Yves-Henri Faure, Nathalie Touze-Foltz

The characteristic flow equation: A tool for engineers and scientists, Rich Lacey

Impact resistance and evaluation of retained strength on geotextiles, C. Cheah, C. Gallage, L. Dawes, P. Kendall

Application design of concrete canvas (CC) in soil reinforced structure, Hui Li, Huisu Chen, Lin Liu, Fangyuan Zhang, Fangyu Han, Tao Lv, Wulong Zhang, Yujie Yang

Behaviour of model footing resting on sand bed reinforced with multi-directional reinforcing elements, M. Hariku-mar, N. Sankar, S. Chandrakaran

Performance evaluation of railway subballast stabilised with geocell based on pull-out testing, M. Mahdi Biabani, Ngoc Trung Ngo, Buddhima Indraratna

Shear behavior of sand-smooth geomembrane interfaces through micro-topographical analysis, Prashanth Vangla, Madhavi Latha Gali

Seismic evaluation of reinforced-soil segmental retaining walls, Feifan Ren, Feng Zhang, Chao Xu, Guan Wang

Experimental study on the improvement of marine clay slurry by electroosmosis-vacuum preloading, Jun Wang, Jianjun Ma, Feiyu Liu, Wei Mi, Yuanqiang Cai, Hongtao Fu, Peng Wang

Feasibility study of copper slag as a structural fill in reinforced soil structures, P.S. Prasad, G.V. Ramana

Deformations of geosynthetic reinforced soil under bridge service loads, Jennifer E. Nicks, Danial Esmaili, Michael T. Adams

Please find the download of the articles at: http://www.sciencedirect.com/science/journal/02661144
For IGS members to have FREE access to the G&G journal articles they MUST log in through the IGS website.

☙ ❧

www.geoengineer.org

Κυκλοφόρησε το Τεύχος #137 του **Newsletter του Geoengineer.org** (Αυγούστου 2016) με πολλές χρήσιμες πληροφορίες για όλα τα θέματα της γεωμηχανικής. Υπενθυμίζεται ότι το Newsletter εκδίδεται από τον συνάδελφο και μέλος της ΕΕΕΕΓΜ Δημήτρη Ζέκκο (secretariat@geoengineer.org).

Ενδεικτικά αναφέρονται:

- Sinkhole Forms in Backyard of Ipswich Home (Video)
- Earthquake in Chile Triggers Landslides Causing Dust Clouds
- Earthquakes in Italy Leave 250 Dead; Rescue Efforts Continue
- Case History - Renovation of the historic Richmond Train Station
- Flood Waters in Nepal Break Through Defense Wall (Video)

http://campaign.r20.constantcontact.com/render?m=1101304736672&ca=33b5c35b-f00f-4120-b265-0517a10a1ac3

ΕΚΤΕΛΕΣΤΙΚΗ ΕΠΙΤΡΟΠΗ ΕΕΕΕΓΜ (2015 – 2018)

Πρόεδρος	:	Γεώργιος ΓΚΑΖΕΤΑΣ, Δρ. Πολιτικός Μηχανικός, Καθηγητής Ε.Μ.Π. president@hssmge.gr, gazetas@ath.forthnet.gr
Α' Αντιπρόεδρος	:	Παναγιώτης ΒΕΤΤΑΣ, Πολιτικός Μηχανικός, ΟΜΙΛΟΣ ΤΕΧΝΙΚΩΝ ΜΕΛΕΤΩΝ Α.Ε. otmate@otenet.gr
Β' Αντιπρόεδρος	:	Μιχάλης ΠΑΧΑΚΗΣ, Πολιτικός Μηχανικός mpax46@otenet.gr
Γενικός Γραμματέας	:	Μιχάλης ΜΠΑΡΔΑΝΗΣ, Πολιτικός Μηχανικός, ΕΔΑΦΟΣ ΣΥΜΒΟΥΛΟΙ ΜΗΧΑΝΙΚΟΙ Α.Ε. mbardanis@edafos.gr, lab@edafos.gr
Ταμίας	:	Γιώργος ΝΤΟΥΛΗΣ, Πολιτικός Μηχανικός, ΕΔΑΦΟΜΗΧΑΝΙΚΗ Α.Ε.- ΓΕΩΤΕΧΝΙΚΕΣ ΜΕΛΕΤΕΣ Α.Ε. gdoulis@edafomichaniki.gr
Έφορος	:	Γιώργος ΜΠΕΛΟΚΑΣ, Δρ. Πολιτικός Μηχανικός, Επίκουρος Καθηγητής ΤΕΙ Αθήνας gbelokas@teiath.gr, gbelokas@gmail.com
Μέλη	:	Ανδρέας ΑΝΑΓΝΩΣΤΟΠΟΥΛΟΣ, Δρ. Πολιτικός Μηχανικός, Ομότιμος Καθηγητής ΕΜΠ aanagn@central.ntua.grn
		Βάλια ΞΕΝΑΚΗ, Δρ. Πολιτικός Μηχανικός, ΕΔΑΦΟΜΗΧΑΝΙΚΗ Α.Ε. vxenaki@edafomichaniki.gr
		Μαρίνα ΠΑΝΤΑΖΙΔΟΥ, Δρ. Πολιτικός Μηχανικός, Αναπληρώτρια Καθηγήτρια Ε.Μ.Π. mpanta@central.ntua.gr
Αναπληρωματικό Μέλος	:	Κωνσταντίνος ΙΩΑΝΝΙΔΗΣ, Πολιτικός Μηχανικός, ΕΔΑΦΟΜΗΧΑΝΙΚΗ Α.Ε. kioannidis@edafomichaniki.gr
Εκδότης	:	Χρήστος ΤΣΑΤΣΑΝΙΦΟΣ, Δρ. Πολιτικός Μηχανικός, ΠΑΝΓΑΙΑ ΣΥΜΒΟΥΛΟΙ ΜΗΧΑΝΙΚΟΙ Ε.Π.Ε. editor@hssmge.gr, ctsatsanifos@pangaea.gr

ΕΕΕΕΓΜ

Τομέας Γεωτεχνικής
ΣΧΟΛΗ ΠΟΛΙΤΙΚΩΝ ΜΗΧΑΝΙΚΩΝ
ΕΘΝΙΚΟΥ ΜΕΤΣΟΒΙΟΥ ΠΟΛΥΤΕΧΝΕΙΟΥ
Πολυτεχνειούπολη Ζωγράφου
15780 ΖΩΓΡΑΦΟΥ

Τηλ. 210.7723434
Τοτ. 210.7723428
Ηλ-Δι. secretariat@hssmge.gr ,
geotech@central.ntua.gr
Ιστοσελίδα www.hssmge.org (υπό κατασκευή)

«ΤΑ ΝΕΑ ΤΗΣ ΕΕΕΕΓΜ» Εκδότης: Χρήστος Τσατσανίφος, τηλ. 210.6929484, τοτ. 210.6928137, ηλ-δι. ctsatsanifos@pangaea.gr, editor@hssmge.gr, info@pangaea.gr

«ΤΑ ΝΕΑ ΤΗΣ ΕΕΕΕΓΜ» «αναρτώνται» και στην ιστοσελίδα www.hssmge.gr